AN ENERGY BASED GENERAL FRAMEWORK FOR DYNAMICAL COMPLEX NETWORKS

A Dissertation

by

CHUN-LIN YANG

Submitted to the Graduate and Professional School of
Texas A&M University
in partial fulfillment of the requirements for the degree of

DOCTOR OF PHILOSOPHY

Chair of Committee,	Chii-Der S. Suh
Committee Members,	Harry Hogan
	Bruce Tai
	Jun Wang
Head of Department,	Guillermo Aguilar

August 2022

Major Subject: Mechanical Engineering

ABSTRACT

Complex networks are ubiquitous in nature. It is essential to understand the mechanism that defines network dynamics and constituent interaction. Defining network behaviors is challenging because network dynamics exist simultaneously at the microscopic (local) level and macroscopic (global) level. A proper description of the dynamics inherent of all complex networks is needed. This study addresses the need and develops a general framework for describing complex networks dynamics. The generality of the general framework is demonstrated using a 20-constituent point mass network and a 6-neuron brain network – examples from two different physical domains. The former is a real-life complex network that is exposed to environmental disturbance and undergoes constant change of network structure due to individual constituent joining and leaving the network. The dynamics of the 20-constituent network is a spatial translational network system whose dynamics is exhibited in the displacement and velocity of individual constituents. A multivariable time-frequency complex network control scheme is also applied to ensure the integrity of the network structure and its robustness to disturbance. The 6-neuron brain network is a complex network in the biology domain whose dynamics is dominated by magnetic flux and exhibited in the form of electrical voltage fluctuations of neuronal membrane.

DEDICATION

This dissertation is dedicated to my loving and supportive family and the kind people who supported me in pursuing my dream. Thank you for having faith in me and participated in this adventure of mine.

ACKNOWLEDGEMENTS

I would like to thank my committee chair, Dr. C. Steve Suh, for his wise guidance in elevating me into a higher intellect level. I am deeply appreciative of Dr. Hogan, Dr. Tai, and Dr. Wang, for all the kindness and support they provided.

Thanks also go to my friends and colleagues for their support.

Finally, to my parents and brother, I deliver my sincere appreciation for their loving and faithful encouragement with their selfless understanding minds and supports.

CONTRIBUTORS AND FUNDING SOURCES

Contributors

All work conducted for the dissertation was completed by the student independently.

Funding Sources

This study was not supported by any funding but with my loving family, guidance of my wise and trusting research advisor, and supporting friends.

TABLE OF CONTENTS

Page

LIST OF FIGURES

LIST OF TABLES

1. PRESENT STATE OF AFFAIRS*

1.1 Overview of Dynamic Complex Network

Complex networks are statistical mechanical systems whose responses are nonlinear and nonstationary. Complex network dynamics involves individual response at the constituent level and global response at the ensemble level [1-5]. Individual constituent has its own dynamics. The relationship of connected constituents is defined by degree of coupling [5] and constituent interaction is governed by coupling laws. Network dynamics is the emerged collective behavior at the ensemble level. Depending on the characteristics of a complex network, constituent dynamics can be the time-derivative of various physical states and the coupling laws are also different. Complex networks are ubiquitous with very different properties. For example, flocking birds have a rather stable and fluid-like collective behavior with nonlinear constituent behavior and nonstationary coupling while power grids are of a static structure, massive blackout could be triggered by a severed coupling. It is difficult to model complex network dynamics. However, there are properties that are common of all networks. A framework for modeling network dynamics applicable to all networks is needed, one that captures the nature of complex network dynamics and helps establish novel network theory.

An extensive literature review indicates that modeling of complex network dynamics focuses, in general, on describing constituent interaction and network structure. Winfree describes biological systems as collections of oscillators [6]. Describing phase synchronization of molecular oscillations in chemical reaction, the Kuramoto model is extensively used to define phase

* Part of this chapter is reprinted with permission from "A General Framework for Dynamic Complex Networks" by Yang, C.-L. and Suh, C. S., 2021, Journal of Vibration Testing and System Dynamics, 5, 87-111, Copyright 2021
by L & H Scientific Publishing, LLC

synchronization of oscillators [7-11]. Coupling strength was proposed to describe the interaction (relationship) between constituents. The Kuramoto model assumes coupling strength as being time-independent and universal between all constituents. However, a clear definition of coupling strength is unavailable. Moreover, constituent relationship in real-life networks is invariably time dependent. Also, each pair of constituents has its unique degree of relationship. Constituent coupling strength as defined by the Kuramoto model is static and universal, which is not true of real-life networks [5].

Adopted for the concept of coupling strength, graph theory is applied to describe network structure. Graph theory is a branch of applied mathematics that studies the relationship between objects. WS models (small world network models) define network structures in which the distance (the number of links) between any two nodes (constituents) is small [12]. BA models (scale free network models) define network structures that present the same characteristics regardless of the size of the network [13]. Although WS and BA models have initiated extensive research, due to the adoption of coupling strength, network structures thus defined are static while the structure of a complex network is invariably dynamical [5]. Moreover, graph theory only considers whether two nodes are connected or not, instead of the physical laws that govern the interaction and connection strength of the nodes. Because static network models disregard the physical laws that govern constituent interactions, graph theory-based network models cannot capture the nature of real-life networks.

The dynamics and structural instability of a complex network can be mitigated through adjusting constituent couplings. However, since network dynamics is not thoroughly understood, conducting proper and effective control of complex networks is difficult. Network controllability is a network control theory [14]. Based on static network models and linear control theory,

network controllability evaluates if a network is controllable with a minimum set of nodes to which control input is inserted. According to network controllability, there always exists a structure in the neighborhood of the uncontrollable structure. By driving the uncontrollable structure toward the controllable neighboring one, the network will eventually become controllable. However, as the wiring diagram of real-life complex networks is usually unknown, network controllability is not applicable [15]. Moreover, because network controllability is based on the LTI control theory and complex networks are nonlinear dynamical systems, network controllability cannot properly address or control complex networks. Also, the specific strategy for maneuvering the uncontrollable structure toward a controllable structure as well as how to find a controllable one is not generally provided. And the maximum matching algorithm is based on static network models that do not capture the dynamical nature of complex networks by following laws of physics. Network controllability is therefore not viable for controlling complex networks.

Many research efforts are devoted to modeling real-life networks. Most, however, fail to address the dynamics of individual constituents and the coupled interaction. Some studies apply static network models to describe real-life networks [16]. However, they are not able to describe the time-dependent nature of complex networks. Other studies focus on describing the mechanism of local dynamics [17].

In general, the reviewed works fail to develop a proper description for 1) the individual constituent dynamics, 2) the coupling dynamics, and 3) the ensemble dynamics involving all the network constituents. As each individual constituent has its own dynamics, there are coupling dynamics governing the relationship between each pair of connected constituents. Moreover, the network has its own dynamics that are nonstationary and nonlinear. Furthermore, real-life networks must obey the law of physics. The literature either assumes static relationship between

constituents, applies inappropriate tools such as graph theory, or ignores the significance of physical laws. As a result, formulation and modeling of complex network dynamics are unsatisfactory and incomplete. It is imperative that a general framework is available for describing complex network dynamics, one that describes the characteristics common of all networks.

Complex networks are special cases of statistical mechanical systems. The dynamics of complex network is the coupled individual constituent dynamics governed by the coupling laws at the microscopic level (constituent level) and the ensemble dynamics at the macroscopic level (network level). Regardless of the physical states individual constituents are in, energy is a fundamental physical property that describes the states. Individual constituent dynamics can be defined by energy. Dictated by physics, individual constituent energy must follow a normal distribution [18]. Network dynamics can be defined through information entropy as a function of individual constituent energy. As individual constituent energy and information entropy are time-dependent, time-dependent network dynamics can be described properly [5]. The relationship between constituents is defined using degree of coupling to describe the dynamics of coupling [5]. Because complex networks are nonstationary and nonlinear, the corresponding spectral responses are broad in bandwidth and time-dependent in the frequency domain [15], requiring that controllers be designed to adjust the constituent couplings both in the time and the frequency domains to maintain structural integrity and dynamic stability [15].

This research presents a general framework for the description of complex network dynamics. A time-frequency control strategy is developed to mitigate complex network dynamics. To demonstrate its generality, the framework is applied to describe the dynamics of network systems from 2 different physical domains including a 20-constituent spatial translational network

which is a statistical mechanical system with coupled constituent dynamics and a brain network which is a neuroscience system.

1.2 Literature Review

1.2.1 Complex Network Dynamics

Complex networks are dynamic systems whose network properties evolve in time. The global dynamics of such systems at the ensemble (macroscopic) level are the manifestation of the coupled constituent dynamics at the individual constituent (microscopic) level. The individual dynamics and global dynamics together define the emergence of collective behaviors such as synchronization and asynchronization at the network level. Network dynamics are nonlinear, non-stationary, and complex. Many efforts have been given to correlate the complex interactions between ensemble constituents with simultaneous collective behaviors as well as critical and abrupt failures when the system is perturbed. Small-world networks and scale-free networks are popular network structures for such efforts [12,13,19,20,21]. However, given that they are tools for static analysis, small-world and scale-free network models are rigid in their definition for network structure, thus requiring that all the network properties to be time-invariant. In addition, being topological tools for defining network structures only at the microscopic level, they are not for addressing network response at the macroscopic level.

Ensemble dynamics is defined by the underlying dynamic network structure and laws of coupling that govern the interactions of ensemble constituents. Concepts of statistical mechanics are essential for defining global dynamics through establishing the relationship between the macroscopic state and the microscopic state [1, 2]. A complex network is a statistical mechanical system with energy distributed among all constituents. Each constituent must maintain a certain amount of energy to be in a corresponding state. The energies and states of all the constituents

must also follow distribution laws defined by a probability distribution function (PDF) [18]. Energy variation of individual ensemble constituents impacts the state of the ensemble. By applying information entropy (or Shannon entropy) [3, 4, 22], the probability distribution of the ensemble energy can be defined to describe the state of the complex network including collective behaviors. With the distribution of individual constituent states defined by the probability distribution function, information entropy determines as to how localized the distribution is under the PDF function. Because the entropy of the ensemble constituent necessarily varies in time as a network structure evolves, thus the stability or otherwise instability of a complex network can be established by exploring the corresponding information entropy. Increasing entropy corresponds to a wider range of distribution of the state of the ensemble constituents, thus indicating a less orchestrated collective behavior while the opposite indicates ordered ensemble dynamics with the constituents engaging in synchronized individual behavior.

1.2.1.1 Network Structure

The structure of a dynamic complex network is defined by the time-evolving connections that connect all the constituents in the network. Appropriate physical laws dictating the forming and sustaining of connections must be followed. Each connection defines how two connected constituents associate with one another by responding to the changing state of the association. The degree of the association is indicated by a coupling whose strength is measured in energy. Weak coupling suggests less influence of one constituent on the other and less energy is involved. Because maintaining the connection that connects two constituents requires energy, the property of each connection is a dynamic function of energy. However, unlike dynamic networks, static network structures are inadequate for resolving the inter-constituent dynamics or the collective behaviors of the networks.

To capture the evolution of a network structure, energy distribution among all the constituents must be established in time. Statistical entropy measures the randomness of the state of a statistical mechanical system while the state of the constituents obeys a probability density function. That is, the structure of a dynamic network can be characterized by statistical entropy and through defining the distribution of the energy of ensemble constituents. Studies on understanding the characteristics fundamental of all complex networks are enormous, with the majority devoted to defining network structures [23]. Graph theory is a prevalent tool using nodes (or constituents) and edges (or connections) to represent network ensemble. Concepts including degree distribution, clustering coefficient, and average path length are properties used to define network structure. The degree of a constituent gives the number of connections a constituent has connecting to other constituents while degree distribution defines the probability distribution of the degrees of all the constituents over the entire network. Clustering coefficient defines how close the neighbors of a constituent are a complete graph. Average path length defines the average number of steps between any two constituents in a network. That is, degree distribution provides a measure of network structure, clustering coefficient indicates the extent to which the constituents in a network group together, and average path length defines the closeness of any two constituents in a network.

A regular graph is a graph in which every constituent has the same degree while such a property is random in a random graph. While most real-world networks are neither completely regular graphs nor fully random graphs, a small-world network by definition has the characteristic of a large clustering coefficient as a regular graph and a small average path length as a random graph. The algorithm for generating a small-world network named the WS model [12] uses a ring lattice, which is a regular graph, and rewires the connections of each constituent randomly with a

defined probability. The model can be tuned to generate networks between completely regular and random graphs. However, Barabási et al. pointed out that the model is limited to fixed constituent numbers - an assumption not generally valid for real-world networks. They proposed a BA model allowing the constituent number to increase at each time step with a preferential law attached to connections with well-connected constituents [13], resulting in a "rich-gets-richer" scenario where constituents with higher degrees ended up with more connections over time. In other words, a constituent late in joining the network will never establish more connections than older constituents. Moreover, since the degree distribution of the BA model follows a power law regardless of the size of the network, the network is also called scale-free.

Assuming the preference for a constituent to attract connections does not always depend on the degree of the constituent, Bianconi et al. proposed a BB model as a modified scale-free network named the fitness model [20]. Similar to the BA model, the BB model introduces new constituents at each time step. Constituents compete for connections, instead of the degree of each constituent, through the "fitness" of each constituent, thus better fitted constituents eventually attract the most connections - a case of "winner-takes-all" regardless of the time duration over which the constituents have presented in the network. An extreme case of the BB model is a star graph where all the constituents have one connection connecting to the fittest constituent. The BB model was mapped to a Bose gas to predict a topological transition between the "rich-gets-richer" phase and the "winner-takes-all" phase.

The WS, BA, and BB models have been influential to the study of complex networks in the past two decades. However, since graph theory addresses mathematically the interconnections of constituents and connections and not the physical properties of such interconnections that define the characteristics of complex networks, these network models do not account for connection

dynamics. As a result, graph theory-based network structures [23] are approximations that do not truly capture the time-dependent nature of dynamic complex networks.

Small-world networks are defined by clustering coefficient and average path length, with the former defining network structure and the latter the relationship between constituents. Clustering coefficient must remain the same if the network structure is to stay intact. The corresponding average path length must also remain the same in time to ensure the same relationship between the constituents. However, while average path length is defined by the average of the shortest path length between all possible pairs of constituents in a network, there often exist multiple shortest paths between two constituents. In the case of weighted graphs, the shortest path between two constituents is the path with the lowest weight if multiple shortest paths exist. While the weight of each connection varies in time, it is likely that the shortest path is switching between all the possible shortest paths in time as well. The relationship between constituents and average path length must also vary in time. As real-world networks cannot be comprehensively defined by clustering coefficient and average path length alone, small-world networks are not a proper network structure definition.

Figs. 1 and 2 present the results corresponding to a small-world network model, Structure 2, to be further elaborated in section 3.1 in the context of the general framework. Structure 2 is based on the WS model. It has its shortest path length initiated from constituent 1 and eventually reached the rest of the constituents in 10 seconds. The weight of each connection is the energy difference between 2 connected constituents. Detail on the definition and determination of connection energy are discussed in that section. Fig. 1(a) is the static structure of the small-world network. Note that the structure stays unaltered at all times. Figs. 1(b), 1(c), and 1(d) along with Table 1 give the connection weights of the structure at t = 0s, 5s, and 10s, respectively. Figs. 2(a),

2(b), and 2(c) provide the corresponding shortest paths from constituent 1 to all other constituents at the 3 time instances considered.

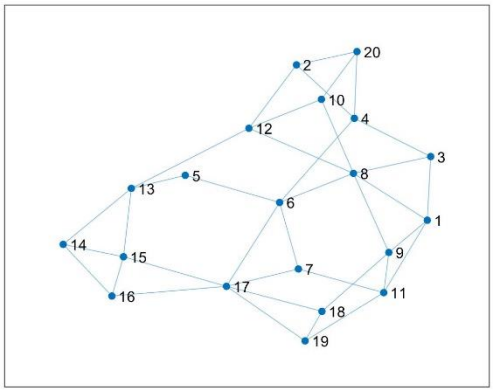

(a)

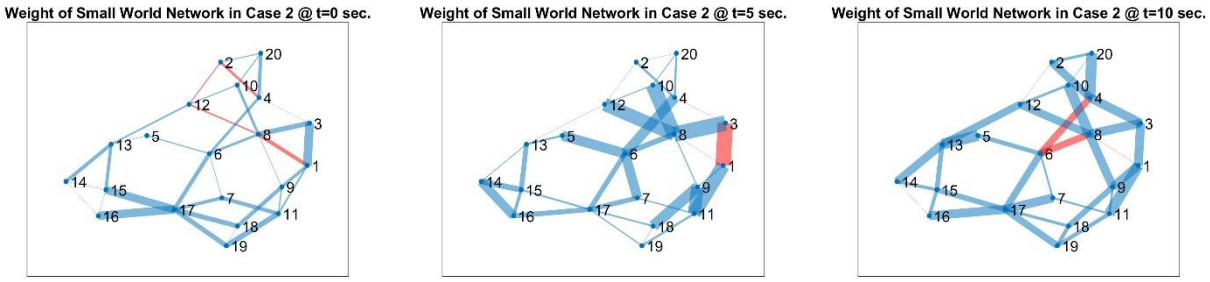

(b) (c) (d)

Fig. 1 (a) 20-constituent static small-world network model considered in Case 2, (b) weights of connections at t=0s, (c) weights of connections at t=5s, and (d) weights of connections at t=5s.

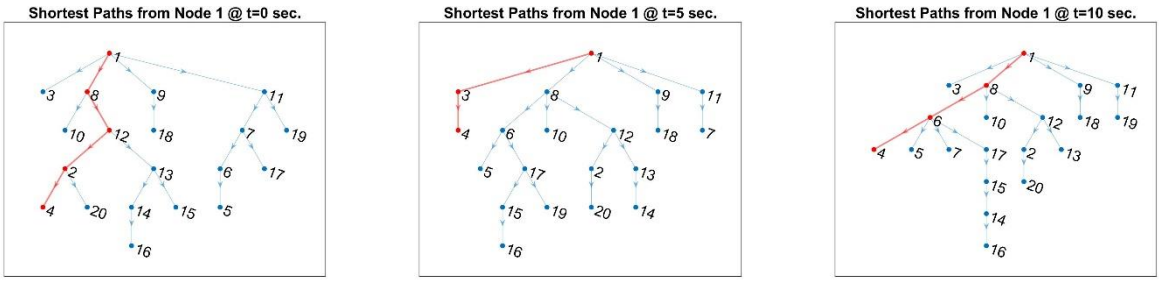

(a) (b) (c)

Fig. 2 Shortest path lengths initiated from constituent 1 considered in Case 2 at 3 different time instances at (a) t=0s, (b) t=5s, and (c) t=10s.

Table 1: Weight of connections in Case 2 at 3 different time instances

End Nodes		Weight of Connections @ t=0s	Weight of Connections @ t=5s	Weight of Connections @ t=10s
1	**3**	0.087587551016085	0.153978681238552	0.090032776716733
1	**8**	0.037834448032312	7.52742281665025e-4	5.80769945940362e-7
1	**9**	0.031985910621667	0.010840303845492	0.087049328112219
1	**11**	0.031985910621667	0.137830525051499	0.109078641069781
2	**4**	0.025384162392762	0.023360260726256	0.081233875871716
2	**12**	0.011058458428669	0.001671547066397	0.001458592730667
2	**20**	0.010072492667219	0.003074680673874	0.027918328220215
3	**4**	0.002377792972332	0.001608719040527	0.089996195412362
3	**8**	0.049753102983773	0.154731423520217	0.090032195946787
4	**6**	0.026370128154212	0.101885583217364	0.069614424420689
4	**20**	0.035456655059980	0.020285580052382	0.109152204091932
5	**6**	0.011542049542330	0.099878243281764	0.044505563487381
5	**13**	0.004833315608894	0.020184124174956	0.108369919107983
6	**7**	0.006225142819775	0.097855218529773	0.019525877049215
6	**8**	0.025760767801892	0.054454559343380	0.069650424955114
6	**17**	0.040289970668874	0.049545863346200	0.069601536787286
7	**11**	0.039304004907424	0.013726510539988	0.019901758295506
7	**17**	0.034064827849099	0.048309355183573	0.089127413836501
8	**9**	0.005848537410645	0.011593046127157	0.087048747342273
8	**10**	0.026746733563343	0.145077175713340	0.104815936435993
8	**12**	0.015688275134674	0.134651428900885	0.079811283675474
9	**11**	0.013919842514662	0.126990221206007	0.022029312957562
9	**18**	0.039304004907424	0.109733930030248	0.057610795907698
10	**12**	0.011058458428669	0.010425746812454	0.025004652760518
10	**20**	0.010072492667219	0.009022613204978	0.004372268190364
11	**19**	0.053223847422086	0.021714923703747	0.040125403587811
12	**13**	0.016781226600655	5.02750450698634e-4	0.074025214340962
13	**14**	0.036442620821431	0.009048849070432	0.081918851741415
13	**15**	0.032595270973987	0.049252697172705	0.048231614914272
14	**15**	0.003847349847443	0.058301546243137	0.033687236827144
14	**16**	8.67361737988403e-19	0.089710221311992	0.033687236827144
15	**16**	0.003847349847443	0.031408675068855	0.035269060194573
15	**17**	0.079593975576298	0.019104441412097	0.053968796080955
16	**17**	0.083441325423741	0.050513116480952	0.089237856275528
17	**18**	0.047984670363761	0.017326553467826	0.029389063266747
17	**19**	0.047984670363761	0.012867920939838	0.068903768544196
18	**19**	2.77555756156289e-17	0.004458632527988	0.039514705277449

While the network structure does not evolve, however, according to the definition for average path length, l_G,

$$l_G = \frac{1}{n^2 - n} \sum_{i \neq j} d(v_i, v_j) \quad (1)$$

where n is the number of constituents and $d(v_i, v_j)$ is the graphical distance between constituent i and constituent j, the shortest path length from constituent 1 to constituent 4, indicated in red in Figs. 1 and 2 and Table 1, switches from path 1-8-12-2-4 with a total weight of 0.09 at t = 0s to path 1-3-4 with a total weight of 0.1556 at t = 5s to path 1-8-6-4 with a total weight of 0.1393 at t = 10s. It is evident that the weights of all the connections have changed in time. Consequently, the shortest path between any two pairs of constituents can change between any possible shortest paths with time-varying length that results in time-varying average path length. That is, albeit rigidly defining the network structure using a constant (time-invariant) clustering coefficient, the corresponding average path length is inherently a function of time. However, the definition of small-world networks requires the clustering coefficient and average path length to stay constant if the network is to remain being "small-world" at all times, implying the insufficiency in defining small-world networks using the 2 parameters. Moreover, static network models are not able to describe the dynamic coupling of all the connected constituents that ultimately manifests into the global dynamics of the network.

One might argue that small-world network models are valid for describing network structures as they evolve using time snapshots [24]. However, time-changing weight of connections results in non-stationary average path length. Consider the traffic network where five cities are connected by multiple roads. Assume that the weight of each road is positively correlated to the traffic load of each road and the connections of the roads stay the same so that the clustering coefficient is a time-invariant constant. The path length of each road is positively correlated to the time required to travel each road. While the traffic load of each road varies in time, the shortest path between any randomly selected two cities also varies. Thus, the required travel time between

the two cities and the shortest path length vary as a function of the traffic and the path length of each road. As the traffic evolves, the average path length of the five-city traffic network also evolves. In addition to resulting in time-varying parameters if the same network structure is to be maintained, small-world networks also do not describe the variation of the weight of each connection. Not being able to predict how a network structure would evolve renders the use of snapshots seriously flawed at the fundamental level.

Like small-world networks, scale-free networks are also inadequate for characterizing dynamic network structures. To construct a network whose degree distribution is of a scale-free, power-law distribution, the growth of new constituents following a preferential attachment process must be defined. Eq. (2) defines the connectivity of the BA model [20]. It is seen that longer a constituent is present in the network, higher is the probability for the constituent to establish connections with newly added constituents as time elapses. In general, older constituents have higher degree than newer constituents. Furthermore, constituent degree distribution can be approximated by the stationary solution given in Eq. (3) regardless of the size of the network. After an extended network growing process, the impact of m on the stationary solution can be neglected as seen in Eq. (3), where γ varies from network to network. As a result, the degree distribution of scale-free networks follows the power law defined by Eq. (3). However, there is no proper physical interpretation for the definition of scale-free networks. First, it is not clear as to after how long the network must develop and how large the network size needs to be to justify neglecting the effect of m. Second, the stationary solution is an approximation of the true scale-free network structure. Lastly, the connectivity is a function of probability without proper physical definition as to how each connection is established and maintained. In other words, with the same

connectivity, networks of different structures can be developed, with each network structure deviating away from the exact stationary solution to a different degree.

$$k_i(t) = m(\frac{t}{t_i})^{\frac{1}{2}}, m_0 = m = 2 \tag{2}$$

$$P(k) = \frac{2m^2}{k^3} \approx k^{-\gamma}, \gamma = 3 \tag{3}$$

where $k_i(t)$ is the connectivity of constituent i at time t, $P(k)$ is the stationary solution of the BA model, t_i is the time when constituent i is added to the network, m_0 is the number of constituents at which the network starts to grow, and m is the number of connections a newly added constituent has.

To illustrate these issues inherent of scale-free networks, networks of 20, 100, 1000, and 2000 constituents using the BA model [20] are considered in Figs. 3 through 6. The network model with 20 constituents follows the network structure defined in section 3.1. in the context of general framework and presented in section 2 as Structure 3. Figs. 3(a) and 3(b) give, respectively, the degree distributions of the 20-constituent and 20,000-constituent scale-free networks. Per the definition given in [20], when growing a n-constituent scale-free network using Eq. (2), iterations must be terminated at the n^{th} step. Or else, the network would end up as a completely connected graph with a degree distribution not following the power law defined by the stationary solution. It is seen that the degree distribution of the 20,000 constituents scale-free network closely follows the power law in Eq. (3) while the degree distribution of the 20 constituents scale-free network does not. This observation suggests degree distribution would only follow the power law if the network size is large enough. To ensure Fig. 3(a) is not a special case, Fig. 3(c) considers the degree distributions of 10,000 sets of the 20-constituent scale-free networks generated using Eq. (2). Note that the degree of any constituent must be an integer. It is seen that while the degree

distribution of the 10,000 sets of the scale-free network follows roughly the stationary solution in Eq. (3), the approximation is of a significant error deviating from the true solution. Note that most networks have more constituents of degree-2 than degree-1. The same is confirmed by all the ascending triangles in Fig. 3(c) where the numbers of constituents of higher degrees are consistently greater than those of the lower degrees. Moreover, there are infinite numbers of possible combination of degree distribution. Thus, the degree distribution of the scale-free network cannot be uniquely defined by the stationary solution in Eq. (3). The simplified stationary power law that neglects the m term in Eq. (3) approximates the degree distribution of the scale-free network with error. Because error becomes significant when the network size is small, it implies that the power-law distribution is not truly scale-free.

To further investigate scale-free networks, networks of 3 different constituent sizes, namely, 20, 100, and 1000 are studied following the BA model. It is noted that 10,000 networks are generated using the same connectivity in Eq. (2) for all the 3 cases. Figs. 4(a), 4(b), and 4(c) give the degree distributions that correspond to 20, 100, and 1000 constituents, respectively. Figs. 4(d), 4(e), and 4(f) present the corresponding numbers of networks that have n-degree (out of the 10,000 networks generated). One could obtain the probability distribution function of degree for each of the network; however, the function is likely to be an approximate solution. Figs. 5(a), 5(c), and 5(e) give the numbers of networks (out of the 10,000 networks generated) having m-constituent with n-degree. Figs. 5(b), 5(d), and 5(f) present the same data as Figs. 5(a), 5(c), and 5(e) with an opposite order of the x-axis (the degree) to provide a better visualization for the lower bars. Figs. 6(b), 6(d), and 6(f) show the same data as Figs. 5(a), 5(c), and 5(e) while using colors to indicate the number of networks having m-constituent with n-degree. Figs. 6(a), 6(c), and 6(e)

display the distributions of m-constituent with n-degree of all the 10,000 networks as the projections of Figs. 6(b), 6(d), and 6(f).

Figs. 4(a), 4(b), and 4(c) provide the same information as does Fig. 3 with 10,000 more sets of networks. They indicate that larger the network size is, closer the degree distribution follows the stationary power law solution. However, as discussed, the degree distributions of all the 3 groups of 10,000 networks cannot be defined exactly by the stationary solution. Figs. 4(d), 4(e), and 4(f) show that the corresponding degree distributions across the networks also follow the power law distribution. It is noted that the degree distributions across the networks do not agree exactly with the power law distribution in all the 3 groups of 10,000 networks. Fig. 4(f) shows that with the same connectivity, it is more likely to generate a network having constituents of 60-degree than 50-degree for the 1,000-constituent network. The same is also observed with Figs. 4(b) and 4(d). It is evident that degree distributions across networks of the same connectivity cannot be properly approximated using a power law distribution function. Furthermore, using the same connectivity to generate either 1 network or multiple networks, the degree distributions of constituents cannot be properly approximated using the stationary solution in Eq. (3). There is no definitive correlation between connectivity and the stationary solution of the scale-free network models.

Figs. 5 and 6 present the statistical relationship between the number of constituents that have degree of n occurred in m number of networks out of the 10,000 networks generated using the same connectivity. It is seen in Fig. 5(c) that for the case of the 100-constituent networks the number of constituents of each degree follows a distribution across the 10,000 networks generated. Similar observations are also made with Figs. 5(a) and 5(e). Figs. 6(b), 6(d), and 6(e) are the top views of Figs. 5(a), 5(c), and 5(e) with the degree distributions of all the 10,000 networks being

stacked up in the same plot for all the 3 groups. Note that colors are used to indicate the number of networks that correspond to the number of constituents of degree indicated therein. As seen in Figs. 3(a), 3(b), 4(a), 4(b), and 4(c), degree distributions cannot be properly approximated using the stationary solution. Larger the network size, better the degree distribution is in agreement with the stationary solution. Figs. 6(a), 6(c), and 6(e) show the distribution of number of constituents with degree n throughout the 10,000 networks. Surprisingly, the probability of the number of constituents of each degree occurs in each set of the network follows a normal distribution. That is, despite the fact that the degree distribution of the network follows the power law, the probability for a constituent with degree n to exist in scale-free networks generated using the connectivity in Eq. (2) is of a normal distributed function. This explains why the degree distribution can only be approximated by the stationary solution for scale-free networks of large network sizes. Scale-free networks do not account for the probability for a constituent to be of a specific degree. To properly define scale-free networks it is required that the number of constituents of each degree be also defined to follow a specific normal distributed function. That is, the stationary solution needs to be revised to have the probability of the occurrence of each degree also defined.

Previous paragraphs indicate that the stationary solution is only applicable to scenarios when the network size is large. Degree distribution as defined by the power-law, the signature characteristic of scale-free networks, is not scale-free. Moreover, the preferential attachment defined by connectivity is also insufficient for generating well-defined network structures. The probability for a constituent of a specific degree to exist in a network is normal distributed. As such, using time snapshots to study scale-free networks evolving in time is flawed. This is particularly so when the network size is small. One could argue that measurements would be valid for scale-free networks that are large in sizes. However, the criteria by which the m term in Eq.

(3) is negligible so that the distribution obeys a power law is not defined. While Fig. 4(c) shows that the degree distributions of 10,000 sets of the 1,000-constituent network deviates significantly from the power law distribution, nature provides abundant examples of stable collective behaviors with a network size under 10 constituents. Bird flocks of 5, 10, 1000, or 10,000 displaying similar collective behaviors of network stability are such examples.

Graph theory does not account for the physical relationship between objects which is nonstationary and nonlinear for most real-world network systems. All graph theory-based networks are static networks. Small-world and scale-free models are inadequate for describing networks and their evolving structures. They provide no mechanism for the wiring and rewiring of connections following laws of physics. Moreover, they assume the connection strength to be uniform and time-invariant for all the connected constituents in a network, which is a contradiction to real-world network systems. While it can be argued that evolutions of small-world network and scale-free network can be approximated using a series of snapshots [24], however, because they are graph theory based, static network models are not applicable to characterize network dynamics. Highly nonlinear in response, input to dynamic networks of whatever magnitude can induce complex system outcome [25]. It is improper to investigate dynamic systems for their behaviors in time using tools developed for static systems. Conversely, schemes formulated using static network models such as virtual structure [26] and leader-follower control [27] would not be valid for mitigating network instability.

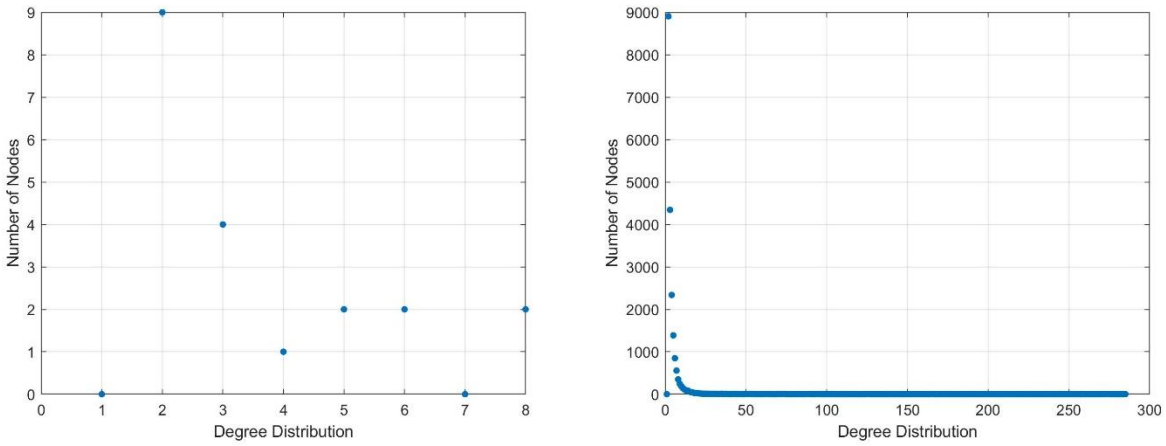

(a) (b)

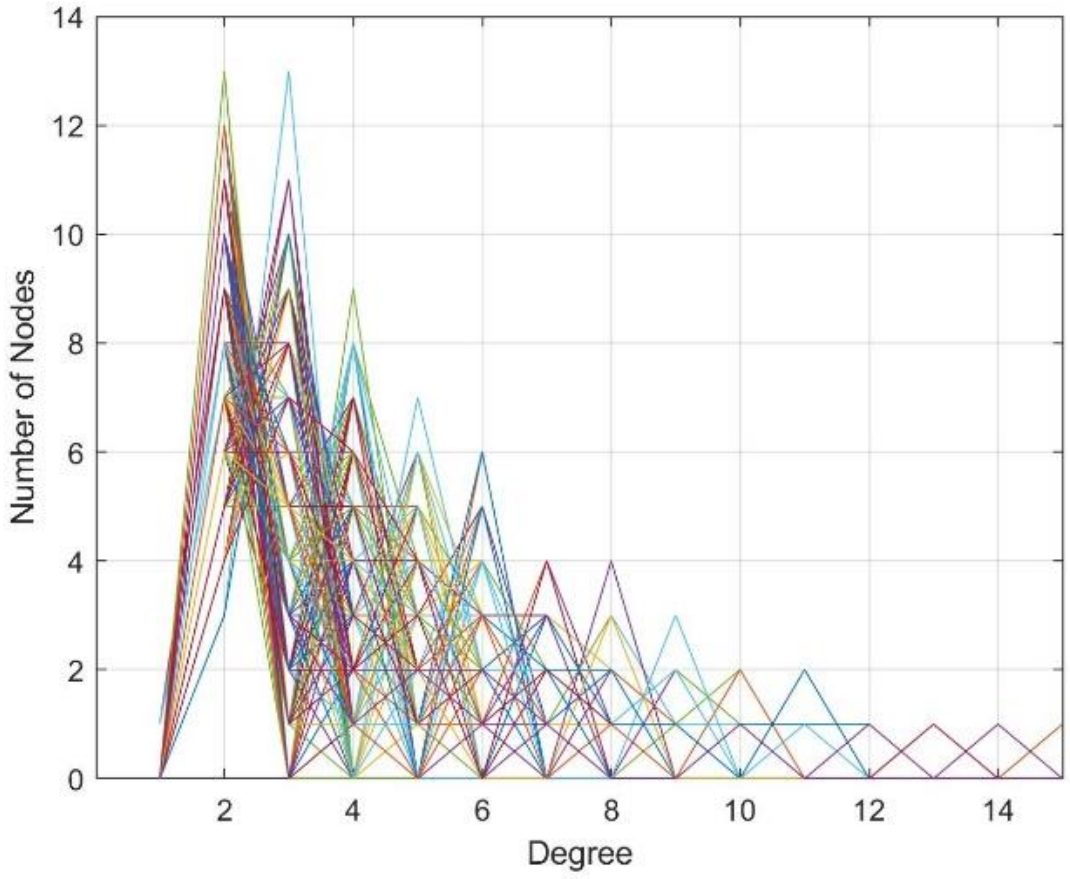

(c)

Fig. 3 Relationship between degree distribution and network size grown by the same connectivity for scale-free network of (a) 20 constituents and (b) 20,000 constituents. (c) Degree distributions of 10,000 sets of 20-constituent scale-free networks.

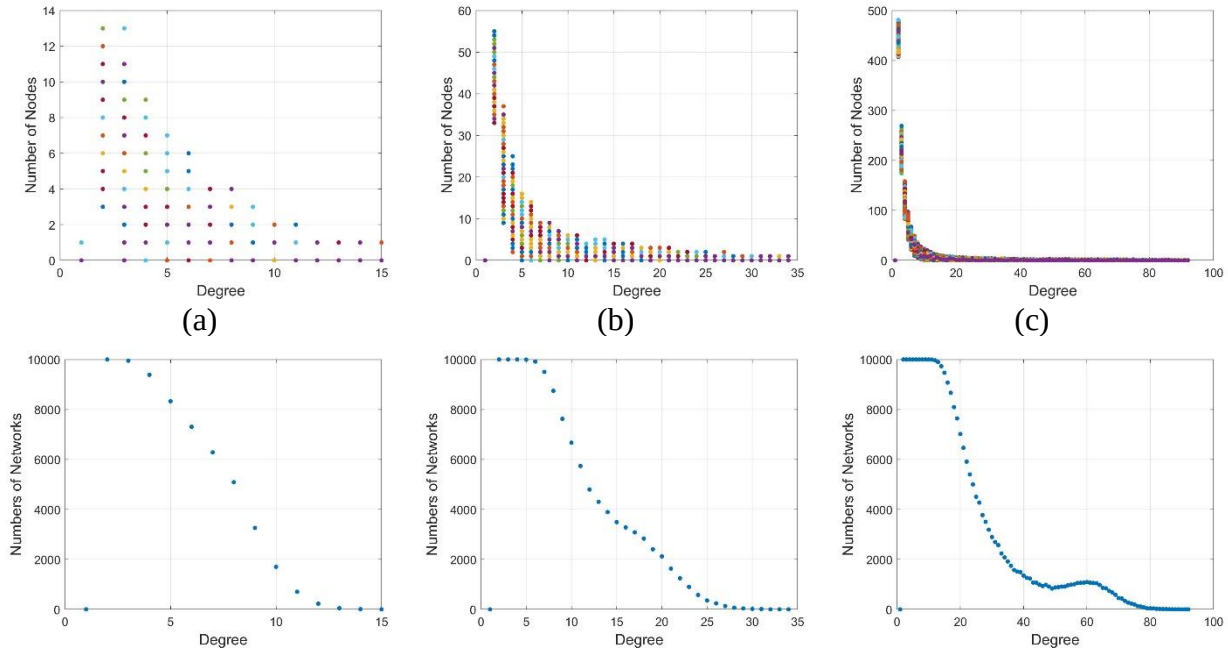

Fig. 4 Degree distributions of 10,000 sets of scale-free networks with (a) 20 constituents, (b) 100 constituents, and (c) 1000 constituents. Degree distributions of the total number of constituents across all the 10,000 networks with (d) 20 constituents, (e) 100 constituents, and (f) 1000 constituents.

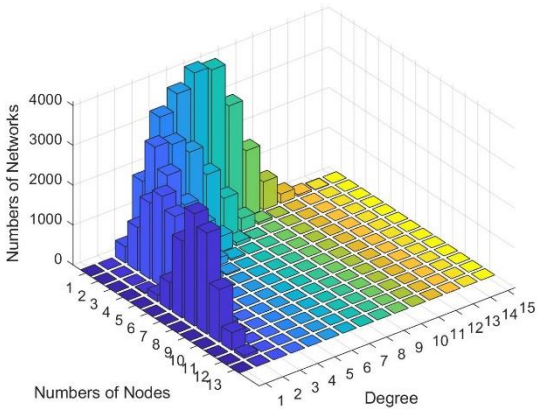

(a)

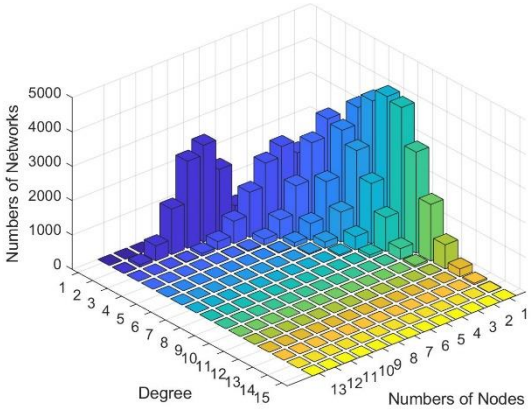

(b)

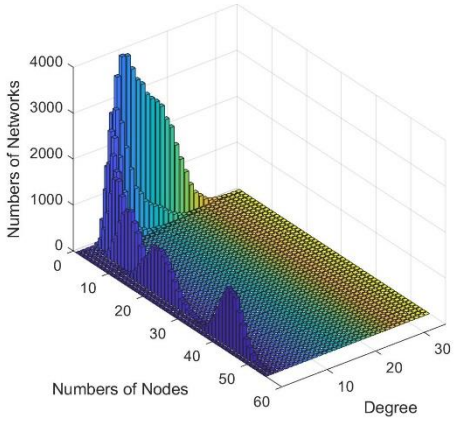

(c)

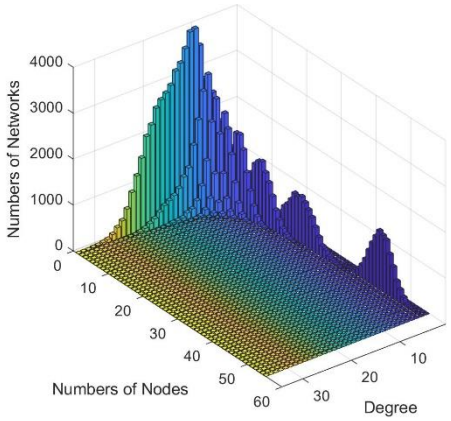

(d)

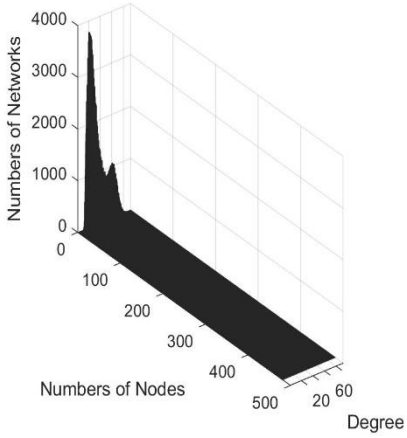

(e)

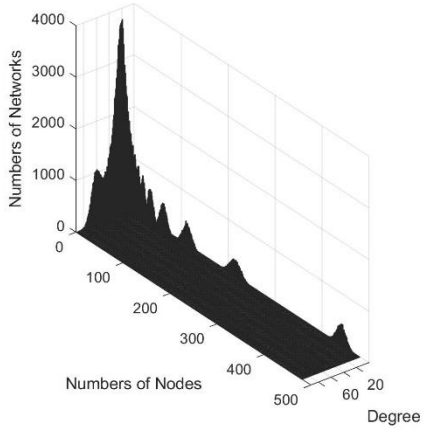

(f)

Fig. 5 Number of networks out of the 10,000 networks generated that has *m* number of constituents with *n* degree for scale-free networks of (a, b) 20 constituents, (c, d) 100 constituents, and (e, f) 1000 constituents.

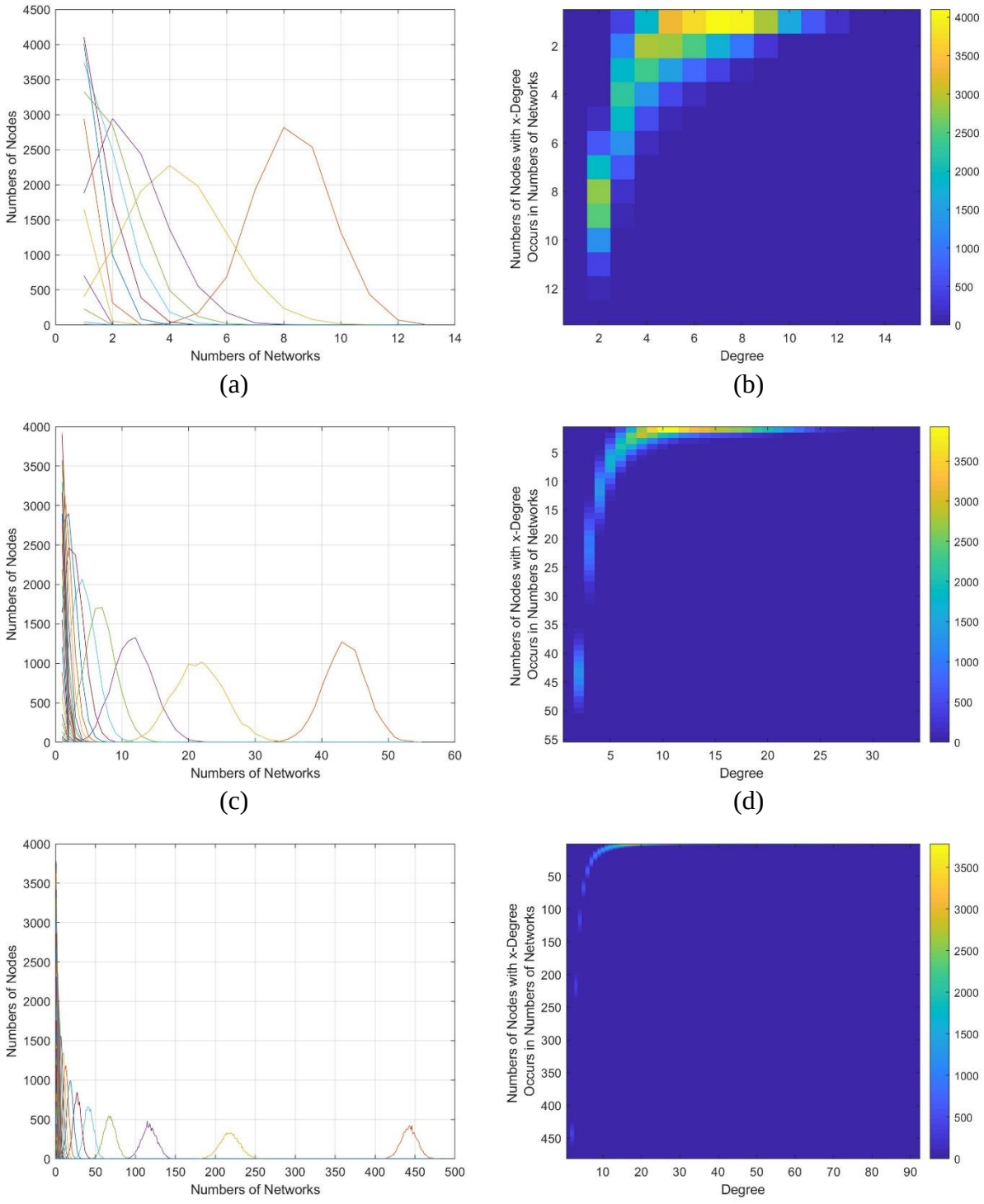

Fig. 6 Distribution of number of constituents with each degree throughout 10,000 sets of (a) 20 constituents, (c) 100 constituents, and (e) 1000 constituents networks. Number of networks out of the 10,000 networks that has *m* number of constituents with *n* degree for (b) 20 constituents, (d) 100 constituents, and (f) 1000 constituents networks.

Small-world and scale-free networks are static models providing topological descriptions for network structures to be defined globally. Static network models are not valid for characterizing network structures as they evolve if the physical and dynamical relationships for all ensemble constituents are not defined at the individual level. In the followings the two network models are reviewed and re-examined in the context of the general framework (to be discussed in detail in section 2. Per graph theory, the degrees of coupling k and J are set to be 1 N/m and 1 s^{-1}, respectively, which correspond to Structures 2 and 3 found in section 3.1. The weight of a connection is the difference of the energies of the two connected constituents. The corresponding k and J are both 0 when no connection is formed. Average path length can be calculated using the weight defined by the energy difference between each pair of connected constituents using Eq. (4) below,

$$l_{GE} = \frac{1}{n^2 - n} \sum_{i \neq j} (E_j - E_i) \tag{4}$$

where E_i is the energy of constituent i and E_j is the energy of constituent j. Using Eq. (4) a small-world network model is constructed. It is noted that the network model is developed in section 3.1 following the general framework presented in section 2. Figs. 1(b), 1(c), and 1(d) plot the weight of each connection and the difference of energy state between each pair of connected constituents of the small-world network as it develops in the 10s window. The corresponding average path length is seen to vary in time in Figs. 7(a) and 10(i). It is evident that the evolution of the average path length is nonlinear and unpredictable. Interpreting network dynamics using the time snapshots of the static network model is therefore flawed.

Because a constituent with a higher energy can establish more connections with other constituents and the probability distribution of ensemble energy can be established using the PDF defined in Eq. (13), scale-free networks can be constructed within the general framework by having

the distribution of constituent energy to follow the power-law probability density function given in Eq. (5)

$$P(E_i) \approx \frac{2m^2}{k^3} \tag{5}$$

Conversely, the probability distribution of ensemble energy of a scale-free network can be calculated to show a power-law distribution. This is exactly what Fig. 7(b) conveys, where the ensemble energy distribution of two 20-constituent scale-free networks of an identical connectivity are plotted. Both lines are of a power-law distribution - the key feature of scale-free networks. Furthermore, Fig. 7(b) indicates that, as have discussed earlier, the contemporary definition for scale-free networks to obey power law distribution is incomplete without also providing a mechanism for the proper distributions of degree of constituent and ensemble energy. Static small-world and scale-free networks can be considered special cases of the general framework through assuming the governing coupling laws to be time-invariant (stationary in time). However, such an assumption would inevitably lead to ill-interpreted collective behavior that is false and incomplete.

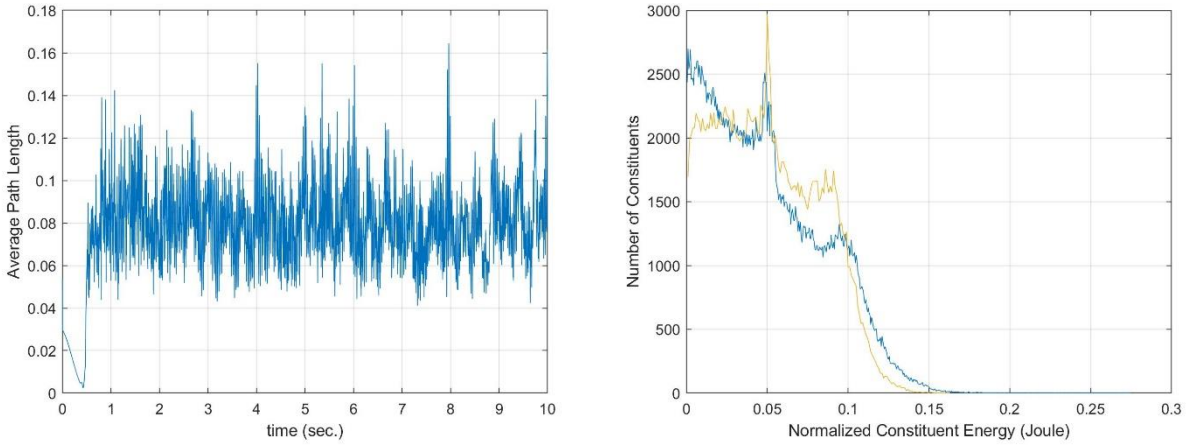

(a) (b)

Fig. 7 Small-world network and scale-free network examined under the general framework. (a) average path length of a small-world network, and b) degree distribution of a scale-free network.

1.2.1.2 Coupling

Network structure is defined by the interconnectivity of the network ensemble. Because network dynamics is the emerged ensemble dynamics of the set of connected constituents, it is essential that the law that governs the coupling of the ensemble constituents be established. Given that network structures are dynamical and oftentimes heterogeneous, the interconnectivity and interaction of ensemble constituents are functions of time and energy. Connection is established and coupling is maintained by the energies contributed by the connected constituents. How much the change of state of one constituent affects the other is defined by the degree of coupling. Higher is the energy of a constituent, more connections of higher degree of coupling it can form with other constituents. Greater the degree of coupling of a connection is, higher the energy is contributed from the connected constituents to the connection to maintain the coupling. Since the energy of each constituent is finite and time-varying, constituents engaged in rigid coupling are less likely to undergo significant change of state in time; that is, the connection between the two connected constituents stays intact while the ensemble evolves. Weaker coupling renders a connection elastic or easily severed.

The Kuramoto model [7-11] is a mathematical tool commonly employed to describe the emergent coherence behaviors of dynamic systems with large numbers of coupled oscillators through defining the interactions between the constituents. Developed to explain the synchronization of oscillating electrons in chemical reactions, the model has the following governing equation

$$\frac{d\theta_i}{dt} = \omega_i + \frac{K}{N}\sum_{j=1}^{N} \sin(\theta_j - \theta_i) , \qquad i = 1 \dots N \tag{6}$$

where θ_i is the phase angle of electron i, θ_j is the phase angle of electron j, ω_i is the frequency of electron i, K is the coupling strength between electrons i and j, and N is the number of electrons. At the initial stage of a chemical reaction, the phase angle of each electron is different. As the reaction proceeds, the phase angle of each electron tends to be normally distributed along the mean phase angle of all the electrons. When the phase angle of the electrons is normally distributed to the mean of the phase angle, the electrons are in a phase-locking state known as synchronization. Synchronization of nonlinear oscillators is ubiquitously observed in bio-neurological systems, physiological systems, and physical systems, to name a few.

The Kuramoto model is generalized to describe the synchronization of coupled constituents engaged in translational motion [28]. In studying complex networks, each of the constituent is a nonlinear oscillator whose state fluctuates about a local equilibrium [29]. To describe the synchronization of constituent dynamics in the 3-dimensional space, the constituents can be taken as undergoing curvilinear motion following Eq. (7)

$$\frac{dx_i}{dt} = v_i + \frac{K}{N}\sum_{j=1}^{N}(x_j - x_i) , \qquad i = 1 \ldots N \tag{7}$$

where x_i is the position of constituent i, x_j is the position of constituent j, v_i is the velocity of constituent i, K is the coupling strength between constituents i and j, and N is the number of ensemble constituents. Many studies were given to define the dynamics of complex networks by defining the coupling law between the ensemble constituents using the Kuramoto model. However, the Kuramoto model only describes the dynamics of coupled oscillators at the individual constituent level, not the global dynamics of the complex network at the ensemble level. In addition, coupling strength K is commonly assumed to be a constant for all connections [7]. As ensemble coupling strength is time-dependent, the interactions between each pair of connected

constituents are therefore not identical. Coupling strength should not be defined or assumed to be the same for all connections. In fact, coupling strength was defined as variables for all connections by Kuramoto [7] to account for the different relationship between each pair of molecules in a chemical reaction. In addition to lacking a proper physical definition for the coupling strength K, dividing K by N to signify equal distribution of the coupling strength among the ensemble constituents is also debatable.

For decades the Kuramoto model has been the preferred mathematical tool for studying the dynamics of static complex networks [25, 30]. However, with the coupling of each pair of connected constituents staying unchanged at all times, static network models are not feasible for resolving the true ensemble dynamics as the complex network evolves. Furthermore, a change to the state of any constituent in the network impacts the state of the entire ensemble at both the constituent and ensemble levels. In chemical reaction, the dynamics of an arbitrary molecule affects all other molecules in the reaction with different degree of impact. A complex network as defined by graph theory is a fully connected graph with various degrees of coupling for each connection. Static network models are therefore special cases of complex networks in which constituent couplings are rigid and time-invariant.

1.2.2 Control of Complex Network Dynamics

Dynamic and structural instabilities of a complex network can be mitigated through adjusting the connections between ensemble constituents. The majority of network control literature focuses on the controllability of network structure and minimal control input. It is stated in structural control theory for complex systems that controlling complex systems is difficult for the following reasons -- in addition to not knowing the inherent system parameters, most either lack accurate wiring diagrams or are without a proper description for the dynamic interactions

between components [31]. Nevertheless, many complex systems control problems are addressed without knowing all the details of the systems. Structural control theory adopts the concept of controllability from linear time invariant (LTI) system control theory to determine whether a complex system can be controlled. Because complex networks and complex systems are closely related, structural controllability of complex networks was investigated and subsequently reported in [32]. According to the literature, network structures can be categorized into (1) inaccessibility, (2) dilation, and (3) cactus. Cactus is the only minimal structure controllability among the three structure categories; that is, only networks constructed by cactus can be controlled. Once its accurate wiring diagram is known or available, the controllability of the network can be determined [32]. Applying graph theory based static network models [12, 13], a maximum matching algorithm is developed for determining the largest set of directed edges of the network without common heads and tails so that a minimum set of nodes can be selected to insert control input [14]. Structural control theory and maximum matching algorithm are tools for designing control inputs once a network structure is evaluated to be controllable.

Structural control theory defines a network using the state space equation below

$$\dot{X}(t) = Ax(t) + Bu(t) \tag{8}$$

where x(t) is the state variable of nodes at t seconds, state matrix A and input matrix B are structured matrices, and u(t) is the input signal [14]. In addition to lacking detailed information about the network, network controllability analysis is based on false assumptions. First, network controllability applies static network models to describe network dynamics. It is flawed to assume node connections as time-invariant while they are physically dynamical. Real-life network structures vary in time. It is more common than not for a physical network to experience disruption to node connections due to environmental disturbance and nodes joining and exiting the network.

Environmental disturbance introduces temporary breakage to the links, and nodes joining and exiting the network cause permanent construction or breakage of the links. Moreover, inserting control input also changes the properties of the links that define the relationship between nodes. Consequently, temporary or permanent link breakage as well as inserting control input can result in network structure alteration. Static network models cannot describe or characterize such time-dependent changes to network structure that would also impact network stability. Applying control input to a static network structure either leads to no control effect in adjusting the relationship between nodes or the collapsing of the network structure. Exploring network controllability using network structure analysis and control methodology is therefore not feasible for studying dynamic networks.

Furthermore, network controllability employs linear control methodology to complex networks whose behaviors are inherently nonlinear and time dependent. Applying LTI control theory for controllability effectively models the coupling between connected constituents as being linear, thus risking misinterpreting the true dynamics of the system. It is claimed that at each uncontrollable state there exists a sufficiently close neighboring state where the node relationship can be controlled [14, 32], implying that by altering the network state to the controllable neighboring state, an uncontrollable network state becomes controllable. For such an assumption to be valid, at least one equilibrium has to exist. However, complex networks are nonlinear dynamic systems having no definitive equilibria that are time-invariant. Moreover, network controllability does not provide any guidelines on how exactly an uncontrollable network state can be altered to the state that is controllable. Considering that network control adjusts the couplings between each constituent members to guide the emergence of desired collective behaviors, it is conceptually flawed to manipulate network property without the support of sound physical laws.

Structural analysis is applicable to only directed networks. Confusions are inevitable when applied to undirected networks in which other criteria are required [32]. Directed networks considered in [32] are literally undirected networks. In directed networks, information and control input can only be transmitted from the tail node to head node. Network controllability is based on directed network structure. However, for network controllability to work, it is required that control input be adjusted based on the feedback from the head node; that is, state information of the head node must also be available to the tail node. With state information allowed to run bi-directionally along edges, directed edges in directed networks are essentially undirected. Most complex networks in nature are undirected networks while directed networks are usually artificial networks following specific definitions that are limited in scope and applicability. In other words, network controllability is not generally applicable to complex networks. Furthermore, dynamic complex networks are systems whose structure is a complete graph with each constituent affecting the dynamics of all other constituents [33]. Network controllability is based on network topology. It is conceptually questionable when the tool is applied to investigate complex networks whose topology does not vary in time.

Dynamic complex networks are statistical mechanical systems with the constituent couplings being nonlinear and nonstationary. To properly control a complex network, a dynamic network model is required - one that describes the underlying dynamics and governs constituent couplings. In the following sections, a multivariable time-frequency network control methodology is applied to control a 20-constituent network model developed following the general framework for dynamic complex networks elaborated in [33].

1.2.3 Complex Network Dynamics

To show that the general framework is truly general, this research uses a 20-constituent translational point mass network and a 6-neuron brain network as examples for describing network dynamics as the function of coupling energy and entropy. Real-life networks are special cases of complex networks. Describing real-life network dynamics is a challenging task because coupled individual dynamics render network dynamics being nonlinear and non-stationary. Individual constituent dynamics can be defined using energy and that individual constituent energies follow a normal distribution. The outward behavior of a complex network is the result of the coupled individual constituent dynamics and ensemble dynamics. Moreover, real-world networks are each under different coupling laws and physical constraints that simultaneously govern individual constituent dynamics and drive network dynamics. A framework feasible for describing complex networks for their local constituent dynamics and global dynamics at the network level is essential.

Many attempts have been devoted to developing models of complex networks such as flocking birds, drone fleets, and brain network [16, 26, 27]. However, these network models fail to capture the dynamics of individual constituent and their coupled interactions that define network dynamics. Some assume a static relationship between the individual constituents using a constant coupling strength without the support of physical laws while others address coupling dynamics without considering the system as a network [16]. As a result, network models available these days are either static network models whose properties do not evolve in time or lacking proper coupling laws to govern the interaction between constituents. Network dynamics is incomplete without constituent dynamics and coupling dynamics been fully defined.

The general framework presented in [33] is formulated to define constituent dynamics and constituent coupling using energy. At the macroscopic level, the concept of the degree of coupling

is proposed to define the law of coupling that governs the time-dependent relationship between individual constituents. Individual constituent dynamics is defined by energy, allowing network dynamics to be quantified using information entropy.

The brain is a dynamical complex network of neurons (nerve cells) whose individual constituent dynamics is driven by the membrane potential of the neurons. The corresponding coupling is governed by the underlying synaptic neural dynamics. Since there are approximately 86 billion neurons in the human brain and the strength of the connection between each neuron changes in time, it is challenging to unveil the dynamics of the brain network. To properly define brain network dynamics, 1) neuron (membrane potential) dynamics and 2) coupling dynamics (synaptic dynamics) must be established. In the context of the general framework for dynamic complex networks, constituent dynamics (neuron dynamics) is defined using energy and the distribution of the energy follows a normal distribution. Since neuron energy is capped and neural response is governed by physical laws, neuron dynamics is bounded and quantifiable, allowing brain network dynamics to be described by information entropy.

A neuron is a system consist of several primary components including 1) a soma as the main cell body, 2) dendrites that receive neural signal, and 3) axons that transmit neural signal. A neuron may or may not have dendrites or axons depending on classification. In general, the axon of a presynaptic neuron can have many axon terminals that connect to different postsynaptic neurons. A postsynaptic neuron can have many dendrites that receive signals from multitudes of presynaptic neurons while a synapse connects axon terminal to dendrites. The membrane potential of postsynaptic neuron varies according to the sodium- (Na^+) and potassium- (K^+) ion flux passing across the chemical gated ion channels on the membrane of the dendrites. The moment the membrane potential rises and reaches a threshold value, the voltage gated ion channels are open

to allow in a huge influx of ions to result in a series of rapid rise and fall of the membrane potential called action potential. The firing of action potential of the presynaptic neuron initiates the synaptic dynamics that couples the dynamics between two connected neurons. When the action potential reaches the axon terminal of the presynaptic neuron, the voltage gated calcium (Ca^{2+}) channels of the axon terminal opens and lead to the releasing of neurotransmitters to the synaptic cleft (the extracellular space between presynaptic and postsynaptic neurons). The released neurotransmitters could be destroyed by enzymes, drift off the synaptic cleft, re-uptake by the presynaptic cell, and be received by the receptor of the dendrite of the postsynaptic cell. The received neurotransmitters trigger the opening of chemically gated ion channels which cause an influx of ions through the membrane of the dendrite that drives the membrane potential and further triggers the firing of action potential of the postsynaptic neuron when the threshold potential is reached, consequently triggering the synaptic dynamics of the next pair of connected neurons. The firing of action potential can be seen as the transmission of signals between neuron connections. In order to maintain the ability to fire action potential, the sodium-potassium pumps maintain the balance of the concentration of ions to establish an electrochemical gradient across the membrane which requires energy provided by adenosine triphosphate (ATP) in the cell. Consequently, the electrochemical gradient across the presynaptic and postsynaptic neuron membrane and the synaptic cleft environment as well as the ATP determines the frequency and intensity of the firing of action potential of each neuron.

One of the fundamental mechanisms in brain neuroplasticity, synaptic plasticity describes the connection strength of neurons as it changes in time. Depending on the firing pattern of action potential between the presynaptic and postsynaptic neurons, excitatory and inhibitory action can be triggered. An excitatory action increases the connection strength, and an inhibitory action

decreases the connection strength. The Ca^{2+} concentration of the postsynaptic neuron increases in response to the activation of excitatory action and decreases in response to the triggering of inhibitory action. With higher Ca^{2+} concentration, the number of the receptor of the neuron increases to receive more neurotransmitters, and vice versa. The availability of neurotransmitter from the presynaptic neuron also affects the connection strength between the neurons.

To describe the behavior of a brain network, the mechanism of individual neuron dynamics and the synaptic dynamics must be properly defined by physical laws. Individual neuron dynamics is driven by the variation of membrane potential that includes post membrane potential and action potential behavior of the membrane. Variation of membrane potential is constrained by the energy required to cause the ion flux and the energy provided by ATP needed to maintain the balance of membrane potential. Therefore, neuron dynamics is defined by energy. Moreover, the synaptic dynamics defines how the membrane potential of the postsynaptic neuron varies by the action potential fired by the presynaptic neuron. Synaptic dynamics are affected by the firing of the action potential of presynaptic neuron, flux of neurotransmitters, and the number of available neurotransmitter receptors on the postsynaptic neuron. Once individual neuron dynamics and synaptic dynamics are properly defined using energy and minding that energy must follow a normal distribution, brain network dynamics can be described using information entropy.

Most brain network models are extensions of the Hodgkin-Huxley (HH) model. However, instead of membrane potential dynamics and synaptic dynamics, the HH model only describes the action potential of an individual neuron. In other words, the model can only partially describe individual neuron dynamics. It cannot describe the coupling dynamics between neurons. Such an approach assumes all neurons fire action potential continuously with a static coupling strength between neurons. The HH model maintains a static brain network with a constant time-invariant

coupling relationship between each pair of neurons. As a result, each neuron in the brain network fires action potential repeatedly with the same action potential profiles identical in time duration and amplitude. This is in disagreement with observations made in physiology. Such neural behaviors would introduce fluctuations to ion concentrations, inadvertently alter the electrochemical gradient of ion across the membrane, and ultimately lead to erroneous action potential profiles. Experimental physiology affirms that, synaptic dynamics, neuron plasticity, and action potential do not fire continuously. While firing of the action potential of the presynaptic neuron results in strong neuron connections, however, excessive firing of the post synaptic neuron blocks the signal transmitted from the presynaptic neuron. HH model-based brain network models therefore are inadequate in resolving the true brain network dynamics where action potentials are fired intermittently and neuron coupling fluctuates according to the firing frequency.

Membrane potentials are in voltage. They are the marked features in neuron dynamics. However, the HH model describes action potential in terms of electrical current, thus obscuring the signature characteristics of neuron dynamics. Describing neuron dynamics using the current induced by ion flux is not straightforward. Neuron dynamics is the manifestation of the fluctuation of membrane potential in terms of voltage.

Literature indicates that focus is either given to establishing individual neuron dynamics or to understanding synaptic dynamics. While investigating both would help have a better understanding of the brain, it would still be inadequate if the brain is not treated as a network of neurons. Electrophysiology measurement data or mathematical curve fitting are predominant techniques applied to brain research. However, they lack the resolution required to resolve the true characteristics of individual neurons. Individual neuron dynamics of is driven by the fluctuation of membrane potential induced by the ion flux across the membrane. Any

measurement made with electrode probes requires the current to flow through the measuring device. In the case of electrophysiology measurement of a neuron, the current is in the form of ion flux. In other words, the ion flux that causes the fluctuation of membrane potential is disturbed every time the neuron is being measured. A tiny difference in input to a nonlinear system would lead the system to evolve towards significantly different outcome. Given the scale of individual neuron dynamics, the flowing of ions through the measuring device is significant enough to cause the membrane potential to behave differently. Not to mention that these electrophysiology measurements are usually done in-vitro, whereby the neurons usually behave differently than they would in undisturbed environment. Though significantly lower than in-vitro, neuron responses are also perturbed when done in-vivo. It is challenging to establish individual neuron dynamics model based solely on electrophysiology measurement data. While electrophysiology measurement data do not portray the true dynamics of an individual neuron, mathematical curve fitting introduces error and obscures the nonlinearity inherent of the neuron. Therefore, it is necessary to establish a governing law to describe the mechanism that defines individual neuron dynamics (such as the variation of membrane potential) so that the brain network model developed in the context of the general framework can properly describe brain network dynamics.

To demonstrate validity, membrane potential profiles generated by the brain network model must be in close agreement with physiological observations made with individual neuron. Although electrophysiology measurement introduces disturbances to neuron dynamics, electrode probes do acquire neuron behaviors on the right time scale. In other words, the temporal resolution of electrophysiology measurements is valid. More specifically, physiology measuring devices have to interact with the captured ion fluxes to convert the interaction into measured output. Measurement reading would vary when there is a strong enough behavioral change of the neuron.

That is, the time scale of neuron dynamics is captured in physiological observations. Therefore, while the magnitude of reported value is questionable, the time scale of the physiological observation data of membrane potential can be considered as accurate and used to establish the feasibility of the membrane potential governing law presented in section 2.

It is important to be aware that no two action potential profiles are identical because the conditions an ion channel are under prior to firing are never the same [34]. Depending on the type of neurons, some neural responses are faster while others are slower. Since the primary objective of the research is to develop a general framework for describing complex networks dynamics, physiological observations made in [34] are used to show in section 4 the feasibility of the framework in creating a brain network model that accurately portrays neuron dynamics. Valid assumptions are made in section 2 in which a brain network model is developed to compensate for the fact that comprehensive neuron physiological measurement data are not available.

Neuron responses resolved by the brain network model presented in the next section are in excellent agreements with physiological observations. The model which is developed in the context of the general framework for dynamical complex networks incorporates a neural coupling law according to the mechanism that underlies synaptic dynamics.

1.3 Research Objective and Task Plan

This study aims to develop a general framework applicable to describing complex networks dynamics that is nonlinear and nonstationary. Insight gained in the study helps to establish a universal network theory. The framework describes complex network dynamics regardless of the domain to which the network belongs. A nonlinear network control strategy is developed to steer complex networks toward displaying desired network dynamics while simultaneously maintaining the integrity and stability of the network structure. The general framework is applied to describe

the dynamics of the following 2 network systems to demonstrate generality: 1) a network of a finite number of discrete masses where individual constituent dynamics is described by the relative position and translational motions of the network constituents [5], and 2) a brain network where neurons do not translate but are coupled through synaptic dynamics manifested by variations of membrane potential and firing of action potential passing along connected neurons [18]. Once network dynamics is properly established, control of network instability is addressed.

The contribution of this study is of many folds. Insight gained through this study will allow researchers to approach complex networks from a new perspective. The general framework provides a universal guideline for describing dynamical networks regardless of the domains in which they are defined, thus allowing network dynamics to be properly described and network property be thoroughly investigated. The developed control scheme provides a novel multivariate design concept for mitigating network instability that is aperiodic, nonstationary, and inherently broad in response bandwidth. With the availability of the brain network model, significance progress can be made in gaining a better understanding for brain dynamics.

This study is cross-disciplinary. Studying complex networks requires knowledges from many different domains and heavy use of mathematical concepts and computational tools. Brain network modeling requires knowledge in biology, neuroscience, and chemistry. Network behaviors in general are more prominent when more constituents are considered. However, as the number of network constituents increases, the demand for computing power for performing simulation and numerical experiment becomes daunting, thus indicative of the challenge in choosing the network size for in-depth exploration. Also, cares must be taken when making assumptions so that a balance is maintained between simplifying the model and not skewing the

true network dynamics. If not properly managed these challenges could deny the research objective from being achieved.

The dissertation is the result of executing the research task plan that was developed to address the stated objective.

1. Formulate the general framework of complex networks dynamics
2. Develop a complex networks control strategy
3. Demonstrate feasibility of the general framework

2. METHODOLOGY*

2.1 The General Framework for Dynamical Complex Networks

To properly define the dynamics of complex networks, a general framework is presented in the present section. Complex networks are time-dependent dynamical networks with coupled constituent dynamics at the constituent level. Concepts fundamental to statistical mechanics [1, 2] are applied to describe the macroscopic (ensemble level) and microscopic (individual constituent level) dynamics and the coupling of ensemble constituents in complex networks. At the constituent level, each constituent moves and couples with all other constituents in pursuant to physical laws. The sum of constituent behaviors emerges the global dynamics of the network system at the ensemble level. Given the computing demand, it is infeasible to resolve ensemble dynamics by time-integrating a large number of constituents for their individual dynamics. Alternatively, ensemble properties are determined by calculating the corresponding information entropy as constituent states evolve. Information entropy is a measure in the probability sense for the randomness of physical variables such as velocity, energy, and temperature in a statistical mechanical system. Each measurement of entropy at the ensemble level indicates an ensemble state. At the constituent level, there are infinite numbers of permissible solutions of constituent states that correspond to the ensemble state. Ensemble dynamics at the system level can be defined by specifying an information entropy and let the constituents evolve to reach their respective states of motion, i.e., constituent dynamics. Connections in complex networks are physically determined

* Part of this chapter is reprinted with permission from "A General Framework for Dynamic Complex Networks" by Yang, C.-L. and Suh, C. S., 2021, Journal of Vibration Testing and System Dynamics, 5, 87-111, Copyright 2021
by L & H Scientific Publishing, LLC

by the potential energy between the connected constituents obeying the Kuramoto model as the law of coupling. Since the state of motion of individual constituent is a function of the energy of the constituent, the energy is established by calculating the corresponding information entropy as information is transmitted in the network system. Networks dynamics can be properly described using the following framework which is generally applicable to all dynamic complex networks

$$E_i(t) = \sum \frac{1}{2} k_{ij}(t) D_{ij}(t)^2 + \frac{1}{2} m_i V_i(t)^2 \tag{9}$$

$$V_i(t+1) = V_i(t) + \sum J_{ij}(t)\, D_{ij}(t) \tag{10}$$

$$D_{ij}(t) = x_j(t) - x_i(t) \tag{11}$$

$$S(E) = -\sum_i p(E_i)\, log\, p(E_i) \tag{12}$$

$$E = \{E_i | i = 1 \sim n, \text{ and } n = \text{number of constituents}\}$$

$$P(E_i) = \frac{1}{\sigma\sqrt{2\pi}} e^{-\frac{1}{2}\left(\frac{E_i - \mu}{\sigma}\right)^2} \tag{13}$$

where $x_i(t)$ is the position of constituent i at t seconds, $x_j(t)$ is the position of constituent j at t seconds, $D_{ij}(t)$ is the measure of connection between constituents i and j at t seconds, $V_i(t)$ is the velocity of constituent i at t seconds, $V_i(t+1)$ is the velocity of constituent i at $t+1$ seconds, $E_i(t)$ is the energy of constituent i at t seconds, $k_{ij}(t)$ is the degree of coupling of connection ij at t seconds, $J_{ij}(t)$ is the degree of coupling of connection ij at t seconds, m_i is the mass of constituent i, $P(E_i)$ is the probability density function (PDF) of the permissible energy level of a constituent, and $S(E_i)$ is the Shannon [4] information entropy of the constituent energy.

The spatial coupling of 2 connected constituents is characterized by an imaginary spring, with the adjustment of the spring in time following the Kuramoto law and the energy of each constituent governed by Eq. (9). Individual constituent velocity is determined in accordance with

the distance between the connected constituents, thus imparting acceleration to each constituent taking into account of all the constituent spatial measures. The parameters k in Eq. (9) and J in Eq. (10) are the degrees of coupling of distance and velocity, respectively, with k being the stiffness of the imaginary spring. Greater is the degree of coupling k, more rigid are the two connected constituents in maintaining their spatial separation. J is the frequency of the change of relative position. Greater is the degree of coupling J, stronger is the tendency for the two connected constituents to approach (attract) to each other. Unlike the coupling strength which is assumed to be a constant for all connections, the degrees of coupling k and J are time-dependent variables [35] of the constituent connection energy.

With the dynamic coupling at the constituent level properly defined using definitive physical parameters, ensemble dynamics can now be determined through calculating the information entropy of the ensemble energy per Eq. (9). As all random variables of physical systems do, ensemble energy is normally distributed [18]. Eq. (13) is the probability density function (PDF) of normal distribution that defines the permissible outcome of the ensemble energy. To define collective behaviors, an entropy is specified for the complex network to search for the solution that satisfy simultaneously both the ensemble and constituent dynamics. Once the ensemble state at the ensemble level is defined by the entropy, the constituents evolve to find the constituent states that correspond to the ensemble state. Since the numbers of the admissible constituent states that satisfy the ensemble state are large, the constituents will 'scan and search through' admissible solutions. Thus, a network could be demonstrating stable dynamic behaviors globally while all the individual constituents engaging in random, asynchronous, and disordered motions.

Collective behaviors are the emergences of constituent dynamics as the ensemble evolves in time. Because the corresponding distribution of ensemble energy is localized, low entropy indicates a more synchronized collective behavior. Following the same reasoning, high entropy signifies a less synchronized collective behavior with widespread ensemble energy.

2.2 Network Dynamics Control Scheme

Network stability and structure integrity can be achieved through adjusting k and J, the 2 DOCs defined within the general framework for complex networks. It was seen in the previous section that 1) constituent couplings are nonlinear and nonstationary and 2) constituent exiting and joining the ensemble impacts network dynamics and network structure, resulting in instability and delayed synchronization. A multivariable control methodology is developed in the section that allows k's and J's to be regulated in the joint time-frequency domain to capacitate the integrity of network structure while maintaining entropy stability.

Nonlinear responses are characterized by their rapidly switching between many orbits of all periods of strange attractors, rendering them being bounded and stable in the time domain while unstably broadband in the frequency domain [36, 37]. Nonlinear responses are also nonstationary. Online system identification is required to capture time-varying system parameters. Initial condition and small perturbation can lead to unstable system behaviors. The wavelet-based time-frequency control architecture outlined in Fig. 8 [36, 38] has demonstrated feasibility in mitigating the deterioration of time and frequency responses of a wide range of nonlinear systems [36-45]. Concept of active noise control is adopted where two adaptive finite impulse response (FIR) filters are placed in parallel to realize time-frequency control and on-line modeling as follows,

$$W_1(n+1) = W_1(n) - \mu_1 TU(n) f(n) \tag{14}$$

$$W_2(n+1) = W_2(n) + \mu_2 TX'(n) e(n) \tag{15}$$

where W1 models the system on-line, W2 is the feedforward controller, T is the wavelet transformation matrix, μ1 and μ2 are optimization step sizes, and $X'(n) = W_1^T TX(n)$. Each adaptive filter uses the filtered-x least-mean-square (FXLMS) algorithm to minimize the mean-square-error. A wavelet transformation matrix is placed in front of the adaptive filters to localize the time event by transforming the discrete signal, x(n), from the time domain to wavelet domain which is essentially a simultaneous time-frequency domain. The adaptive filters update the weights of the wavelet coefficients according to the error, e(n). A multivariable control scheme is also developed which runs two time-frequency nonlinear controllers in parallel to mitigate the responses induced by cutting force along different directions [38, 40].

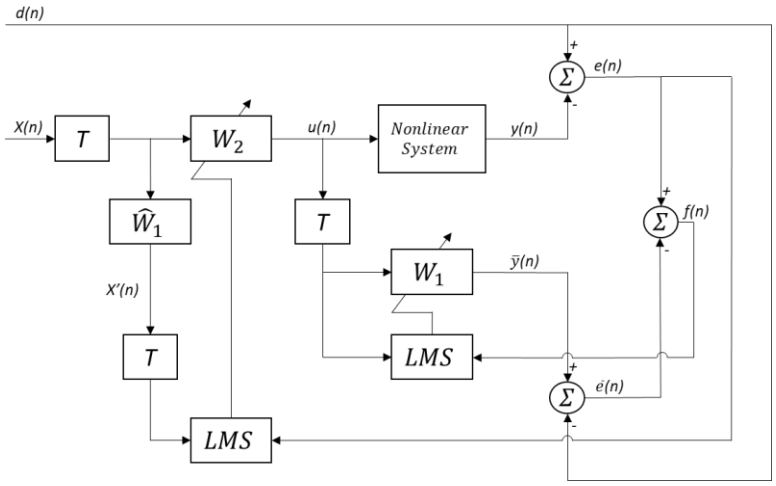

Fig. 8 Configuration of wavelet-based time-frequency control

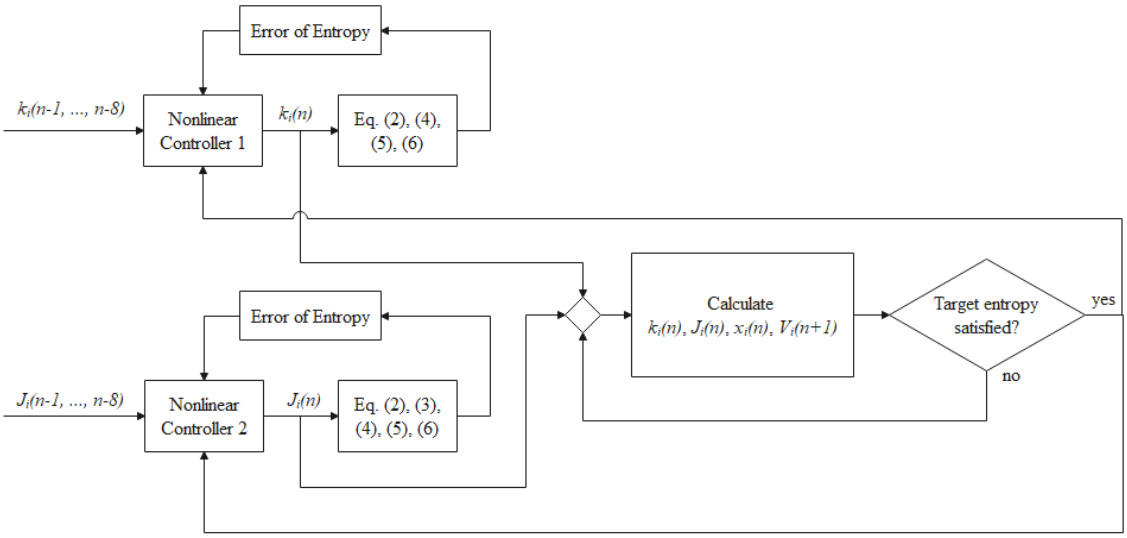

Fig. 9 Multivariable complex network control scheme

Network dynamics is determined by entropy which is a function of both DOCs k and J. Complex networks can be put under the jurisdiction of a multivariable time-frequency controller to maintain network structure stability through adjusting constituent DOCs. Fig. 9 illustrates the control concept having two time-frequency controllers operated in parallel, each regulating a DOC in response to error which is the deviation of network entropy from the target entropy.

2.3 Dynamics of Real-Life Networks

In this section, a brain network model is developed in the context of the general framework for dynamical complex networks. Real-life network dynamics modeling is a challenging task. At the individual constituent level, individual constituent dynamics is defined by energy. Real-life networks exist in the physical world. They are under physical laws and subject to the constraints associated with the laws. Their respective coupling energies must follow a normal distribution by which information entropy is determined. Thus, the essence of the general framework is defining constituent dynamics and coupling using energy enables ensemble dynamics to be described using entropy. The following steps embody the general framework:

1) Establish the mechanisms that underlies constituent dynamics and coupled dynamics

2) Identify the state that drives constituent dynamics

3) Define constituent dynamics using energy

4) Define coupling laws using potential energy and kinetic energy

5) Define corresponding degree-of-coupling k and degree-of-coupling J

2.3.1 Brain Network Model

Brain networks are complex networks composed of coupled neural cells. The focus of this study will be upon neurons in particular. Individual neuron dynamics is driven by membrane potential changes caused by ion flux across the membrane. Ion flux is a function of the cumulative cross-sectional area of open ion channels and electrochemical gradient. The cumulative cross-sectional area of a postsynaptic neuron is determined by the action potential firing of the presynaptic neuron. Membrane potential fluctuations can be considered as the superposition of different sources of changes: (1) postsynaptic potential, (2) action potential, and (3) change of membrane potential introduced by ion pumps. Postsynaptic potential is the stage of the membrane

potential before reaching threshold at which action potential is fired. Postsynaptic potential is a function of ligand gated ion channels on the postsynaptic neuron and synaptic dynamics. Thus, postsynaptic potential changes indicate the behavior of the postsynaptic neuron as a receiver receiving signals (neurotransmitters) from the presynaptic neurons. Action potential is the stage of membrane potential where the threshold potential is reached and triggers the voltage gated ion channels to allow a sudden large amount of Na^+ influx to cause depolarization and K^+ outflux with a delay in time from the triggering moment to cause repolarization. At the moment an action potential is fired, postsynaptic neurons are triggered by the presynaptic neuron signal to transmit information by releasing neurotransmitters. Hence, the amplified signal is transmitted further to the next line of postsynaptic neurons down the signal chain by releasing neurotransmitters. In preventing the state of neurons from stalling for a prolonged period of time induced by unbalanced ion concentration (due to significant ion flux through voltage gated ion channels), ion pumps work to reestablish and maintain the ion concentration to guarantee a proper electrochemical gradient of ions. Therefore, to define brain network dynamics in terms of voltage changes, mechanisms that cause 1) postsynaptic potential, 2) action potential, and 3) ion pumps dynamics must be determined following the laws of physics.

A brain network model is developed in the context of the general framework in Eqs. (16)-(26). The model incorporates a law that governs the driving mechanisms of neuron dynamics. The law resolves membrane potential dynamics by identifying the mechanisms behind postsynaptic potential (Eq. 17), action potential (Eq. 18), and ion pump dynamics (Eq. 26). The relationship between the neurotransmitters released by the presynaptic neurons and the cumulative cross-sectional area of the ligand gated ion channels on the postsynaptic neuron is described by Eqs. (28)-(38). Action potential firing mechanism of the postsynaptic neuron is described by Eq.

(24). The relationship between pumping cycles of ion pumps and ion concentration of the postsynaptic neuron is described by Eqs. (26) and Eqs. (39)-(45).

In the sections that follow, computed neuron membrane potentials are shown to match the time scale of the action potential profile in Fig. 22 of [46]. Prominent features are noted in the referenced action potential profile indicating a depolarization of 1 millisecond in duration, a repolarization of 1 millisecond in duration, and a 1 millisecond delay from the moment the action potential is triggered.

2.3.2.1 Membrane Potential – Individual Neuron Dynamics

Individual neuron dynamics is driven by membrane potential changes which is a function of ion flux. Assume a postsynaptic neuron N having d number of dendrites receiving triggering signals of neurotransmitter species j from presynaptic neurons M. Neuron N allows i species of ion flux flow across the membrane to induce membrane potential variations. Membrane potential at the next time instant as defined in Eq. (16) is the sum of the membrane potential at the present moment with the change in voltage introduced by the ion flux across the membrane. Change of membrane potential is contributed by the voltage change of the postsynaptic potential defined in Eq. (17), the action potential defined in Eq. (18), and the Na^+-K^+ ion pumps defined in Eq. (26) and Ca^{2+} ion pumps defined in Eq. (44). The mechanism behind membrane potential variations is described by the electrochemical gradient in Eqs. (19) and (20), the cumulative area of the ligand gated channels in Eq. (22), and ion flux in Eq. (21).

$$V_{mN}(t+1) = V_{mN}(t) + V_{mN_{lgd}}(t) + V_{mN_v}(t) + V_{pN}(t) \tag{16}$$

$$V_{mN_{lgd}}(t) = \sum_d \sum_i \left(\frac{\nabla \overline{\mu_{NMi}}(t) \alpha_{d_{Nij}}(t) J_{Ni}(t) \Delta t}{e V_{Ni}(t)} \right) \tag{17}$$

$$V_{mN_v}(t) = \sum_i \left(\frac{\nabla\overline{\mu_{NMi}}(t)\, \alpha_{Nvi}(t)\, J_{Ni}(t)\, \Delta t}{eV_{Ni}(t)} \right) \tag{18}$$

$$\nabla\overline{\mu_{NMi}}(t) = \nabla G_{NMi}(t) + Z_i F V_{mN}(t) \tag{19}$$

$$\nabla G_{NMi}(t) = RT(t) \times \ln\left(\frac{c_{Nout}(t)}{c_{Nin}(t)} \right)_i \tag{20}$$

$$J_{Ni}(t) = -\frac{D_i (c_{Nout}(t) - c_{Nin}(t))_i}{RT(t)} \frac{\partial\overline{\mu_{NMi}}}{\partial x} \tag{21}$$

$$\alpha_{d_{Nij}}(t) = n_{d_{N_{ij\_trig}}}(t) A_{li} \tag{22}$$

$$\alpha_{Nij}(t) = \sum_d \alpha_{d_{Nij}}(t) \tag{23}$$

$$\alpha_{Nvi}(t) = n_{Nvi}(t) A_{vi}$$

$$, where \begin{cases} n_{NvNa^+}(t) = 1.06 \times 10^7 \; if \; V_{mN}(t) \geq threshold\ potential \\ n_{NvK^+}(t) = 2.76 \times 10^7 \; if \; V_{mN}(t) \geq threshold\ potential \\ n_{NvCa^{2+}}(t) = 2.81 \times 10^5 \; if \; V_{mN}(t) \geq threshold\ potential \\ n_{Nvi}(t) = 0 \; if \; V_{mN}(t) < threshold\ potential \end{cases} \tag{24}$$

$$eV_{Ni}(t) = \left(\frac{\nabla\overline{\mu_{NMi}}(t)}{mol} \right) \times n_{AP_{Na^+}} \times \frac{1}{Amp_{AP}} \tag{25}$$

$$where\ n_{AP\_Na^+} \cong 2 \times 10^6 \; and \; Amp_{AP} \cong 0.1[volt]$$

$$V_{pN}(t) = V_{pNNa^+}(t) + V_{pNK^+}(t) + V_{pNCa^{2+}}(t) \tag{26}$$

where $V_{mN}(t+1)$ and $V_{mN}(t)$ are the membrane potentials of neuron N at time t+1 and t, respectively. $V_{mN_{lgd}}(t)$, $V_{mN_v}(t)$, and $V_{pN}(t)$ are voltage variations caused by ligand gated ion channels, voltage gated ion channels and ion pump channels of neuron N. $\nabla\overline{\mu_{NMi}}$, in the unit of [Joule/mol], is the electrochemical gradient of ion species i between the synaptic cleft of neurons M and N and the intercellular space of dendrite d of neuron N. $\alpha_{d_{Nij}}$, in the unit of [m^2], is the availability of ligand gated ion channels of ion species i of neuron N specific to neurotransmitter species j. α_{Nvi}, in the unit of [m^2], is the availability of voltage gated ion channels of ion species

i of neuron N. J_{Ni} is the ion flux of ion species i through the membrane of neuron N in the unit of [mol/m^2·s]. $eV_{Ni}(t)$ is the electronvolt of the ion species i of neuron N in the unit of [Coulomb]. mol is the mole number 6.022×10^{23}, Δt is the duration of each calculation iteration in the unit of [s]. Z_i is the valency of the ion species i, F is the capacitance of the membrane of the whole neuron N in the unit of [Faraday], ∇G_{NMi} is the chemical potential (or gradient) of ion species i between the synaptic cleft of neurons M and N and the intercellular space of neuron N in the unit of [Joule/mole], R is the ideal gas constant in [Joule/K·mole], T is temperature in Kelvin [K], c_{Nout} and c_{Nin} are the concentrations of ion species i outside and inside of the membrane of neuron N in the unit of [mol/m^3], D_i is the diffusion constant of ion species i in the unit of [m^2/s], $\alpha_{d_{Nij}}$ is the availability of ligand gated ion channels of ion species i of neuron N specific to the neurotransmitter species j on dendrites d in the unit of [m^2], $n_{d_{N_{ij\_trig}}}$ is the number of triggered ligand gated ion channels type l of ion species i of neuron N specific to neurotransmitter species j on dendrites d, A_{li} is the area of ligand gated ion channel type l of ion species i in the unit of [m^2], n_{Nvi} is the number of triggered voltage gated ion channels of ion species i of neuron N, A_{vi} is the area of voltage gated ion channel of ion species i in the unit of [m^2], V_{pNNa^+} is the voltage fluctuation caused by the Na^+ ion pump channels of neuron N in the unit of [V], V_{pNK^+} is the voltage fluctuation caused by the K^+ ion pump channels of neuron N in the unit of [V], $V_{pNCa^{2+}}$ is the voltage fluctuation caused by the Ca^{2+} ion pump channels of neuron N in the unit of [V]. Eq. (16) is the membrane potential dynamics of neuron N, Eq. (17) is the change of voltage through ligand gated ion channels of ion species i, Eq. (18) is the change of voltage through voltage gated ion channels of ion species i, Eq. (19) is the electrochemical gradient of ion species i between the synaptic cleft of neurons M and N and the intercellular space of neuron N which is the sum of the chemical potential shown in Eq. (20) and the electrical potential of ion species i, Eq. (21) is the

flux of ion species i across the ion channel, Eq. (22) is the availability of ion channel specific to neurotransmitter specie j and ion specie I, Eq. (25) is the charge of ion specie i which depends on the valency of ion species i. Note that eV_{Ni} is a modification of electronvolt eV specific to the neurons. A more detailed discussion about eV_{Ni}, V_{pN}, V_{pNNa^+}, V_{pNK^+}, and $V_{pNCa^{2+}}$ is provided in later passages. Furthermore, these parameters are essential and feasibly calculable to determine the membrane potential (and its change over time) for a neuron.

Assuming there are N individual neurons and each neuron has d number of dendrites, the dynamics of an individual neuron N is defined by the dynamics of its membrane potential as shown in Eq. (16) which caused by the ion flux through the triggered ion channels and ion pumps on all the dendrites of neuron N. For each neuron N, 1) different species of ion could all contribute to the change of membrane potential, 2) each type of the ion can only flow through one or a few types of ion channels and ion pumps, and 3) each type of ligand gated ion channel is triggered by a specific specie of neurotransmitter while voltage gated ion channels is triggered by reaching the threshold potential. This study assumes there are i species of ion, j species of neurotransmitter, l types of ligand gated ion channels, and i types of voltage gated ion channels. A more detailed explanation of the relationship between ion species, neurotransmitters, and ion channels will be provided in the later sections. Influence of leak channels to the membrane potential dynamics is not considered in this study. The electrochemical gradient $\nabla\overline{\mu_{NMi}}$ is the potential energy of ion species i per mole which is the sum of chemical potential and electrical potential of ion species i. According to Eqs. (19) and (20), the dynamics of electrochemical gradient is dominated by the change of ion concentration across the membrane. Compared to other parameters that are also contributing to the change of membrane potential dynamics, human body temperature fluctuates much more subtly both in amplitude and frequency in general. Therefore, the dynamics of

membrane potential is primarily driven by the fluctuation of ion concentration gradient across the membrane due to ion flux. Hence, ion flux must be described properly so that membrane potential dynamics can be properly defined.

Ion flux, one of the dominant mechanical phenomena responsible for neuronal voltage fluctuations, is driven by diffusion in biological systems where the flux is defined through Fick's first law as shown in Eq. (21) in the unit of [mol/m^{2}s]. $\alpha_{d_{Nij}}$ is the available cross-sectional area of activated ion channels of ion species i on dendrite d of the postsynaptic neuron N. Therefore, the amount of ion passing through the membrane per second through the ion channels can be calculated by multiplying the available cross of ion channel and ion flux. As the electronvolt of neuron eV_{Ni} defines the energy required to translate 1 charge of ion species i across the membrane of neuron N as shown in Eq. (25) (a more detailed discussion will be provided in the later passages), the equivalent charge in coulombs due to ion influx can also be calculated. Since the definition of voltage is energy per charge, the fluctuation of membrane potential is calculated by multiply the potential energy (electrochemical gradient) $\nabla\overline{\mu_{NMi}}$ and the number of ions that flow across the membrane in addition to the voltage change caused by ion pumps as shown in Eq. (16). Consequently, the dynamics of membrane potential of neuron N is described.

Ensuring the preliminary brain network model is reliable incorporates generating 1) the fundamental individual neuron dynamics, 2) inter-neuron coupled dynamics, so that 3) a set of simulated brain network dynamics is close enough to the fundamental characteristic of real-life brain network dynamics exhibiting the feasibility of the general framework. The following passages investigate the consistency of physical units in the brain network model, the membrane potential dynamics that is correlated to the ligand gated channels (postsynaptic potential), the voltage gated channels (action potential), and ion pump driven membrane potential dynamics to

establish the credential of the proposed simplified brain network model. Assumptions made by this study are also shown below.

2.3.2.2 Consistency of Physical Units

Since Eq. (16) is the governing law of membrane potential dynamics proposed by this study which defines the individual neuron dynamics, it is crucial to ensure the physical units of each parameter are balanced on both side of the equation.

$$V_{mN}(t+1) = V_{mN}(t) + \sum_d \sum_i \left(\frac{\nabla \overline{\mu_{NMi}}(t) \left(\alpha_{Nij}(t) + \alpha_{Nvi}(t) \right) J_{Ni}(t)\, \Delta t_{li}}{eV_{Ni}} \right) + V_{pN}(t) \tag{27}$$

$$[volt] = \left[\frac{joule}{joule}\right] = [volt] + \frac{\left[\frac{joule}{mol}\right] \times ([m^2] + [m^2]) \times \left[\frac{mol}{m^2 \cdot s}\right] \times [s]}{[joule]} + [volt]$$

Eq. (27) shows the units of all parameters in Eq. (16) are balanced. Therefore, the governing dynamical law of membrane potential defined through Eq. (16) obeys physical constraints. Moreover, membrane potential is the measurement of the potential energy of cell membrane in the form of voltage. Voltage is the measurement of the energy that a charge requires for it to move between two points in space. In the case of membrane potential of a neuron, the voltage measurement is the potential energy that an ion requires to flow across the membrane. Furthermore, electronvolt (eV) defines the kinetic energy required for 1 single ion or electron to flow across an electric potential of one volt in vacuum from rest. In an ideal environment, 1 eV equals to the exact value 1.602×10^{-19} joule. In other words, in an ideal environment each ion of 1 charge causes 1 volt of potential energy rise or drop requiring 1 eV of energy equal to 1.602×10^{-19} joule. However, a biological cell is a complex system and is not an ideal environment where 1 eV is defined. The energy required for 1 charge of ion to flow across the

neuron membrane and cause fluctuation in electric potential of 1 volt should be time-dependent and more than 1.602×10^{-19} joule due to the time-dependent environmental condition which is not in vacuum state. Therefore, this study defines the electronvolt of neuron eV_{Ni} as shown in Eq. (25). Since 1) physiological observation reveals roughly 2 to 100 million sodium ions are required to across the neuron membrane throughout the entire action potential firing process, 2) the amplitude of membrane potential of an action potential firing, Amp_{AP}, is around 0.1 volt (-70mV to 50mV), 3) electrochemical gradient ($\nabla\overline{\mu_{NMi}}(t)$) defines the potential energy of ion species i per mole, and 4) law of energy conservation, one can obtain the kinetic energy required for 1 charge of ion species i to cause 1 volt of membrane potential rise or drop by multiplying the following: a) the potential energy of per ion species i, $\left(\frac{\nabla\overline{\mu_{NMi}}(t)}{mol}\right)$, b) the number of sodium ions across the membrane of a neuron throughout the entire action potential firing process, $n_{AP\_Na^+}$, and c) the reciprocal of the amplitude of action potential in volt, $\left(\frac{1}{Amp_{AP}}\right)$. In this study, $n_{AP\_Na^+}$ is assumed as 2 million and Amp_{AP} is assumed as 0.1 volt. As a result, the electronvolt of neuron eV_{Ni} is a function of electrochemical gradient $\nabla\overline{\mu_{NMi}}(t)$. Through the neuron specific electronvolt eV_{Ni}, the governing law of membrane potential dynamics, Eq. (16), describes the dynamics of membrane potential properly.

2.3.2.3 Dynamics of Ligand Gated Ion Channels

Both the analog and digital dynamics of the membrane potential are described in the same mathematical form as shown in Eq. (17) and (18). However, the definition of the availability α_{ij} of ligand gated and voltage gated ion channels is different as shown in Eq. (22) and (24). Since the focus of this study is to propose a general framework that describes the dynamics of complex networks and a control strategy, this study only considers a few commonly studied types of ligand-

gated ion channels (AMPA receptors and NMDA receptors) that is significant in describing the basic brain network dynamics and some assumptions are applied to simplify the research question.

To simplify and limit the possible scenario of brain network dynamics be considered in this study, the AMPA receptors (AMPAR) and NMDA receptors (NMDAR) are the only two types of ligand gated ion channels to be considered because of the significantly developed literature in these receptor subtypes in particular and their significant implications in brain neuron structure stability and synaptic plasticity (local alterations in coupling configurations steering global brain dynamical response). Moreover, the ion flux pass through AMPARs is composed mainly by Na^+ and K^+. NMDARs are additionally uniquely permeable to Ca^{2+}. This study assumes AMPARs only allow Na^+ and K^+ flux and NMDARs only allow Ca^{2+} flux for simplicity to more prominently capture Ca^{2+} concentration dynamics which have significant implications upon the magnitude and direction of synaptic plasticity. The availability of ligand gated ion channels of analog dynamics of the membrane potential is defined as below.

$$\varphi_{Nd_{NTlj}}(t) = NT_{MNd_{lj}}(t) - NT_{Nd_{ezcj}}(t) - NT_{MNd_{rlj}}(t)$$

$$,where \begin{cases} NT_{MNd_{lj}}(t) = high\ concentration\ if\ AP_M\ fires \\ NT_{MNd_{lj}}(t) = low\ concentration\ if\ AP_M\ not\ fires\ long\ enough \end{cases} \tag{28}$$

$$J_{Nd_{NTlj}}(t) = -D_j \frac{\partial \varphi_{Nd_{NTlj}}}{\partial x} \tag{29}$$

$$A_{Nd_{NT_{lj\_total}}}(t) = J_{Nd_{NTlj}}(t) \times A_{Nd} \times \Delta t \times A_{NT_{lj}} \tag{30}$$

$$A_{Nd_{N_{j\_trig}}}(t) = A_l \times n_{Nd_{N_{j\_trig}}}(t) \tag{31}$$

$$P_{Nd_{N_j}} = \frac{A_{Nd_{NT_{lj\_total}}}(t)}{A_{Nd_{N_{j\_trig}}}(t)} \tag{32}$$

$$n_{Nd_{N_{j\_trig}}}(t) = n_{Nd_{N_{j\_trig}}}(t-1) + n_{Nd_{N_{j\_avl}}}(t) \times P_{Nd_{N_j}} \tag{33}$$

$$n_{Nd_{N_{j\_MAX}}}(t) = n_{Nd_{N_{j\_avl}}}(t) + n_{Nd_{N_{j\_trig}}}(t) \tag{34}$$

$$\Delta t_{AMPARi} = 1.5 \times 10^{-3}\ sec.$$
$$\Delta t_{NMDARi} = 225 \times 10^{-3}\ sec. \tag{35}$$

where $\varphi_{Nd_{NTlj}}$ is the concentration of neurotransmitter species j that activates ligand gated ion channels type l on dendrite d of neuron N in the unit of [mol/m^3], $NT_{MNd_{lj}}$ is the concentration of neurotransmitter species j released by the presynaptic neuron M that activates ligand gated ion channels type l on dendrite d of neuron N in the unit of [mol/m^3], $NT_{Nd_{ezlj}}$ is the concentration of neurotransmitter species j that activates ligand gated ion channels type l which are degraded by enzymes in the synaptic cleft that connected to dendrite d of neuron N in the unit of [mol/m^3], $NT_{MNd_{rlj}}$ is the concentration of neurotransmitter species j that activates ligand gated ion channels type l be re-uptake by the presynaptic neuron M in the unit of [mol/m^3], $J_{Nd_{NTlj}}$ is the neurotransmitter flux that triggers ligand gated ion channels type l on dendrite d of neuron N in the unit of [mol/m^{2}s], D_j is the diffusion constant of neurotransmitter species j in the unit of [m^2/s], $A_{Nd_{NT_{lj\_total}}}$ is the summation of the cross-sectional area of all neurotransmitter species j that activates ligand gated ion channels type l on the surface of dendrite d of neuron N in the unit of [m^2], A_{Nd} is the surface area of dendrite d of neuron N in the unit of [m^2], Δt is the duration of each calculating iteration in the unit of [s], $A_{NT_{lj}}$ is the cross-sectional area of neurotransmitter species j that activates ligand gated ion channels type l in the unit of [m^2], $A_{Nd_{N_{j\_trig}}}$ is the total cross-sectional area of ligand gated channel type l triggered by neurotransmitter species j on dendrite d of neuron N in the unit of [m^2], A_l is the cross-sectional area of each ligand gated ion channel type l in the unit of [m^2], $n_{Nd_{N_{j\_trig}}}$ is the number of triggered ligand gated ion channel

type l, $P_{Nd_{N_j}}$ is the estimated probability of each ligand gated ion channel type l triggered by neurotransmitter species j, $n_{Nd_{N_{j\_avl}}}$ is the number of available ligand gated ion channel type l on dendrite d of neuron N, $n_{Nd_{N_{j\_MAX}}}$ is the total number of available ligand gated ion channel type l on dendrite d of neuron N, Δt_{AMPARi} and Δt_{NMDARi} are the opening duration of the triggered AMPAR and NMDAR receptor that allow ion flux of species i respectively in the unit of [s].

Eq. (28) to (35) describes the mechanisms of ligand gated ion channels, AMPAR and NMDAR, considered in this study. Assuming a postsynaptic neuron N has dendrite d that is receiving neurotransmitter from presynaptic neuron M. Eq. (28) describes the physiological observation of the fluctuation of neurotransmitter concentration in synaptic cleft. The concentration of neurotransmitter species j rises to a high level if the presynaptic neuron M fires action potential (AP) and drops to a low level if the presynaptic neuron M does not fire AP for a prolong duration. Neurotransmitter concentration can be decreased due to enzymatic degradation in the synaptic cleft and re-uptake by the presynaptic neuron M for reuse to conserve energy consumption. With the remaining concentration of neurotransmitters, the flux and number of neurotransmitters in the synaptic cleft can be calculated shown in Eq. (29). Due to lack of study in establish a proper description in the probability of each species of neurotransmitters triggering the corresponding ligand gated ion channels, this study uses the ratio between the cumulative cross-sectional area of the neurotransmitters of each species and the available ligand gated ion channels of each type to establish a rough estimation the probability of triggering each ligand gated ion channel as shown in Eq. (32). Lastly, each triggered AMPAR and NMDAR are not available to further receive more neurotransmitters. And each triggered AMPAR and NMDAR returns to available state (allowing ion flux) in the following time scales of Δt_{AMPARi}, 15 ms, and Δt_{NMDARi}, 225 ms, seconds from the moment of triggering. As a result, the coupling relationship between

the presynaptic neuron M and the postsynaptic neuron N is defined through the concentration of released neurotransmitters from neuron M and the probability of triggering the ligand gated ion channels of neuron N by the released neurotransmitters. It is noteworthy that ion concentration is proportional to probability of ligand-gated ion channel activation and respective ion flux significantly determining the level of influence a presynaptic neuron has upon a postsynaptic neuron.

Synaptic plasticity is a key phenomenon that changes the receiver behavior of a postsynaptic neuron in adjusting the degree of coupling to the connected presynaptic neurons. Mg^{2+} blockage to the NMDARs is one of the key mechanisms of spike timing dependent plasticity (STDP) which is one of many forms of synaptic plasticity. Also, Mg^{2+} is directly correlated to Ca^{2+} concentration in postsynaptic neuron since NMDARs is more permeable to Ca^{2+}. Therefore, Mg^{2+} blockage is considered in this study through Coulomb's law as shown in Eq. (36) to ensure a realistic NMDARs behavior. As this study only develops the preliminary brain network model in proving the generality of the proposed general framework of complex network, details in synaptic plasticity will not be further discussed. Also, since NMDARs is more permeable to Ca^{2+}, Mg^{2+} blockage significantly controls Ca^{2+} concentration in the postsynaptic neuron. This study assumes NMDARs only permeable to Ca^{2+}.

$$F_{Mg^{2+}} = K\frac{q_{Mg^{2+}}Q_{mN}}{r^2} \tag{36}$$

$$Q_{mN} = C_m V_{mN} \tag{37}$$

$$\frac{F_{Mg^{2+}}}{m_{Mg^{2+}}} = a_{Mg^{2+}} \tag{38}$$

where $F_{Mg^{2+}}$ is the electrostatic force reacting on the Mg^{2+} that is close to the membrane of neuron N in the unit of [N], K is the coulomb's constant in the unit of $[\frac{N\cdot m^2}{C^2}]$, $q_{Mg^{2+}}$ is the charge of the

Mg^{2+} in the unit of [C], Q_{mN} is the charge of the membrane of neuron N in the unit of [C], C_m is the capacity of the membrane of neuron N in the unit of [F], V_{mN} is the membrane potential of neuron N in the unit of [V], $m_{Mg^{2+}}$ is the mass of Mg^{2+} in the unit of [kg], $a_{Mg^{2+}}$ is the acceleration of Mg^{2+} in the unit of $[\frac{m}{s^2}]$. Thus, trivial double integration can be utilized to approximate the location of the Mg^{2+} ion within the pore of the NMDAr to determine the level of blockage (if any).

2.3.2.4 Dynamics of Voltage Gated Ion Channels

Once the mechanisms that cause analog dynamics of membrane potential, postsynaptic potential, is described as aforementioned, the mechanisms that causes digital dynamics of membrane potential, action potential, is of the same principle but with different triggering condition in general. While ligand gated ion channels are triggered by neurotransmitters released by presynaptic neurons, voltage gated ion channels are triggered by the membrane potential of the postsynaptic neuron. When the membrane potential of a postsynaptic neuron rises from a resting potential and reaches the threshold potential, voltage gated ion channels on the same postsynaptic neuron are triggered to allow ion influx. Due to the number of voltage gated ion channels is usually many times larger than the number of ligand gated ion channels on neurons, membrane potential usually presents spikes with very sharp slope in time when voltage gated ion channels are triggered. As aforementioned, the voltage rise of action potential depolarization is caused by a sudden large influx of Na^+ for a short period of time and follows by a sudden large outflux of K^+ that causes the voltage drop repolarization of action potential. In other words, their exist in a time delay in the triggering of Na^+ and K^+ voltage gated channels that is crucial in defining the action potential profile. Since this study aims to use the common referred action potential profile as shown in Fig. 22 of [46] in proving the credential of the general framework, this study assumes all voltage gated Na^+ channels are triggered at the threshold potential, -50 mV, and all voltage gated K^+ channels

are triggered 1 millisecond after the threshold potential is reached. Triggered voltage gated Na^+ channels close when the repolarization of action potential drops below the threshold potential. Triggered voltage gated K^+ channels follow the same procedure but also with time delay of 1 millisecond to ensure K^+ channels open after Na^+ so the observed action potential profile due to spike depolarization and repolarization are accurately reproduced with what is observed.

The contribution of voltage gated Ca^{2+} channels to the dynamics of action potential is also be considered in this study. Since Ca^{2+} primarily plays roles as a secondary message to trigger biological mechanisms such a various modes of synaptic plasticity [47], it is beneficial to consider the effect of voltage gated Ca^{2+} channels to the dynamics of action potential to set the stage for future study even though the detailed analysis of synaptic plasticity is outside the scope of this study. Moreover, although Ca^{2+} influx through voltage gated Ca^{2+} channels do not contribute as significantly to the profile of action potential as Na^+ influx through voltage gated Na^+ channels do, the dynamics of voltage gated Ca^{2+} channels is one of the key factors to synaptic plasticity of individual neuron dynamics that causes change in the number of ligand gated ion channels and further alters the signal receiving behavior of the neuron. In other words, this can significantly influence the coupling strength between neurons. In this study, the triggering and closing procedure of voltage gated Ca^{2+} channels are assumed to follow the same procedure of voltage gated Na^+ channels which triggered when membrane potential is higher than the threshold potential and are closed when membrane potential is lower than the threshold potential. The detailed analysis of synaptic plasticity will not be provided.

With the description and assumption of voltage gated Na^+, K^+, and Ca^{2+} channels defined, the action potential dynamics is described clearly through the preliminary brain network model.

2.3.2.5 Dynamics of Ion Pumps

In maintaining the membrane potential responsive to triggering of presynaptic neuron dynamics, the ion concentration must be restored to a resting state upon perturbed ion concentrations due to ligand-gated and voltage-gated ion channel ionic flux. Thus, the out of balanced ion concentration will lead to reverse of electrochemical gradient in ion flux direction. As a result, incorporating the mechanism of ion pumps to the brain network model is crucial in describing the dynamics of neuron membrane potential. However, the available physiology observation documentation and data of ion pumps are not comprehensive enough for developing a general governing law of ion pumps as this study performed for ligand gated and voltage gated ion channels. In alternation, this study developed a mathematical equation, Eq. (39), in describing ion pump dynamics through mathematical curve fitting technique with some assumptions according to the observation data of [48, 49]. The fundamental premise of these equations are that ion-pump activity (ion flux) will be higher when ion concentrations are further away from resting potential conditions and vice-versa. Worth to keep in mind as aforementioned, mathematical curve fitting technique overlooks the higher order terms that preserve the characteristic of a nonlinear system. The governing law of ion pump dynamics, Eq. (44), this study developed will need to be revised once a proper and comprehensive physiological observation of ion pumps are available.

[48, 49] conduct a curve fitted relationship between Na^+ efflux and Na^+ concentration of Na^+-K^+ pump from the experimental data of rat. Although [48] did provide a few different equations of Na^+-K^+ pumps. These equations are either be further fitted to models proposed by other studies or incorporated with some coefficient with no support of physics laws. Moreover, these equations define change of membrane potential due to Na^+-K^+ pumps as a function of Na^+ and K^+ concentration. As previously discussed, the electronvolt, eV, of neuron membrane is a

time dependent variable and a function of electrochemical gradient $\nabla\overline{\mu_{NMi}}(t)$ which is further a function of ion concentration, the proposed equations in [48] overlook fundamental factors that contribute to the change of membrane potential caused by Na^+-K^+ pumps. In other words, these Na^+-K^+ pumps equations cannot describe the dynamics of Na^+-K^+ pumps properly.

The mechanism of ion pumps has to be properly described since the effect of the ion pumps is crucial to the dynamics of membrane potential. Although there are not enough physiological observation data for one to develop a proper dynamics equation in describing the mechanism of ion pumps properly, based on the best of our knowledge of physiology of ion pumps, this study provides 1) a preliminary descriptions to Na^+-K^+ pumps that describe the mechanism properly with an estimated relationship between pump cycle per unit of time and Na^+ concentration of the postsynaptic neuron, and 2) a rough estimation of Ca^{2+} pumps dynamics that does not described the mechanism properly.

It is a fact that the dynamics of Na^+-K^+ pump of human and rat are both function of Na^+ concentration. This study assumes Na^+-K^+ pumps of human and rat are similar enough, the normalized Na^+-K^+ pump Na^+ efflux versus Na^+ relationship conducted by Blom et al in Fig. 5(a) of [49], can be denormalized and mapped to a human condition through Na^+-K^+ pump conditions of human body. Since the $\alpha 1$ curve of Fig. 5(a) shown in [49] is of a step function or Heaviside step function form, this study uses the smooth approximation shown in Eq. (39) of the same curve. Instead of defining the direct relationship between Na^+ concentration to membrane potential in voltage, Eq. (40) first describes the relationship between Na^+ concentration of neuron N to the number of Na^+ be pumped out from neuron N in a given time then the correspond change of membrane potential in voltage can be obtained through Eq. (44). Further, since every 2 K^+ are

pumped into the membrane while 3 Na^+ are pumped out through the same Na^+-K^+ pumps, the 2 to 3 ratio between K^+ and Na^+ has to be obeyed and is constrained through Eq. (43).

Compared to Na^+-K^+ pump, the available underlying knowledge of Ca^{2+} pump and its physiology is even more incomprehensive. Therefore, this study simply uses the concentration difference of Ca^{2+} from the lowest commonly observed value to the current calculated value in neuron N to estimate the number of Ca^{2+} pumped out from neuron N in each simulation iteration as shown in Eq. (44). Note that Eq. (44) is a very rough estimation which does not describe the mechanism of Ca^{2+} pumps properly. The underlying logic is that rate of Ca^{2+} expulsion increases if intracellular Ca^{2+} rises significnalty above its normal, homeostasis levels and vice versa. The mathematical form that describes Ca^{2+} pump should eventually be similar as the one that describes Na^+-K^+ pumps. Revising to Eq. (43) is a must when a comprehensive physiological observation of Ca^{2+} pumps is available.

$$V_{pN}(t) = V_{pNNa^+}(t) + V_{pNK^+}(t) + V_{pNCa^{2+}}(t), \tag{26}$$

$$n_{pNNa^+} = \left(\frac{1}{1 + e^{-aC_{NNa^+in}{}^2 - bC_{NNa^+in} - c}}\right) \times CPI_{pNa^+K^+} \times Vol_{meme} \times n_{pNNa^+K^+} \tag{39}$$

$$,where \begin{cases} a = -0.003936 \\ b = 0.3919 \\ c = -4.227 \\ C_{NNa^+in} = Na^+ concentration\ of\ neuron\ N \end{cases}$$

$$CPI_{pNa^+K^+} = \left(\frac{CPM_{pNa^+K^+} \times 3}{60}\right) \times \Delta t \tag{40}$$

$$,where\ CPM_{pNa^+K^+}\ (cycle\ per\ \min of\ Na^+K^+\ pump) \cong 8000\ to\ 10000$$

$$n_{pNNa^+K^+} = 8 \times 10^4 \sim 3 \times 10^7 \tag{41}$$

$$n_{pNK^+} = \frac{-2}{3} \times n_{pNNa^+} \tag{42}$$

$$n_{pNCa^{2+}} = \left(\frac{e^{C_{NCa^{2+}}} - 0.009}{10^{28}}\right) \times \Delta t$$
$$, where\ n_{pNCa^{2+}} = 0\ if\ n_{pNCa^{2+}} < 0.009 \tag{43}$$

$$V_{pNi}(t) = \sum\nolimits_i \left(\frac{\nabla\overline{\mu_{NMV}}(t) n_{pNi}(t)}{eV_{Ni}}\right) \tag{44}$$

$$\nabla\overline{\mu_{NMVi}(t)} = \nabla\overline{\mu_{NMi}}(t) \tag{45}$$

where V_{pN} is the voltage fluctuation of the membrane potential of neuron N caused by all the ion pumps in the unit of [V], V_{pNNa^+}, V_{pNK^+}, and V_{pNCa^+} are the voltage fluctuation of the membrane potential of neuron N caused by the Na^+ and K^+ through Na^+ -K^+ pump, and Ca^{2+} through Ca^{2+} pumps accordingly in the unit of [V], n_{pNNa^+} is the number of Na^+ pumped out of neuron N according to the concentration of Na^+ in neuron N, C_{NNa^+in} is the concentration of Na^+ in neuron N in the unit of [mol/m^3], Vol_{meme} is the volume of the static electric force effective zone on the inside of the membrane of neuron N where the ion effecting zone is in the unit of [m^3], $n_{pNNa^+K^+}$ is the number of Na^+-K^+ pumps neuron N has, $CPI_{pNa^+K^+}$ is the number of cycle of Na^+-K^+ pumps per simulation iteration, $CPM_{pNa^+K^+}$ is the number of cycle of Na^+-K^+ pumps per minute, Δt is the duration of each calculating iteration in the unit of [s], n_{pNK^+} is the number of K^+ pumped out of neuron N, $n_{pNCa^{2+}}$ is the number of Ca^{2+} pumped out of neuron N according to the concentration of Ca^{2+} in neuron N, $C_{NCa^{2+}in}$ is the concentration of Ca^{2+} in neuron N in the unit of [mol/m^3], V_{pNi} is the change of membrane potential of ion species i of neuron N in the unit of [V], $\nabla\overline{\mu_{NMVi}}$ is the electrochemical gradient of ion species i across the membrane of neuron N in the unit of [joule/mol], $\nabla\overline{\mu_{NMi}}$ is the electrochemical gradient of ion species i between the synaptic cleft of neuron M and N and intercellular space of dendrite d of neuron N in the unit of [joule/mol].

With the descriptions of the Na^{+}-K^{+} pump and Ca^{2+} pump, the preliminary brain network model could estimate the dynamics in membrane potential in regard to the refractory time period after hyperpolarization primarily driven by active ion transport through the aforementioned ion pumps. Since the change of membrane potential caused by the ion pumps requires energy by consuming ATP, one should establish the relationship between the energy that ATP provides to a neuron and the number of ions be pumped out through each type of ion pump to refine the description of the mechanism of ion pumps when correlated physiological observation data is available. Moreover, since the preliminary brain network model describes the individual neuron dynamics through energy in the context of complex network, it is more direct and clearer to use ATP consumption of neuron in develop the description of ion pump dynamics.

Consequently, this study describes individual neuron dynamics (membrane potential dynamics) and the synaptic dynamics by using physics laws to properly describe the mechanism that drives (1) postsynaptic potential through Eq. (17), (2) action potential through Eq. (18), and (3) ion pump dynamics through Eqs. (26) and (44). From this point and on, the general framework could be applied to describe brain network dynamics by describing individual neuron dynamics through energy and defining the degree of coupling in establish the coupling dynamics (synaptic dynamics) of neurons. Since the energy distribution of all systems exist in the world of physics follows normal distribution, information entropy describes the dynamics at the network level by defining the individual energy distribution. The following sections will demonstrate how one could describe real-life network dynamics in the context of the general framework using the preliminary brain network model as an example.

2.3.2.6 Define Brain Network Dynamics Using the General Framework

In the previous section, a preliminary brain network model is developed which describes the individual neuron dynamics and synaptic dynamics properly according to the mechanisms driving the behavior of postsynaptic potential, action potential, and ion pump dynamics. This section will use the preliminary brain network model to demonstrate how to describe real-life network dynamics in the context of the general framework of complex network.

The general framework of complex network is general to complex network systems in all domains of physics because the individual dynamics of the constituents are defined through energy. Energy is a dimensionless physics property that defines the change of states in time (the dynamics) of an object. Therefore, energy is the proper and in fact the only physics property that defines the dynamics of an object applicable generally to different domains of physics. In other words, the first step to describe network dynamics using the general framework is to define the individual dynamics through energy. Since the general framework shown in Eq. (9) through Eq. (13) is present in the case of a 20-constituent point mass network that translate in space, the general framework is presented in the physical domain of mechanical translational motion in space. However, the brain network dynamics is driven by the membrane potential of individual neurons that is measured in voltage, mechanical-electrical analogies need to be applied to transform the general framework shown in Eq. (9) to another domain of physics that is suitable for brain networks. Once the individual neuron dynamics be defined through energy, the degree of coupling (DOC k and DOC J) between the neurons can be established. As aforementioned, the energy distribution of systems in the world of physics follows normal distribution. Information entropy defines the distribution of individual neuron energy. Finally, the dynamics of the brain-network is described at the network level.

In the case of brain neurons, the driving state of individual neuron dynamics is the time-dependent membrane potential behavior (the dynamics of membrane potential) of each neuron. Since membrane potential is measured in voltage whose change is caused by the ion flux through the ion channels, neuron cells can be viewed as electrical cell batteries in electrochemical domain. The electrical potential energy of the individual neuron N is the charge of the ions contained in the cell membrane multiply with membrane potential as

$$PE_{mN}(t) = q_{mN}(t)V_{mN}(t) \tag{46}$$

in the unit of [J] where $q_{mN}(t) = \sum_i q_{mN_i}(t)$ is the total ion charge of all ion species i contained in the cell membrane in the unit of [C], and $V_{mN}(t)$ is the membrane potential of neuron N in the unit of [V]. The kinetic energy of neuron N

$$KE_{mN}(t) = \sum_i \left(\left(\sum_d I_{mN_{lgdi}}(t) \right) + I_{mN_{vi}}(t) + I_{mN_{pi}}(t) \right) \times V_{mN}(t)\Delta t \tag{47}$$

is the charge of ion flux across the membrane that introduce change to the potential energy of neuron N and further drives the dynamics of the membrane potential of neuron N due to change in the number of ions inside neuron N. The kinetic energy of neuron N, $KE_{mN}(t)$ in the unit of [J], is contributed by the change of ion charge $q_{mN_{lgdi}}(t)$ in the unit of [C] across the ligand gated ion channels, $q_{mN_{vi}}(t)$ in the unit of [C] across the voltage gated ion channels, and $q_{mN_{pi}}(t)$ in the unit of [C] across the ion pumps where $\sum_i \sum_d I_{mN_{lgdi}}(t) = \sum_i \sum_d \frac{q_{mN_{lgdi}}(t)}{\Delta t}$ in the unit of [A] is the ionic current of all ion species that flow through all dendrites of neuron N, $\sum_i I_{mN_{vi}}(t) = \sum_i \frac{q_{mN_{vi}}(t)}{\Delta t}$ in the unit of [A] is the ionic current of all ion species that flow through the voltage gated channels of neuron N, and $\sum_i I_{mN_{pi}}(t) = \sum_i \frac{q_{mN_{pi}}(t)}{\Delta t}$ in the unit of [A] is the ionic current of

all ion species that flow through ion pumps of neuron N. Therefore, the individual neuron energy is defined as Eq. (48) in the unit of [J].

$$E_{mN}(t) = PE_{mN}(t) + KE_{mN}(t) \tag{48}$$

Once the individual neuron energy is defined, the degree of coupling can be further defined. In regard to the 20-constituent point mass model as aforementioned in section 2.1, degree of couplings, DOC k and DOC J, define the relationship between each pair of connected constituents. DOC k is related to the potential energy portion of the individual constituent dynamics

$$E_i(t) = \sum \frac{1}{2} k_{ij}(t) D_{ij}(t)^2 + \frac{1}{2} m_i V_i(t)^2 \tag{9}$$

in the sense of how much the state of constituent i will change according to constituent j. DOC J is related to kinetic energy portion of the individual constituent dynamics, where the governing law

$$V_i(t+1) = V_i(t) + \sum J_{ij}(t)\, D_{ij}(t) \tag{10}$$

is defined in the sense of how frequent the state of constituent i will be adjusted according to constituent j. As shown in Eq. (46) and Eq. (47), in the case of brain neuron dynamics, the potential energy of neuron N is the ion charge it holds and the kinetic energy of neuron N is the change of ion charge per unit of time of neuron N. It is clear that ion flux across the membrane of neuron N is the fundamental parameter that causes change of state (the dynamics) of membrane potential V_{mN}. Therefore, to transform the DOC k, incorporated in Eq, (9), and DOC J, incorporated Eq. (10), to the version appropriated for brain networks, this study chooses the mechanical-electrical analogy which deems 1) mechanical displacement equivalent to magnetic flux (ion flux in the case of individual neuron dynamics) and 2) velocity of mechanical system equivalents to electrical voltage. The DOC k of individual neuron N in brain networks is defined as

$$DOCk_{mN_i}(t) = q_{mN_i}(t) \tag{49}$$

which is essentially the charge of neuron N in the unit of [C]. In other words, the larger measurement of DOC k of neuron N shows the larger number of ions neuron N holds. Consequently, a larger DOC k corresponds to more difficulty in changing the state of neuron N in terms of membrane potential and vice versa. Similarly, the DOC J of individual postsynaptic neuron N is defined as

$$DOCJ_{mNM_{di}}(t) = \sum_d \sum_i \left(\frac{\nabla \overline{\mu_{NMi}}(t) \alpha_{d_{Nij}}(t) \Delta t}{eV_{Ni}(t)} \right) \tag{50}$$

which is the ligand gated ion channel portion of the governing law of individual neuron dynamics (the time-evolution of postsynaptic potential)

$$V_{mN_{lgd}}(t) = \sum_d \sum_i \left(\frac{\nabla \overline{\mu_{NMi}}(t) \alpha_{d_{Nij}}(t)\, J_{Ni}(t) \Delta t}{eV_{Ni}(t)} \right) \tag{17}$$

excluding the ion flux $J_{Ni}(t)$ term. Notice that as aforementioned, not all ion flux across the membrane of neuron N is triggered by the signal (neurotransmitters) transmitted by the presynaptic neuron M, only the analog dynamics (postsynaptic potential) reflects the signal receiving behavior of neuron N. Therefore, the DOC J of individual postsynaptic neuron N is defined only with the ion flux across ligand gated ion channels instead of all types of ion channels and pumps. The DOC J of individual postsynaptic neuron N is in the unit of $\frac{[m^2]\cdot[s]}{[mol]}$, which defines the number of ion species i in mole are allowed to cross the available ligand gated ion channels that is triggered by the neurotransmitter species j released by the presynaptic neuron M in the duration time of consideration. Consequently, the larger measurement of DOC J of neuron N indicates a higher number of ions are allowed to flow across the ligand gated channels of neuron N that are triggered by neurotransmitter species j released by neuron M in the time span of consideration. As a result, the more change of state neuron N undergoes in terms of postsynaptic potential changes due to the

state of the presynaptic neuron M in the same time period corresponds to greater values of DOC J and vice versa.

To this point, the brain network dynamics is defined at the microscopic level (the individual neuron level) as the individual neuron dynamics is defined through energy, Eq. (46), (47), and (48), and the coupled relationship is defined through the degree of couplings, Eq. (49) and (50). Finally, the brain network dynamics at the macroscopic level (network level) can be further defined. As aforementioned, individual neuron energies should follow a normal distribution

$$P(E_{mN}) = \frac{1}{\sigma\sqrt{2\pi}} e^{-\frac{1}{2}\left(\frac{E_{mN}-\mu}{\sigma}\right)^2} \tag{51}$$

as all systems in real-life do. As a result, information entropy can be applied to define brain network dynamics at the network level as

$$S(E_m) = -\sum_N p\big(E_{mN}(t)\big)\, log\, p\big(E_{mN}(t)\big) \tag{52}$$

where $E_m = \{E_{mN} | N = 1 \sim n,$ and $n =$ number of neurons$\}$ is the set of individual neuron energies.

In summary, the brain network dynamics is defined following the general framework for dynamical complex networks. At the individual neuron level, 1) individual neuron dynamics is defined using energy and 2) coupling dynamics between neurons is defined using degree of couplings. As individual neuron energies follow a normal distribution, information entropy is employed to define brain network dynamics at the network level.

3. STATISTICAL MECHANICAL SYSTEMS *

3.1 Complex Network Models

Three types of networks, namely, a general complex network (Structure 1), a WS small-world network model (Structure 2), and a BA scale-free network model (Structure 3) are investigated in the section, with the corresponding network structures illustrated in Figs. 10(a), 10(b), and 10(c). It is seen that while the majority constituents in the small-world network structure are of the same or similar degree, the scale-free network is featured with high degree constituents that are hubs and low degree constituents that reply on hubs to reach other low degree constituents. All 3 are 20-constituent networks. The WS small-world network [12] is initially a graph of degree of 4 with each connection re-wired to other constituents with a re-wiring probability $p = 50\%$. Using Eq. (11) and normalized ensemble energy, the average path length of the small-world network is 0.0537 Joule at t=0s. The BA scale-free network model [13] has initially 2 constituents. New constituents are added to the network with the connectivity $k_i(t) = m(t/t_i)^{\frac{1}{2}}$, $m_0 = m = 2$ as defined in Eq. (2) until all 20 constituents are added to the network. An iteration time step of 0.0005 seconds is used. Network constituents interact with one another according to the general framework and the entropy of the probability of ensemble energy at the ensemble level holds constant for the complex network to maintain the same ensemble dynamics. Constituent and ensemble network states are simultaneously calculated to monitor changes of network properties in time.

---

* Part of this chapter is reprinted with permission from "A General Framework for Dynamic Complex Networks" by Yang, C.-L. and Suh, C. S., 2021, Journal of Vibration Testing and System Dynamics, 5, 87-111, Copyright 2021
by L & H Scientific Publishing, LLC

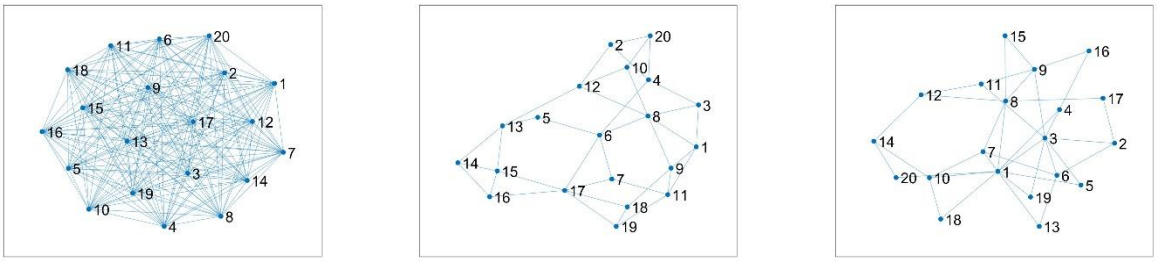

(a) (b) (c)

Fig. 10 (a) General complex network, (b) small-world network, (c) scale-free network

At t=0s all the constituents are evenly spaced on a circle of 5-meter in radius with the center of the circle overlapping with the Cartesian origin of the x-y plane. An initial velocity of 0 m/s is given to all the constituents. In Case 1, the degrees of coupling k=0.5 N/m and J=0.5 s^{-1} are initially specified to all the connections. In Case 2 and Case 3, the degrees of coupling k and J are assumed to be 1 N/m and 1 s^{-1}, respectively, for all connections. Note that k and J are both time dependent variables in Case 1 while being constants in Case 2 and Case 3. Since the separation between each connected pair and the degree of coupling k are known, the potential energy of each connected pairs is known using Eq. (9), thus the energy and the probability of energy of each connected pair can be calculated. The information entropy of the whole network is obtained through Eq. (12). The initial state of the complex network at both the constituent and ensemble levels are given as knowns.

The constituent trajectory of each network case is plotted in Figs. 11(a), 12(a), and 13(a) with a circle and a cross indicating the initial and final positions, respectively. The corresponding velocities are given in Figs. 11(b), 12(b), and 13(b). Constituent energies are placed in Figs. 11(c), 12(c), and 13(c) alongside the normalized constituent energy in Figs. 11(d), 12(d), and 13(d). The time histories of the degree of coupling J are found in Figs. 11(e), 12(e), and 13(e) and the time histories of the degree of coupling k are seen in Figs. 11(f), 12(f), and 13(f). The red lines in Figs.

11(g), 12(g), and 13(g) indicate the initial entropy while the blue lines show the variation of the corresponding entropy in time. Because information entropy indicates the dynamic state of the network ensemble, low measurements correspond to collective network behaviors that are more synchronized while the opposite suggests ones that are less synchronized. Figs. 11(h), 12(h), and 13(h) give the normalized probability of constituent energy per the PDF of normal distribution.

Measurements based on graph theory are also made. Figs. 11(i), 12(i), and 13(i) present the average path lengths defined in Eq. (4) using the normalized ensemble energy. The weight of each topological connection is defined as the normalized energy difference between the two connected constituents. Thus, the path length between any two constituents also shows the difference in the energy state. That is, shorter is the path length between two constituents, closer is the energy states of the two constituents. Because the energy states between two connected constituents are closer, information transmits faster through paths of shorter length. Also, smaller the average path length, faster a network would reach synchronization after a disturbance is introduced to the network. The variations of the average path length in all 3 cases are evidently nonlinear and non-stationary. The average path length of Case 1 is approximately 1-tenth of the other 2 cases', demonstrating a feature that is distinctive and different from the other 2. The average path length of Case 2 is slightly greater than Case 3's but of similar pattern. Because transmission of coupling energy in Case 1 is much faster than the other 2 cases, the rate of reaching emergent phenomena such as synchronization and asynchronization as described by the network model is also faster. Lastly, it is readily seen from the 2 average path length plots in Figs. 12(i) and 13(i) that Case 2 and Case 3 generate highly similar network structures.

The distribution of the normalized ensemble energy shown in Figs. 11(j), 12(j), and 13(j) serve the same objective as degree distribution does. At each of the 20,000 iterations used to

generate the results, for all the 3 cases, the normalized energy of each constituent is noted every 0.0005J ranging from 0 to 1J. Fig. 11(j) shows the energy is distributed between 0.05J and 0.065J and localizes at 0.05J. The distribution is seen to follow Eq. (10). The distribution for Case 3 in Fig. 13(j) is seen to follow the power law defined in Eqs. (2) and (3) and also is in agreement with Eq. (5). Fig. 12(j), which corresponds to Case 2, demonstrates a trend that is identical to Fig. 13(j). This is expected because with the degrees of coupling $k = 1\ N/m$ and $J = 1\ s^{-1}$ for all the connections, the distribution of constituent energy is positively correlated to the distance and velocity of the constituent according to Eq. (9). When constituent energy, position, and velocity follow the same trend, the corresponding energy distribution and degree distribution should also demonstrate the same trend. Figs. 12(a) and 13(a) show the constituents in both cases all begin their motions on a circle of 5.0m in radius in the x-y plane and converge to a distance smaller than 0.1m at the end of the simulation. Figs. 12(b) and 13(b) show that both constituent velocities vary between 0 and 10 m/s 0.5 seconds after the simulations began. Figs. 12(c), 12(d), 13(c), and 13(d) show that the constituent energies of both cases vary within the same range 0.5 seconds after the simulations began. The black lines in Figs. 12(c) and 13(c) indicate that the total ensemble energy of both cases vary within a tight range. Figs. 12(d) and 13(d) show that the normalized ensemble energy of both cases vary between 0 to 0.15J. Since the constituent energy, position, and velocity of both Case 2 and Case 3 all demonstrate the same trend and vary within the same range, their corresponding constituent energy distributions are also of similar features. This is because the degree distribution of Case 3, the scale-free network model, and Case 2, the small-world network model, were all defined by the stationary solution in Eq. (5). This observation along with the one made earlier with the average path length seems suggest that the two different network structures are identical in interpreting network dynamics.

Case 1 which is the general network is plotted in Fig. 11. While the constituents interacting with one another, properties such as constituent energy, degrees of coupling k and J, constituent position and velocity are all nonstationary at the constituent level. Emergent ensemble dynamics is the consequence of these constituent properties being coupled together. While the constituent properties are inherently time-varying and complex, however, the corresponding information entropy of the network system as seen in Fig. 11(g) stays relatively stable, thus signifying dynamic stability. Had the variation magnitude of the information entropy been greater, the state of the ensemble dynamics of the complex network would have been unstable.

It is also noted that there are 3 distinct stages in the evolving dynamics. In the initial stage, all constituents engage in mutual interaction, acquire acceleration as dictated by the Kuramoto law, and move toward each other. As the constituents approach one another, the potential energy decreases while the kinetic energy remains at maximum. As a result, the network evolves to a more stable state while maintaining the same collective behavior. Once the constituents are close enough to one another, the network moves into a stage in which all the network properties vary in time facilitating the ensemble to evolve and settle in a state of equilibrium. The entropy is seen to oscillate during the stage, signifying that the network system is in dynamic inequilibrium but not of a degree sufficient to disrupt the initial collective behavior. Eventually the network reaches a stage of dynamic equilibrium with the entropy restored to the initial value and ensemble energy stabilized. As the complex network develops from a random initial ensemble state to a stabilized ensemble state, the mandate that system dynamics be maintained results in the emergence of synchronization with the constituents swirling about one another at the same velocity.

Upon being excited or perturbed, a complex network may evolve and synchronize with the ensemble energy follows a defined probability distribution. Or it may collapse. In Case 1, the

network evolves toward synchronization. However, the corresponding degrees of coupling k and J stay fluctuating when network dynamic equilibrium is reached. Since the spatial relationship between the constituents remains dynamical, the degrees of coupling k and J must evolve accordingly.

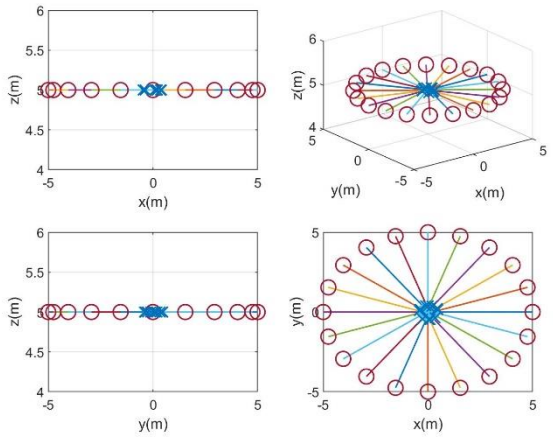

(a)

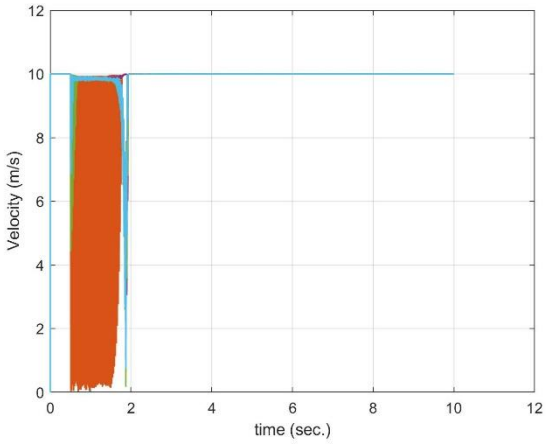

(b)

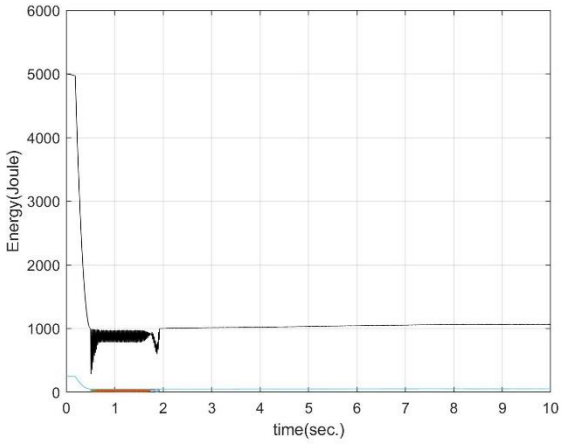

(c)

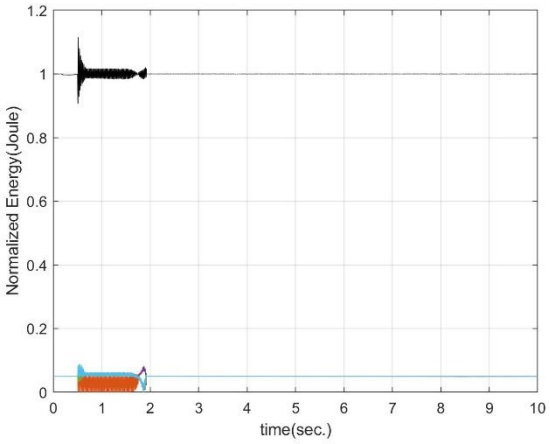

(d)

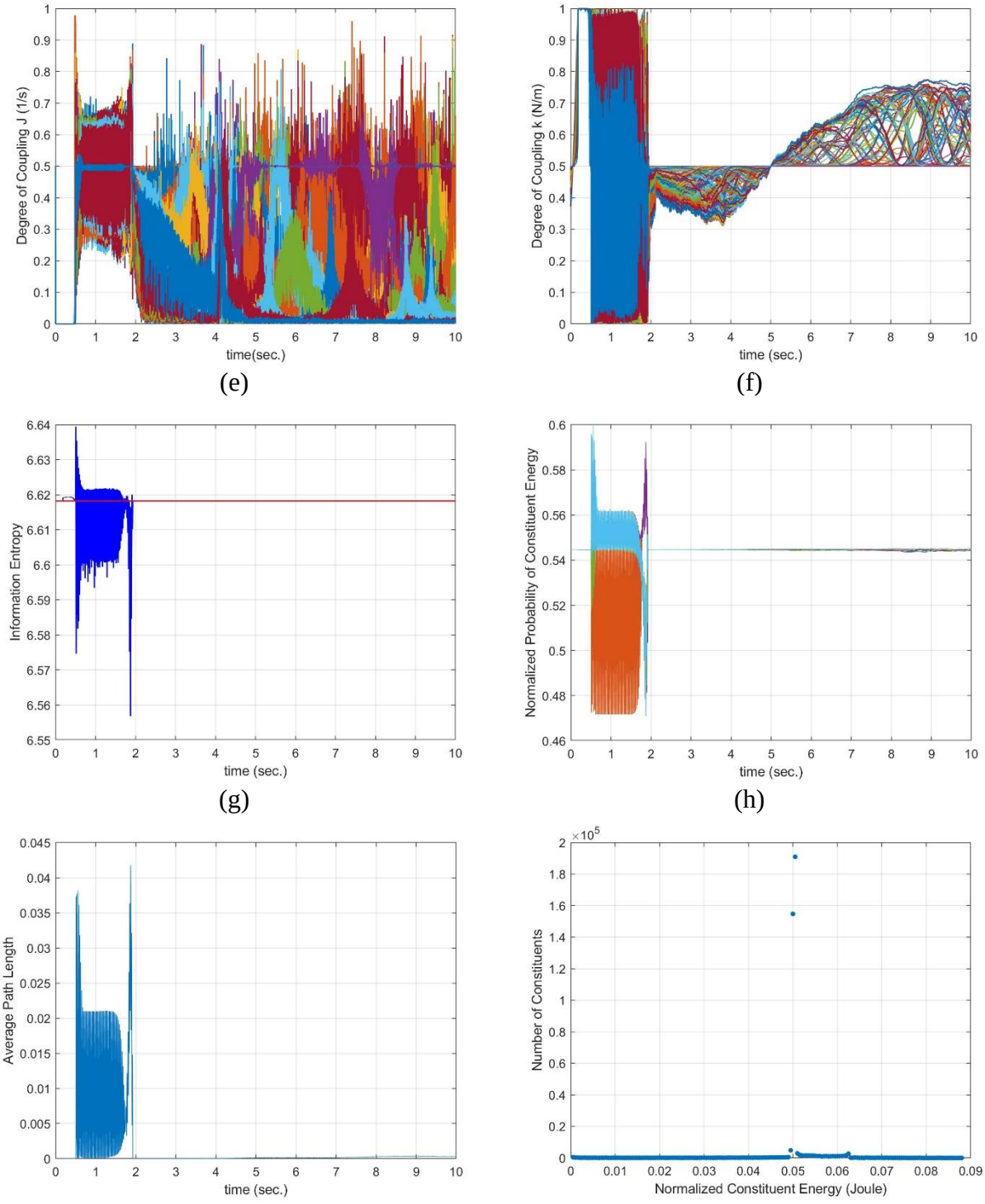

Fig. 11 Case 1-- 20-constituent general framework network model (a) Trajectory, (b) Velocity, (c) Constituent energy, (d) Normalized constituent energy, (e) Degree of coupling *J*, (f) Degree of coupling *k*, (g) Entropy, (h) Probability of entropy, (i) Average path length, and (j) Constituent Energy distribution

Figs. 12 and 13 show that while Case 2 and Case 3 are static structures, with the exception of the degrees of coupling k and J which are held as constants, their corresponding network properties are time-varying. Similar to Case 1, both cases feature an initial stage in the first 0.5 seconds within which the entropy is seen to increase with decreasing constituent energy, thus signifying that the networks are evolving to seek to reach equilibrium. However, the two cases never reach dynamic equilibrium within the 10 seconds time window as Case 1 does. A change of dynamic state experienced by a network constituent will impact the dynamic state of the entire ensemble. With some constituents connected and some not, the small-world and scale-free networks considered in Case 2 and Case 3 have less connections than the Case 1 network of the same number of constituents has. As coupling is less extensive, the time needed for Case 2 and Case 3 to reach dynamic equilibrium with all the constituents being in sync would therefore be significantly longer. In addition, through allowing constituent coupling to be updated at the constituent level. the time dependent degrees of coupling k and J in Case 1 construct a dynamic network that enable energy to be transmitted and distributed among different sections of the network at the ensemble level. With the degree of coupling being either 1 or 0, Case 2 and Case 3 are inherently rigid - a property not at all favorable for mitigating instability.

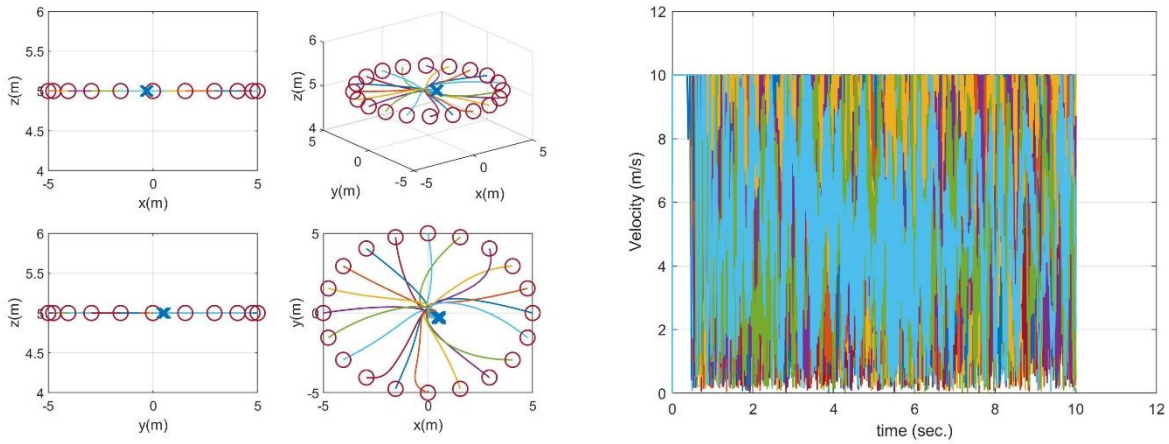

(a) (b)

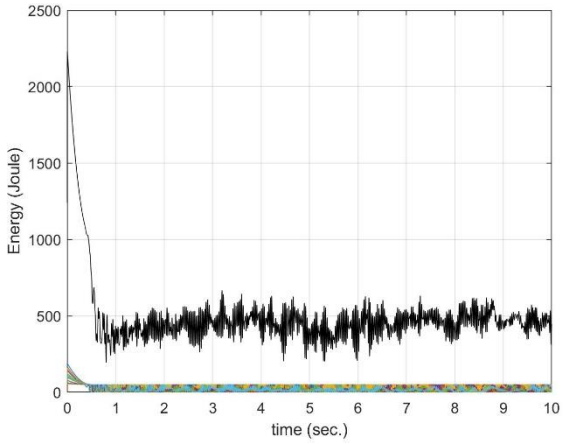
Energy (Joule)
time (sec.)

(c)

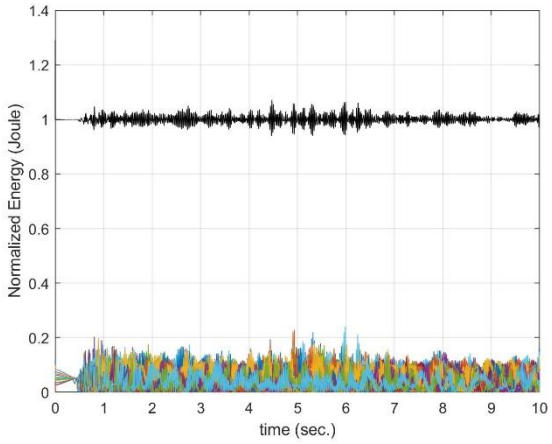
Normalized Energy (Joule)
time (sec.)

(d)

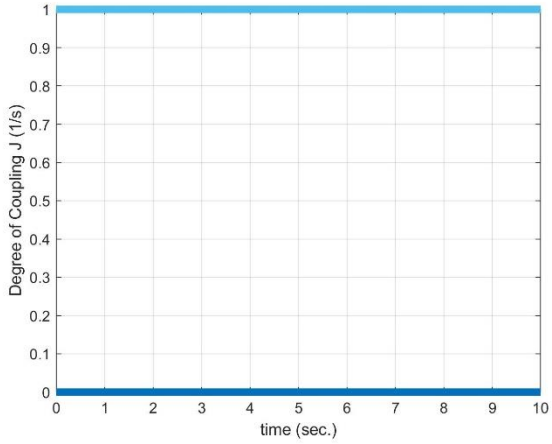
Degree of Coupling J (1/s)
time (sec.)

(e)

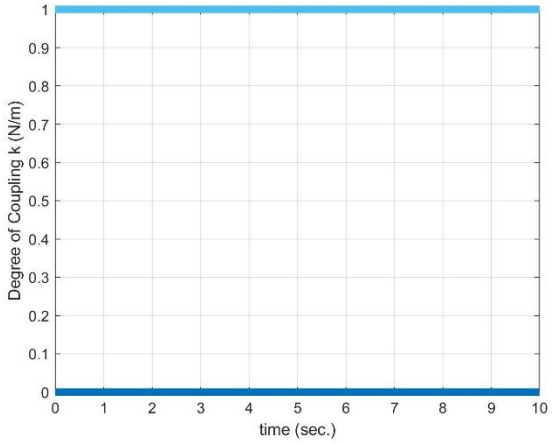
Degree of Coupling k (N/m)
time (sec.)

(f)

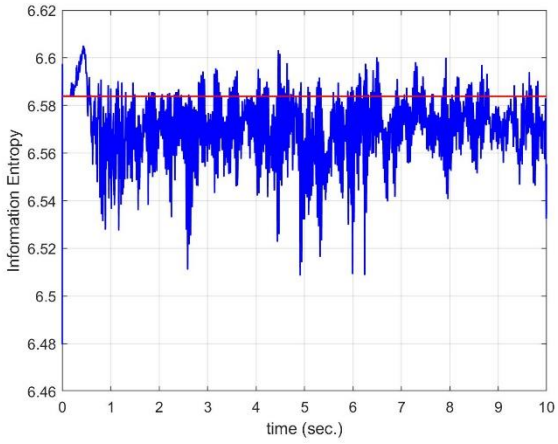
Information Entropy
time (sec.)

(g)

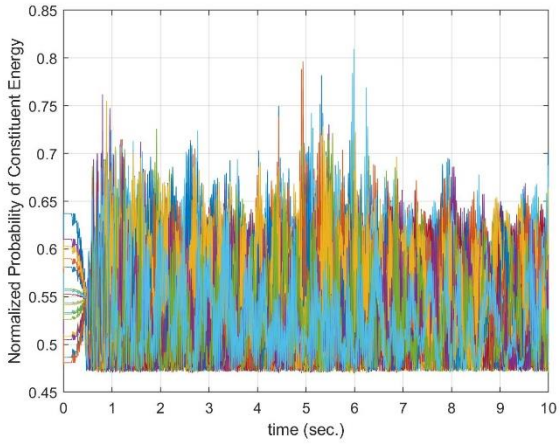
Normalized Probability of Constituent Energy
time (sec.)

(h)

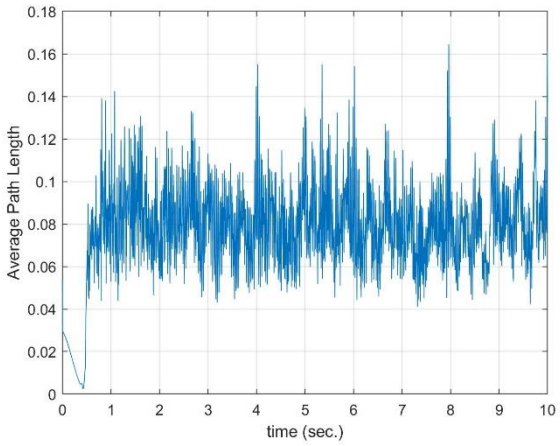

(i)

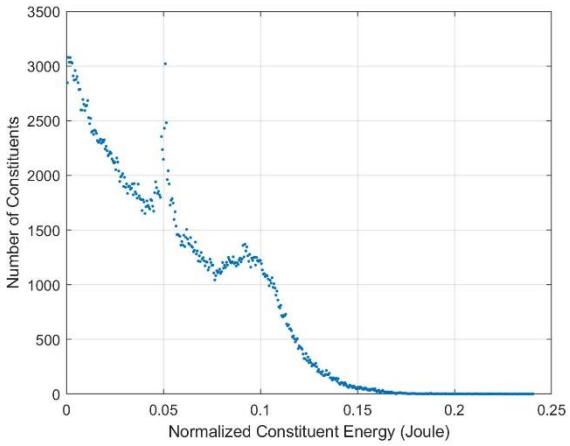

(j)

Fig. 12 Case 2 -- 20-constituent WS small-world network model of degree = 4, p = 50% (a) Trajectory, (b) Velocity, (c) Constituent energy, (d) Normalized constituent energy, (e) Degree of coupling *J*, (f) Degree of coupling *k*, (g) Entropy, (h) Probability of entropy, (i) Average path length, and (j) Constituent Energy distribution

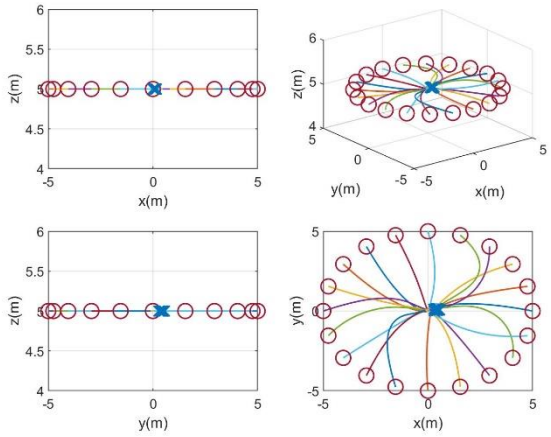

(a)

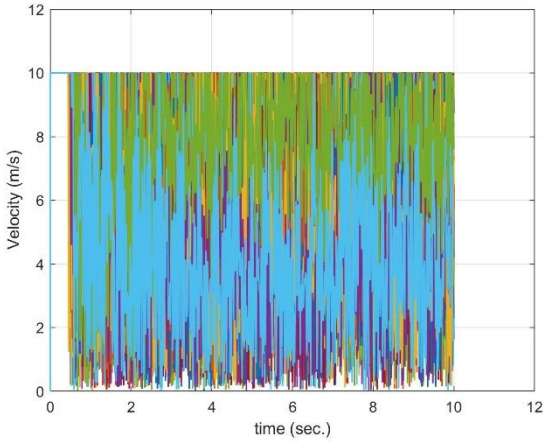

(b)

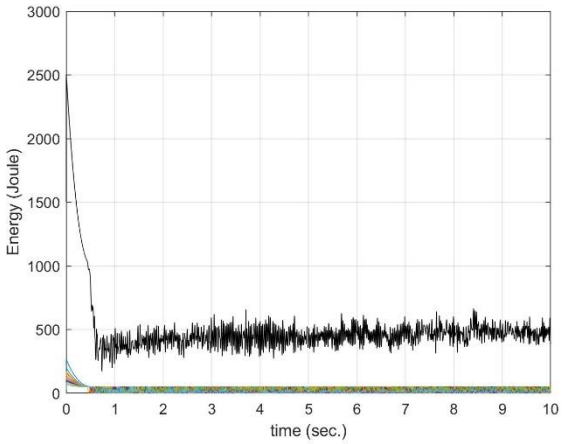

(c)

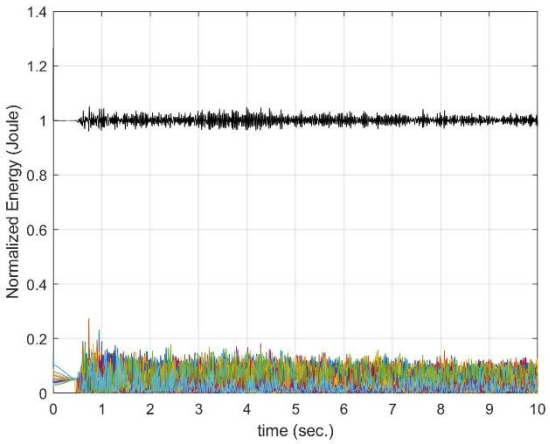

(d)

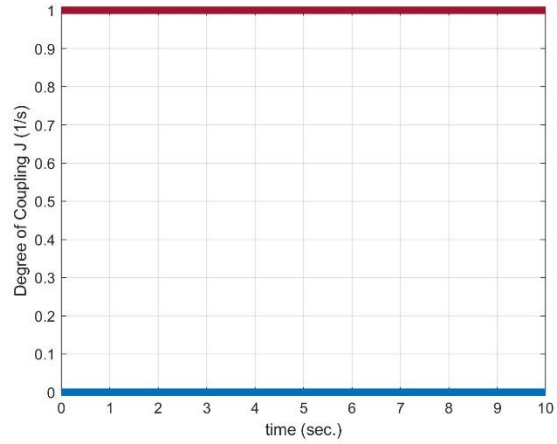

(e)

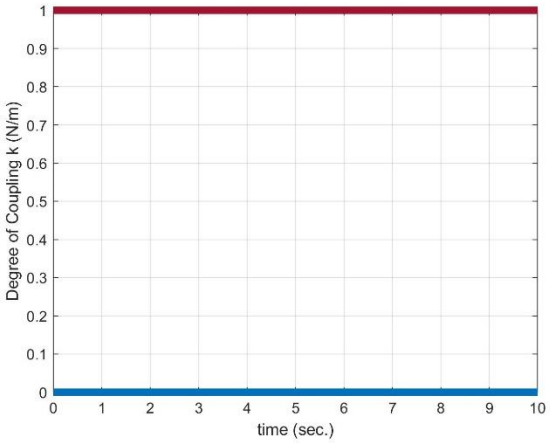

(f)

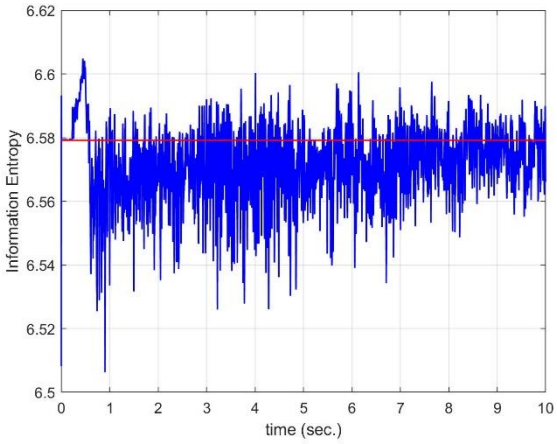

(g)

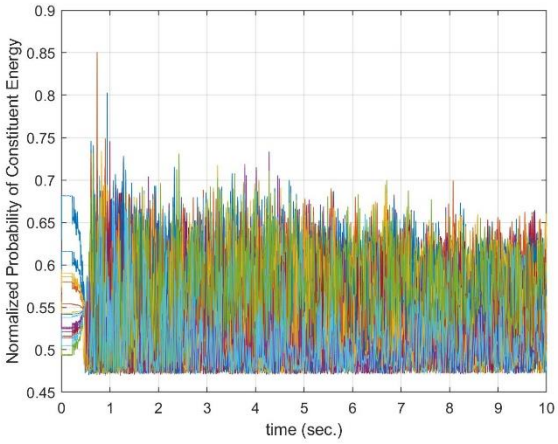

(h)

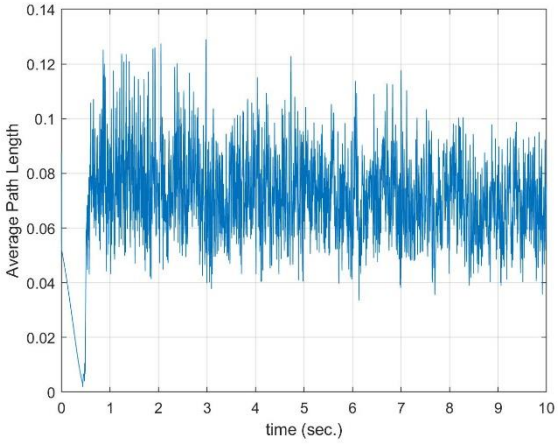

(i)

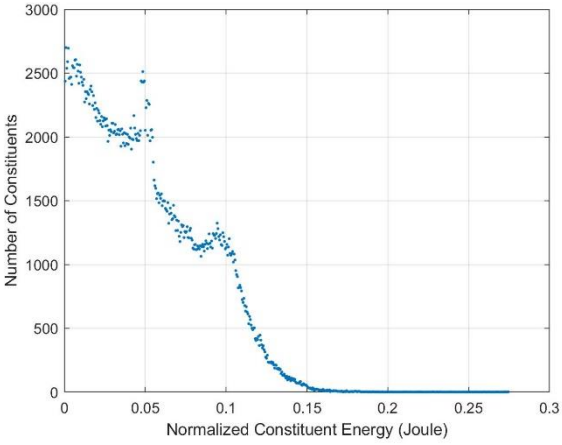

(j)

Fig. 13 Case 3 -- 20-constituent BA scale-free network model with $\mathbf{k_i(t) = m(t/t_i)^{\frac{1}{2}}}$, $\mathbf{m_0 = m = 2}$ (a) Trajectory, (b) Velocity, (c) Constituent energy, (d) Normalized constituent energy, (e) Degree of coupling *J*, (f) Degree of coupling *k*, (g) Entropy, (h) Probability of entropy, (i) Average path length, and (j) Constituent Energy distribution

Figs. 12(b) and 13(b) shows that the velocities of all the constituents vary wildly in Case 2 and Case 3 while no such velocity variations in the equilibrium state for Case 1 as seen in Fig. 11(b). Also, Figs. 11(c), 12(c) and 13(c) show that the total constituent energy for Case 2 and Case 3 are half of Case 1's. The average path length in Case 1 in Fig. 11(i) is about 1 tenth of its counterparts' in Figs. 12(i) and 13(i). The corresponding probability of constituent energy in Figs. 12(h) and 13(h) are seen to not only oscillate more prominently but also with a greater magnitude than Fig. 11(h). The implication for having less connections is that more energy is required to keep rigidly connected constituent pairs having a large energy gap between them. As a result, Figs. 12(h) and 13(h) indicate that Case 2 and Case 3 have less total constituent energy to go around for the ensemble to respond to disturbance. Therefore, static networks are more likely to collapse under impact and disturbance than general complex networks. This is insightful as to why natural complex networks are resilient and robust while artificial networks following static network models are vulnerable to attack and prone to collapse.

Fig. 12(g) shows that the peak entropy oscillates while the error between the equilibrium and initial entropy decreases over time. Also oscillating with decreasing amplitude and error, however, the peak entropy for Case 3 in Fig. 13(g) does not demonstrate similar features as Case 2's. It is evident from Figs. 12(g), 12(h), 13(g), and 13(h) and Figs. 12(c), 12(d), 12(i), 13(c), 13(d), and 13(i) that the two static network models convey similar properties at the constituent level. These observations support the commonly accepted statement that small-world networks are less centralized networks while scale-free networks are more centralized networks. The average distance of small-world networks is greater than that of scale-free networks. Consequently, disturbances would bounce back and forth in small-world networks before diminishing. It is not the case with scale-free networks where any constituent variation would

transmit through the hubs to reach other constituents in the ensemble. As disturbances are received by and distributed through hubs, thus oscillation amplitudes in Case 3 decrease gradually without showing many oscillation peaks.

The general framework makes explicit the underlying constituent and ensemble dynamics of the complex network in Case 1, allowing the collective behaviors of the ensemble to be described following physical laws using parameters having definitive physical units. Case 2 and Case 3 are special cases of the general framework with time-invariant degrees of coupling. Investigating networks by taking time snapshots of the graph theory-based, topological network structures risks misinterpreting the true network dynamics. Furthermore, the small-world network in Case 2 and the scale-free network in Case 3 do not differentiate themselves in the average path length and degree distribution, thus rendering similar interpretations for the underlying network.

3.2 Control of Complex Network Models

Complex networks could experience (1) interruption to connections such as breakage of transmission signal between communication towers, or among drone fleets, that causes temporary change to network structure, and (2) disruption induced by changing the number of constituents such as the removal or addition of a constituent (commonly seen in flocking birds and schooling fish) characterizes by a permanent change to the network structure. Both scenarios could have an immediate impact on network structure, aggravating network stability and structural integrity and delaying eventual synchronization. Table 2 shows the three scenarios of disruption and the three control cases for a 20-constituent complex network considered in the investigation. In Scenario 1 the network evolves under the steering of the Kuramoto law to eventual synchronization without being disrupted. In Scenario 2 the network is perturbed by a temporary disturbance to constituent connections where the probability of connection breakage follows a normal distribution. The

disruption in Scenario 2 impacts the connection quality and perturbs the structural integrity of the network. In Scenario 3, the network is not only experiencing the same disruption as in Scenario 2, but also disrupted with permanent disturbances caused by constituents detaching from the ensemble and joining the network. In Scenario 3 the network is so severely perturbed that the varying number of constituents destabilizes structural integrity and results in a permanent alteration to the network structure. Nonlinear time-frequency control (to be elaborated in the sections that follow) is applied to the three scenarios to investigate the resilience of the perturbed network in response to disruption and the resulted instability. Controls are applied to 1 constituent in Case B and to all the constituents in Case C before being evaluated against Case A, the baseline case, where no control is exerted. The three scenarios subject to no control are considered in the present section where entropy time history and the phase of k-J coupling are presented.

Table 2. Scenarios of disruption and cases of control

Scenario 1 – No Disruption		
Case A Control applied to 0 constituent	Case B Control applied to 1 constituent	Case C Control applied to all constituents
Scenario 2 – Temporary Disruption (Random breakage of connections)		
Case A Control applied to 0 constituent	Case B Control applied to 1 constituent	Case C Control applied to all constituents
Scenario 3 – Temporary and Permanent Disruptions (Random breakage of connections and departure and joining of constituents)		
Case A Control applied to 0 constituent	Case B Control applied to 1 constituent	Case C Control applied to all constituents

At t=0s, the same initial conditions are specified to all the cases in which 20 constituents are evenly spaced out on the peripheral of a 5-meter in radius circle with zero velocity. The center of the circle overlaps with the origin of the Cartesian x-y plane. Initial degrees of coupling k=0.5 N/m and J=0.5 s-1 are given to all the connections. As the distance between each constituent and the degrees of coupling are known, the constituent energy and entropy of the network are also known. An iteration time step of 0.0005 seconds is followed. The entropy of the probability of the ensemble energy is held constant to maintain invariant network dynamics. Constituent and ensemble states are computed to monitor network parameters as they evolve in time.

Fig. 14 illustrates the spatial relationship of the constituents of Case A in Scenario 1. Fig. 14(a) shows the constituent trajectories with a circle and a cross indicating the initial and final positions, respectively. Fig. 14(b) shows the velocity of the constituents in time. Fig. 14(c) plots the variation of the distance between each constituent in time. The average distance of all the constituents is given in Fig. 14(d). Crosses in the time-snapshots in Fig. 14(e) through Fig. 14(l) indicate the positions of the constituents at 8 different time instances. The circles indicate the position at t=0s. At approximately t=3.2s the constituents are seen to start swirling toward one another with the distance increasing between them. The increasing of distance stabilizes at t=10s and the ensemble moves as a group. The spatial relationship between each pair of constituents is seen to vary in Fig. 14 at the constituent level and result in different stages at the ensemble level. At each stage, the spatial relationship at the ensemble level lasts long enough to be observed without significant variation. While constituent positions and velocities are explicit, as indicated by Eqs. (9)-(13), properties that define network dynamics including entropy, energy, probability distribution of constituent energy, and DOCs k and J are implicit. These dynamic properties are indicative of the state of stability of the network.

Case A in Scenario 1

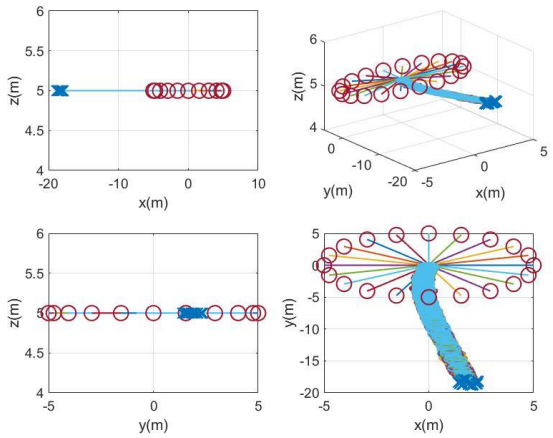

(a)

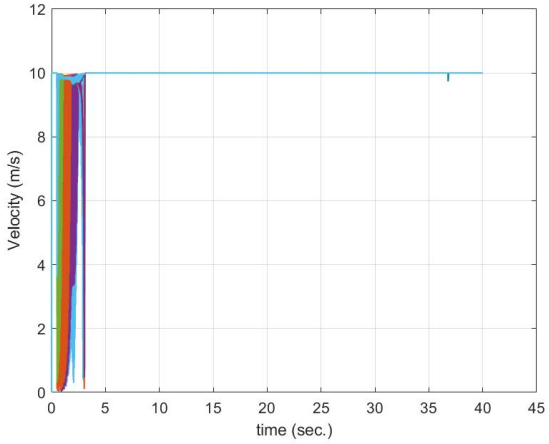

(b)

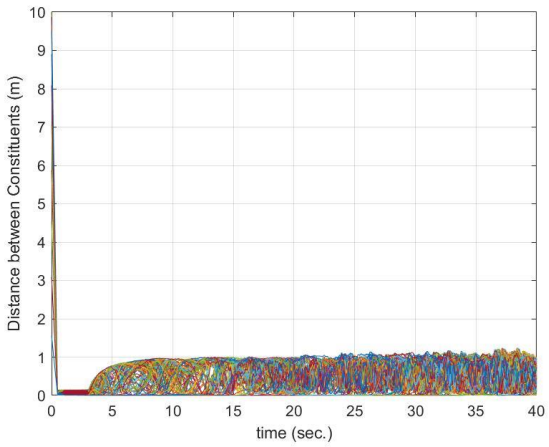

(c)

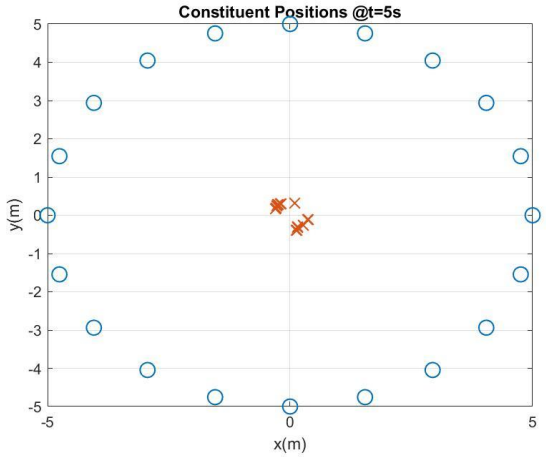

(g)

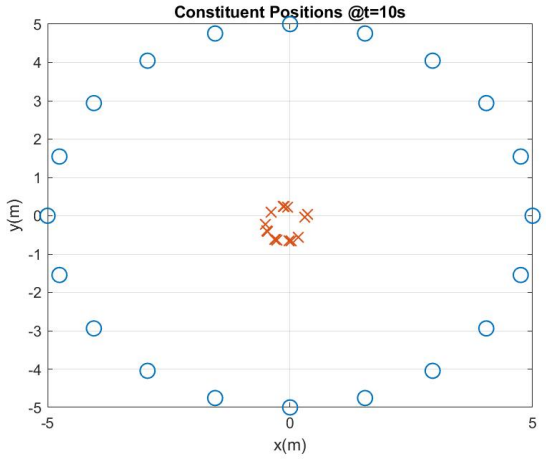

(h)

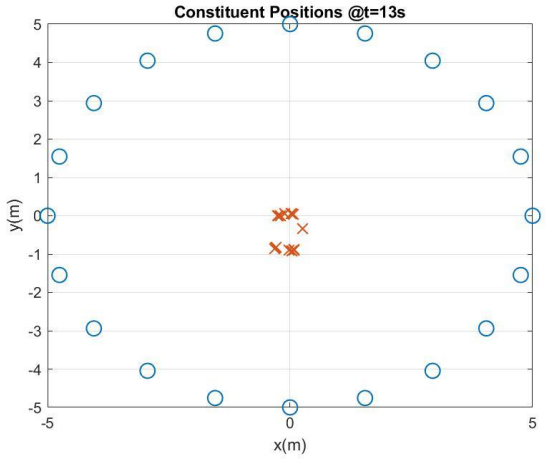

(i)

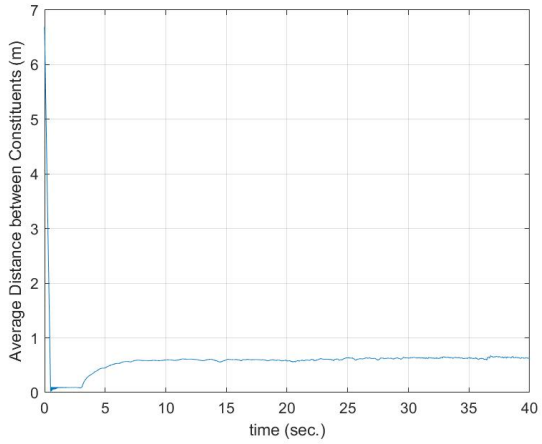

(d)

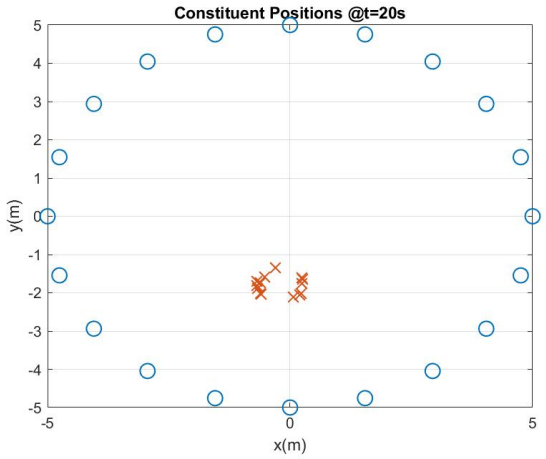

(j)

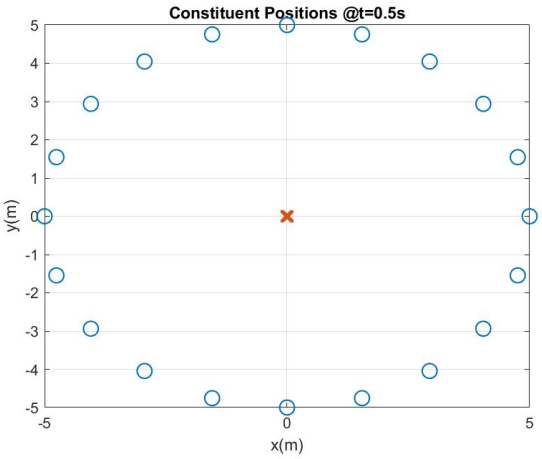

(e)

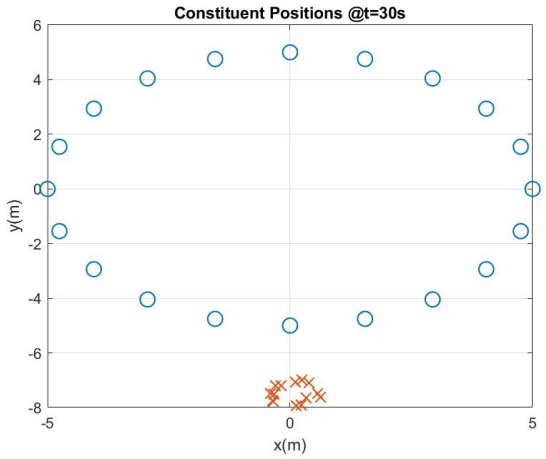

(k)

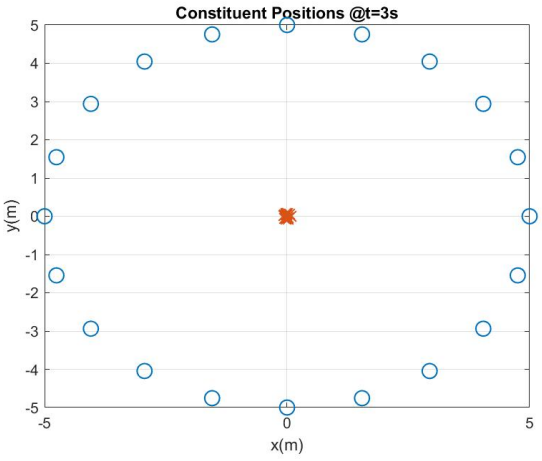

(f)

(l)

Fig. 14 Case A in Scenario 1 – 20-constituent network under no disturbance and not being controlled. Constituent (a) trajectory, (b) velocity, (c) time variation of distance, (d) time variation of average distance, (e) constituent positions at t=0.5s, (f) constituent positions at t=3s, (g) constituent positions at t=5s, (h) constituent positions at t=10s, (i)

constituent positions at t=13s, (j) constituent positions at t=20s, (k) constituent positions at t=30s, and (l) constituent positions at t=40s.

The implicit properties associated with Case A in Scenario 1 are displayed as time histories in Fig. 15. Fig. 15(a) shows the entropy of the 20-constituent network as it stabilizes at t=3.2s. Because Kuramoto law steers collective behavior and dictates eventual synchronization, constituent energy and entropy are seen to stabilize as the network evolves. However, the spikes and broadband response seen in the instantaneous frequency (IF) of the entropy in Fig. 15(b) show that while entropy is stable in the time-domain it is unstable in the frequency-domain. The IF indicates the effort taken by the constituents in adjusting the couplings. This suggests that network control needs be exerted both in the time and frequency domains simultaneously. Moreover, the variations of IF of the entropy is related to the variations of the degrees-of-coupling k and J in Figs. 15(c) and 15(d). Entropy is a function of constituent energy and degrees-of-coupling k and J, with the latter being the most fundamental parameters as they are incorporated with the coupling law defined by Eq. (10). The variations of k and J in Figs. 15(c) and 15(d) suggest that, as a result of obeying the Kuramoto law in Eq. (9), constituent couplings are rapidly adjusted to maintain the stability of entropy. Frequent variations of k and J speak to the instability of the network structure, thus more effort is required of all the constituents to maintain structural integrity. Should there be disturbance to the network, network structure would be even more unstable, and more time would be required to reach synchronization. As it reflects the variations of k and J, IF of entropy is another indicator of network stability and structural integrity.

The time progressions of DOC k (horizontal axis) versus DOC J (vertical axis) in Figs. 15(f), 15(g), 15(h), and 15(i) indicate the evolution of the constituent relationship. Each figure shows the time progression (over a duration of 10 seconds) of phase portraits (each phase portrait illustrates the DOC record for 1 second). This time progression is shown by the phase portrait

from top to bottom. The column on the left gives the k-J phase plots of all the connections. Dictated by the Kuramoto law, the distributions of k-J phase plots are seen to converge to a finite bounded range after t=4s signifying that the network is evolving toward synchronization. Network synchronization is reached when all the k-J phases converge to a point. The range of k-J phase plots indicates that the dynamic response of constituent couplings is nonlinear [36-40]. As the constituents' states evolve, the k-J phases also shift. This shift of k-J phases is better observed using the column on the right where the averaged k (horizontal axis) versus the averaged J (vertical axis) of all the couplings are plotted. The time progression of the averaged k-J phases is seen to cluster and rapidly stabilize to zero along the vertical axis at t=4s and to 0.2 at t=30s along the horizontal axis. That is, constituent couplings reach the steady-state at t=30s. Closer the averaged k-J phase cluster gets to the coordinate origin at (0,0), less frequent the constituent couplings are adjusted, thus signifying a more "relaxed" relationship between connected constituents. A "rigid" coupling is resulted when the cluster approaches coordinates (1,1). It is seen that DOCs evolve toward the state of synchronization with the couplings becoming less "stiff".

Constituent energy is a function of k and J, the degrees-of-couplings. As indicated by Eqs. (9) and (10), low DOC corresponds to low constituent energy. The total energies in Figs. 15(e) and 15(j), with the latter being a rescaled plot of the former for better clarity, therefore indicate the trend of the averaged k-J phases. As the averaged k-J phases cluster, constituent couplings in Figs. 15(f)- 15(i) along with the constituent energies in Figs. 15(e) and 15(j) are seen to evolve toward a low energy state in which coupling adjustment for maintaining entropy stability is less frequent. In other words, k and J not only become synchronized under the steering of the Kuramoto law, they also enable a network state that requires less energy to maintain stable constituent relationship.

Case A in Scenario 1

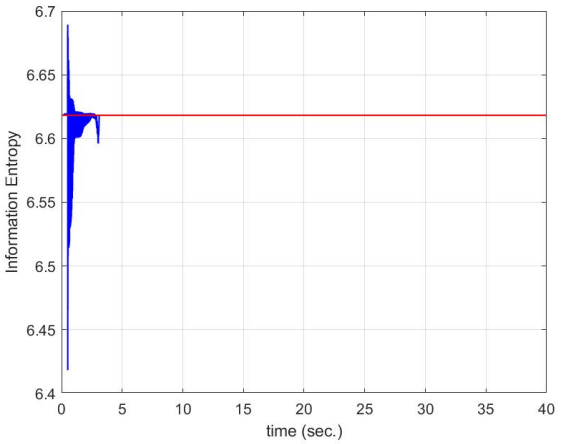

(a)

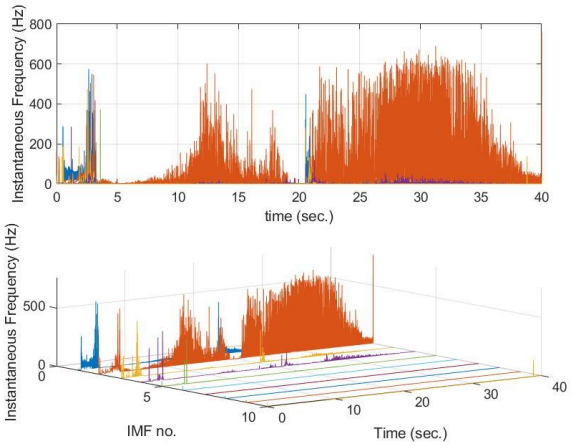

(b)

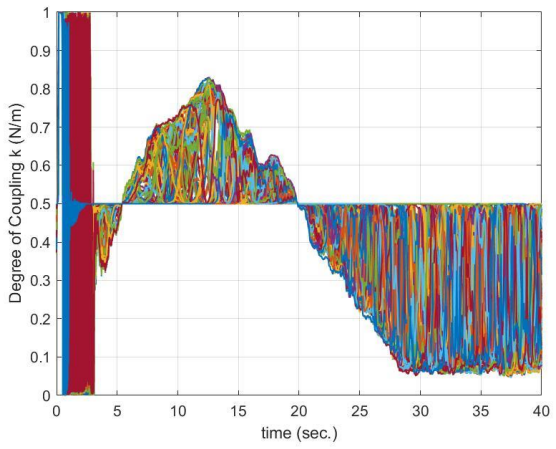

(c)

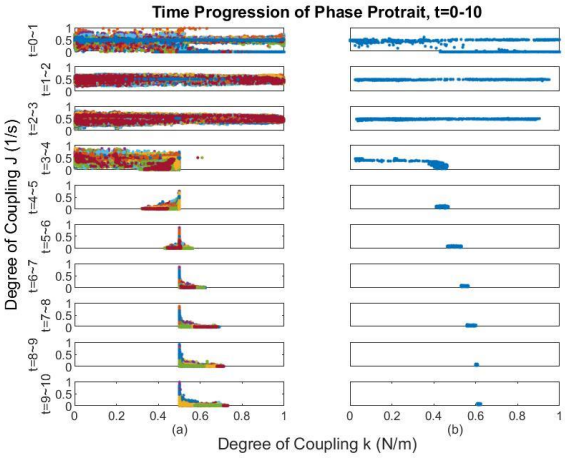

(f)

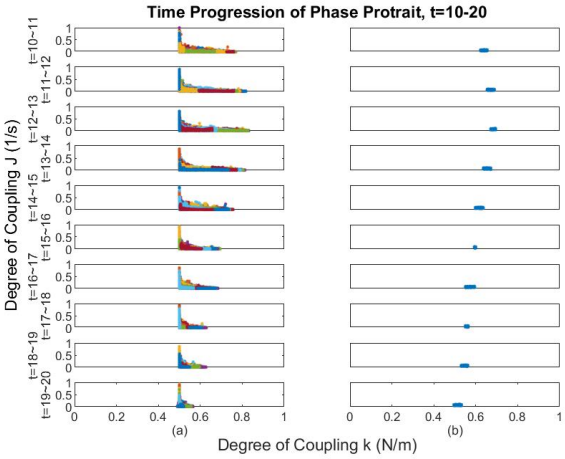

(g)

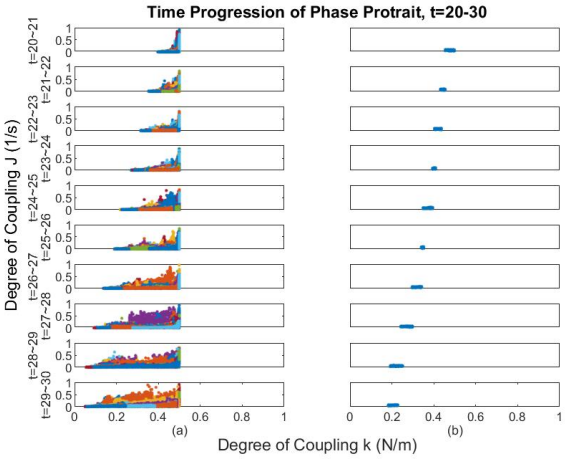

(h)

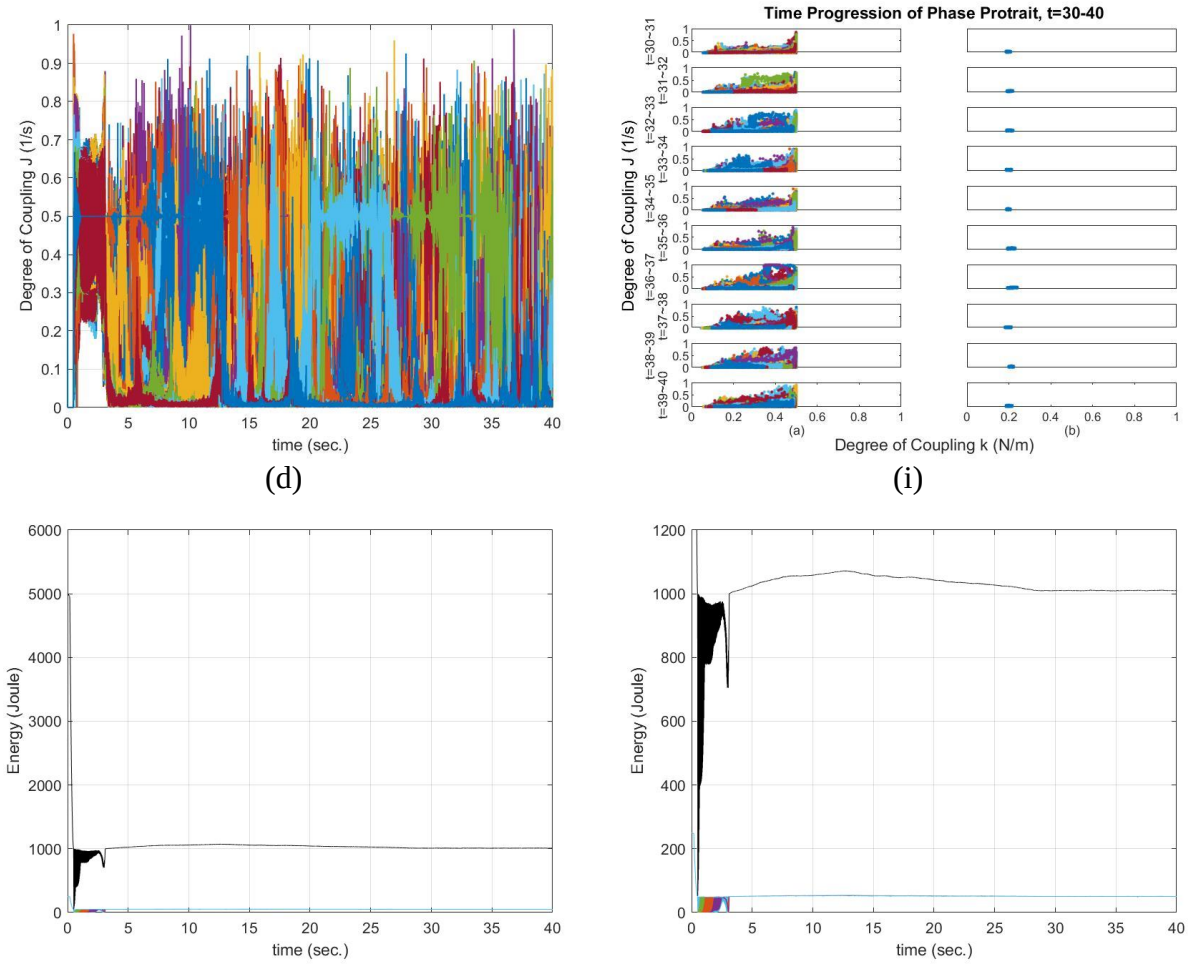

Fig. 15 Case A in Scenario 1 – 20-constituent network under no disturbance and not being controlled. Constituent (a) entropy, (b) instantaneous frequency of entropy, (c) DOC k, (d) DOC J, (e) energy, (f) time history of k-J phase from t=0s to t=10s, (g) time history of k-J phase from t=10s to t=20s, (h) time history of k-J phase from t=20s to t=30s, (i) time history of k-J phase from t=30s to t=40s, and (j) constituent energy (a zoomed-in on Fig. 15(e)).

Case A in Scenario 2 is presented in Figs. 16(a)- 16(e) where the constituent couplings of the 20-constituent network are subject to random temporary breakage following the probability of normal distribution. Fig. 16(a) shows that entropy converges to the target value at t=3.2s as does Fig. 15(a) but with prominent oscillations. Since connections are abruptly broken in random, the IF response of the entropy in Fig. 16(b) is broad in bandwidth, thus indicating that DOCs undergo rapid adjustment to ensure entropy stability. The time progression of k-J phases in Fig. 16(c)

depicts a state that is not as synchronized as Case A in Scenario 1 in the first 10 seconds. Figs. 16(d) and 16(e) shows similar trends as Figs. 15(e) and 15(j) but with a lower constituent energy before stabilizing at t=3.2s. Compared to Case A in Scenario 1, the disturbed network requires more time to reach synchronization.

Case A in Scenario 3 is presented in Figs. 16(f)- 16(j) where the network experiences changing numbers of constituents and random coupling breakage subject to a disturbance identical to the one described in Scenario 2. Network structure in the scenario undergoes both temporary and permanent alterations. The 20-constituent network has one of the constituents detach from it at t=1s and subsequently rejoin at t=4s. A constituent that was not a member of the network joins the network at t=7s. Entropy in Fig. 16(f) is seen to respond to the leaving and joining of constituents accordingly. Figs. 16(f), 16(i), and 16(j) show that both the entropy and energy (1) vary significantly after the constituent detaches from the ensemble, (2) swiftly restore back to the level before detachment when the detached constituent rejoins the ensemble, and (3) register an increase when the constituent joins the ensemble. The IF of entropy in Fig. 16(g) is a broadband response of oscillating amplitudes which indicates the level of effort network constituents are taking to maintain entropy stability. The k-J phase plot in Fig. 16(h) shows that the averaged k-J phase moves toward the coordinate origin as a result of constituent couplings becoming weaker when there are fewer constituents. The averaged phase moves to the opposite extreme of the plot when there are more constituents with stronger couplings. Like Case A in Scenario 2, Case A in Scenario 3 takes more time to reach synchronization than Case A in Scenario 1. It is seen from comparing the response of Case A in Scenario 1 at t=0~3.2s with the response of Case A in Scenario 3 at t=0~7s that after the constituent rejoins the ensemble, the time the network takes to restore back to the dynamic state that was perturbed by the detached constituent is evidently longer.

Constituent leaving and rejoining the ensemble not only impacts the stability of network structure, it also delays the emerging of collective behaviors. In addition, although entropy is stable after the constituent joins the ensemble, the IF of entropy varies in such a way that signifies that the network is dynamically unstable.

Network stability is perturbed, structural integrity is compromised, and synchronization is delayed for both the cases above in response to connection breakage and changing constituent count. To mitigate the impact induced by the noted disruptions it is essential that constituent couplings are controlled to maintain entropy stability and structure integrity. This can be achieved by manipulating degrees-of-couplings k and J. However, it was also observed in the cases associated with Scenarios 2 and 3 that while entropy is stable in the time domain, the corresponding IF of entropy indicates dynamic instability in the frequency domain. This implies that DOCs k and J need be adjusted in both the time and frequency domains in a timely manner if the noted impact is to be properly mitigated.

Case A in Scenario 2

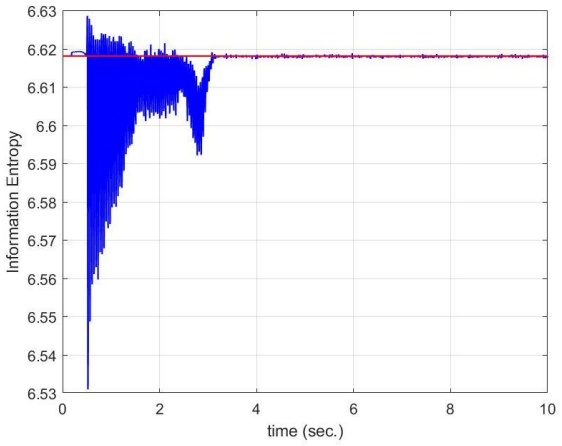

(a)

Case A in Scenario 3

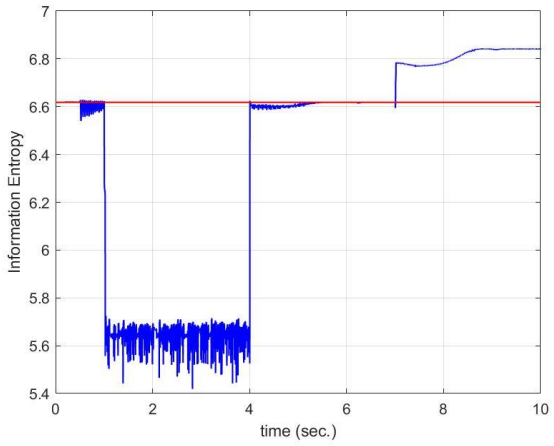

(f)

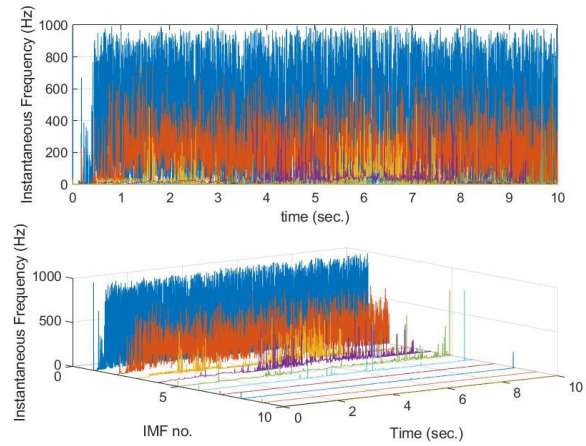
Instantaneous Frequency (Hz)
time (sec.)
Instantaneous Frequency (Hz)
IMF no.
Time (sec.)

(b)

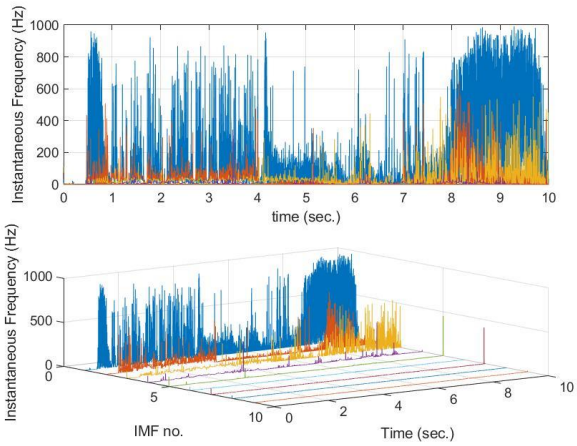
Instantaneous Frequency (Hz)
time (sec.)
Instantaneous Frequency (Hz)
IMF no.
Time (sec.)

(g)

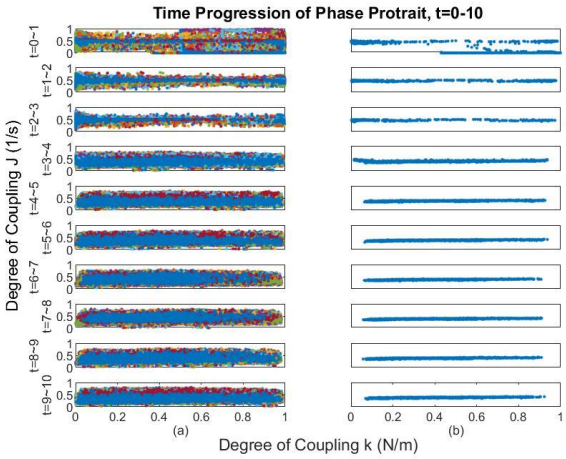
Time Progression of Phase Protrait, t=0-10
Degree of Coupling J (1/s)
t=0~1
t=1~2
t=2~3
t=3~4
t=4~5
t=5~6
t=6~7
t=7~8
t=8~9
t=9~10
(a)
(b)
Degree of Coupling k (N/m)

(c)

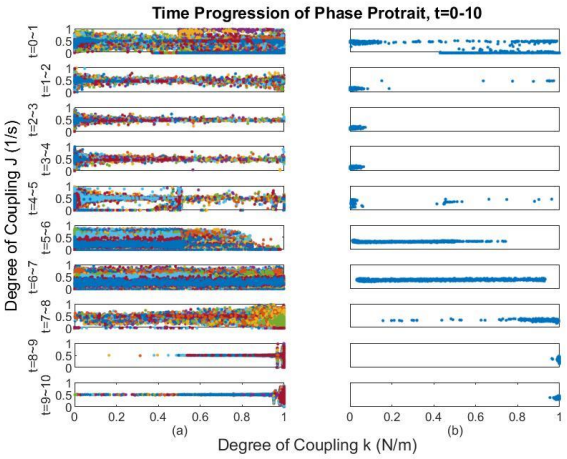
Time Progression of Phase Protrait, t=0-10
Degree of Coupling J (1/s)
t=0~1
t=1~2
t=2~3
t=3~4
t=4~5
t=5~6
t=6~7
t=7~8
t=8~9
t=9~10
(a)
(b)
Degree of Coupling k (N/m)

(h)

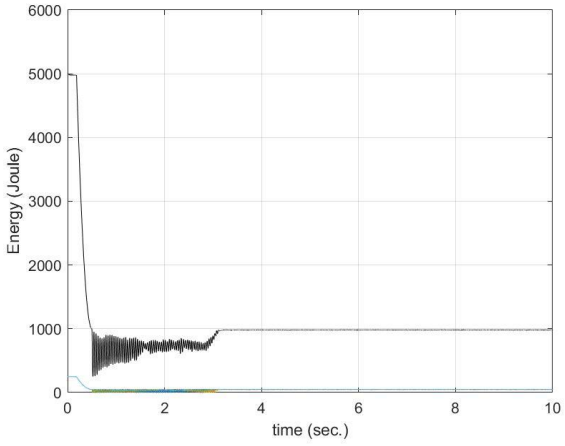
Energy (Joule)
time (sec.)

(d)

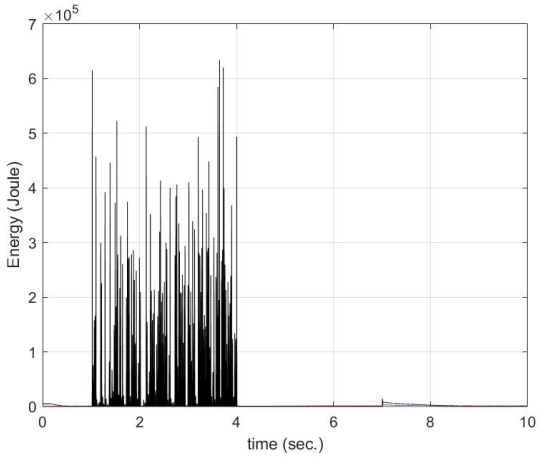
×10^5
Energy (Joule)
time (sec.)

(i)

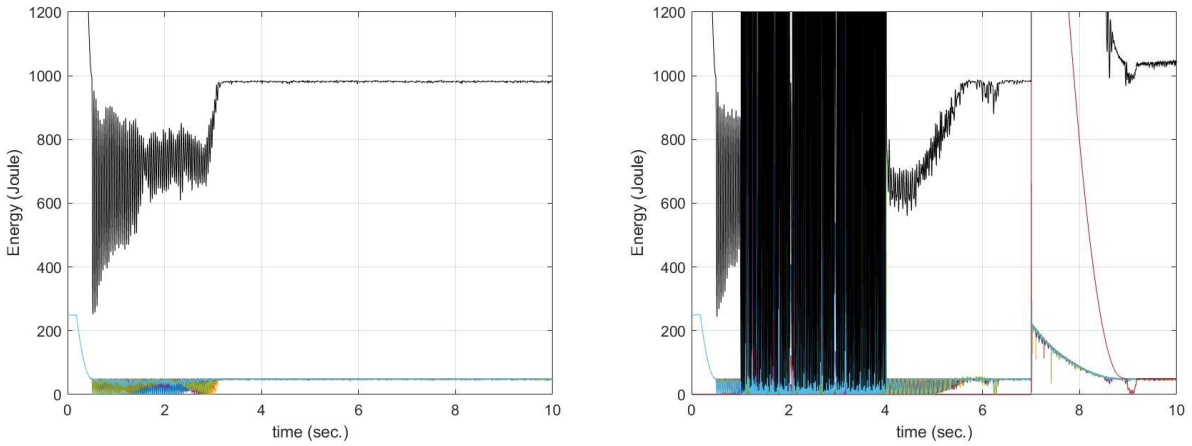

(e) (j)

Fig. 16 Case A in Scenario 2 (left column) – 20-constituent network experiencing random temporary connection breakage with none of the constituent being controlled in (a) through (e). Case A in Scenario 3 (right column) – 20-constituent network experiencing random temporary connection breakage with 1 constituent detached from the network at t=1s and re-join the network at t=4s and a constituent join the network at t=7s in (f) through (j). (a) and (f) entropy, (b) and (g) instantaneous frequency of entropy, (c) and (h) time progression of k-J phases between t=10s and t=20s, (d) and (i) constituent energy, and (e) and (j) constituent energy (zoomed-ins on Fig. 16(d) and Fig. 16(i), respectively).

As the dynamics of individual constituent is coupled with the ensemble's, network stability along with structure integrity can be achieved through tweaking network constituents. However, as is seen in the followings, control exerted through multitudes of couplings demonstrates better robustness in mitigating the instability induced by temporary or permanent disturbance than when a relatively small number of constituents are involved. The controlled Cases B and C in Scenarios 1, 2, and 3 are presented in the section. In all cases, controllers are brought online at t=1s. Fig. 17 shows the controlled Cases B and C in Scenario 1. The results in Figs. 15 and 17 show the difference between the uncontrolled and controlled cases of an undisturbed network. Fig. 18 shows the controlled Case B in Scenario 2 and 3. Fig. 19 shows the controlled Case C in Scenario 2 and 3. The results in Figs. 16, 18, and 19 show the comparison between the uncontrolled and controlled cases of the network under disturbances.

Similar to Case A in Scenario 1 in Fig. 15(a), the entropy seen in Fig. 17(a) also stabilizes at t=3.2s. However, the corresponding instantaneous frequency oscillations in Fig. 17 (b) are significantly reduced, signifying less efforts are required for adjusting DOCs k and J. Case B in Scenario 1 is evidently more stable than Case A in Scenario 1. The k-J phase plots seen in column (a) in Figs. 17(c), 17(d), 17(e), and 17(f) also suggest that Case B in Scenario 1 demonstrates a higher degree of synchronization than Case A in Scenario 1. As constituent couplings are relaxed, less energy is required of the constituents in keeping entropy stable. Column (b) in Figs. 17(c), 17(d), 17(e), and 17(f) shows similar trends as Case A in Scenario 1. That k's and J's are both becoming stabilized is also evident from Figs. 17(g) and 17(h) where the total constituent energy is seen to reach a steady state.

As the time-frequency control scheme successfully ensures the stability of the network structure, controlling a complex network through only one or a few constituents is not ideal. As aforementioned, disturbance and breakage negatively impact the stability of complex network and prolong the time to reach synchronization. When a network is controlled through only one constituent, the controller is unable to affect the constituent at the other end of an unstable or interrupted connection.

Case B in Scenario 1

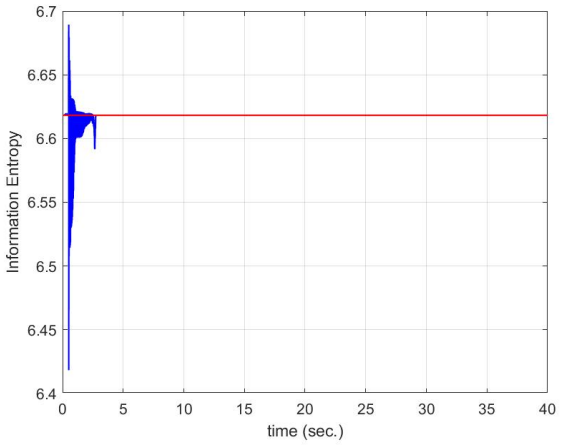

Case C in Scenario 1

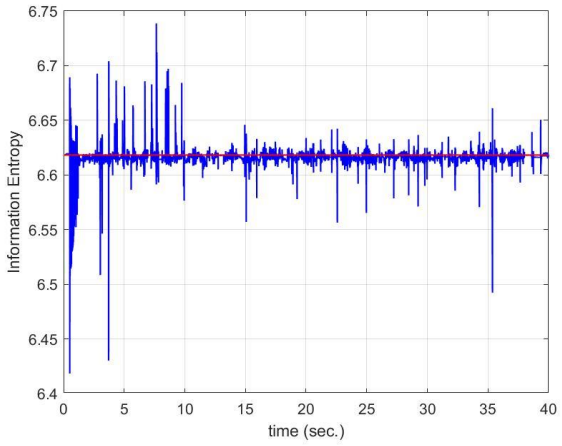

(a)

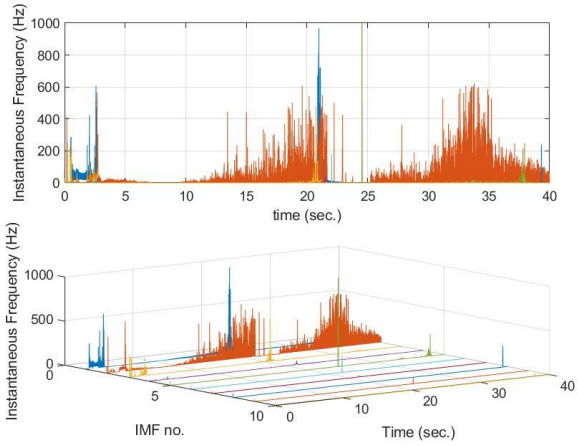
Instantaneous Frequency (Hz)
time (sec.)
IMF no.
Time (sec.)

(b)

(i)

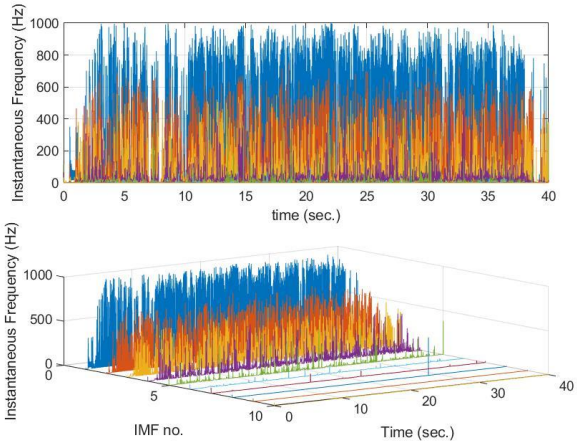
Instantaneous Frequency (Hz)
time (sec.)
IMF no.
Time (sec.)

(j)

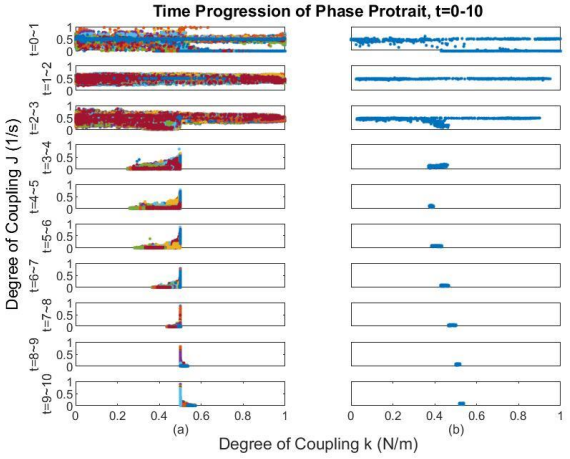
Time Progression of Phase Protrait, t=0-10
Degree of Coupling J (1/s)
Degree of Coupling k (N/m)

(c)

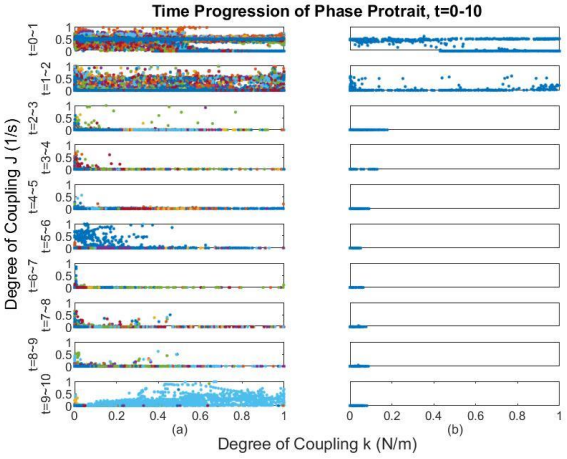
Time Progression of Phase Protrait, t=0-10
Degree of Coupling J (1/s)
Degree of Coupling k (N/m)

(k)

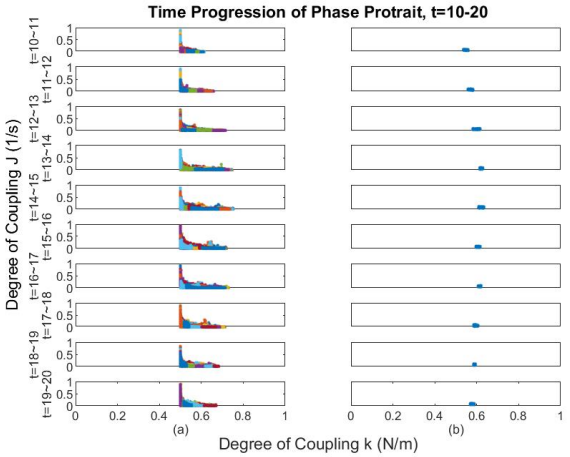
Time Progression of Phase Protrait, t=10-20
Degree of Coupling J (1/s)
Degree of Coupling k (N/m)

(d)

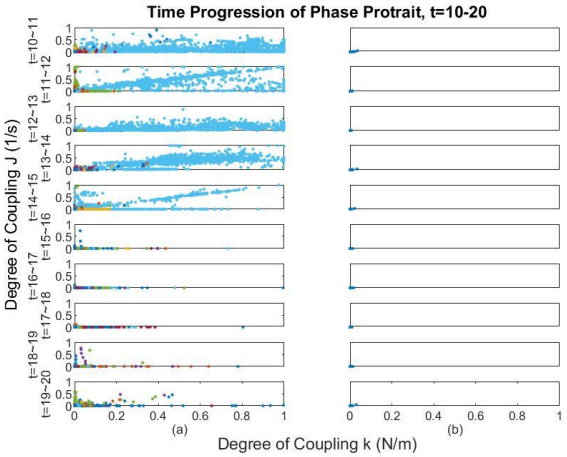
Time Progression of Phase Protrait, t=10-20
Degree of Coupling J (1/s)
Degree of Coupling k (N/m)

(l)

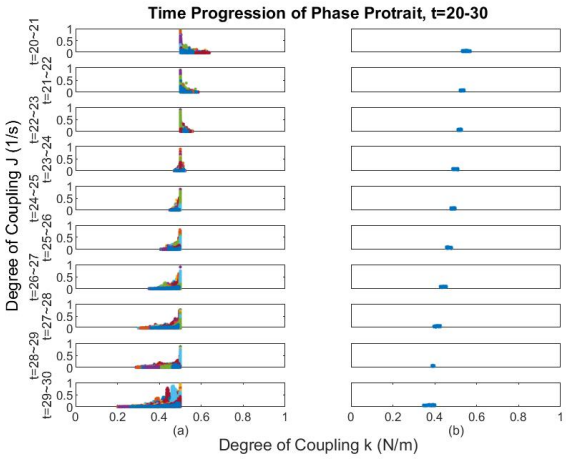
Time Progression of Phase Protrait, t=20-30
Degree of Coupling J (1/s)
t=20~21
t=21~22
t=22~23
t=23~24
t=24~25
t=25~26
t=26~27
t=27~28
t=28~29
t=29~30
(a)
(b)
Degree of Coupling k (N/m)

(e)

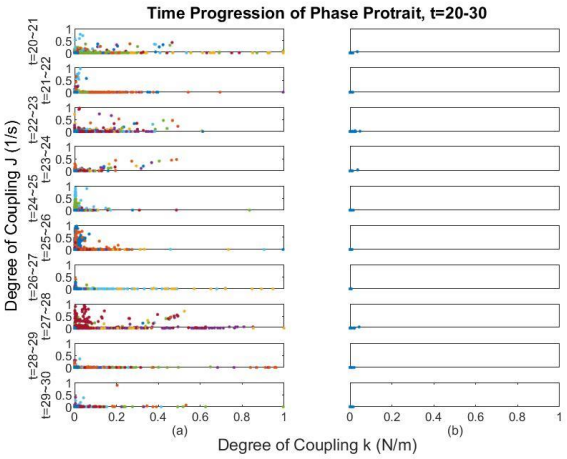
Time Progression of Phase Protrait, t=20-30
Degree of Coupling J (1/s)
t=20~21
t=21~22
t=22~23
t=23~24
t=24~25
t=25~26
t=26~27
t=27~28
t=28~29
t=29~30
(a)
(b)
Degree of Coupling k (N/m)

(m)

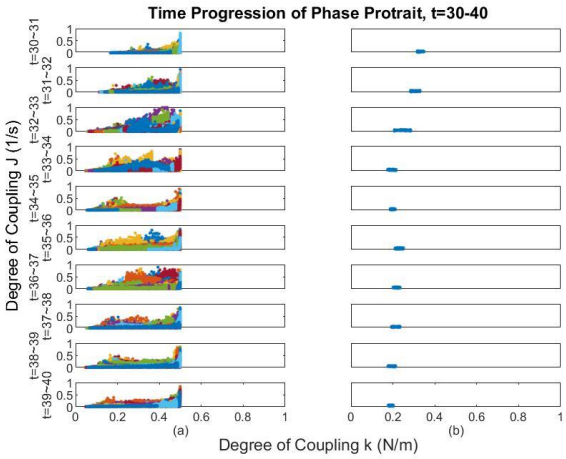
Time Progression of Phase Protrait, t=30-40
Degree of Coupling J (1/s)
t=30~31
t=31~32
t=32~33
t=33~34
t=34~35
t=35~36
t=36~37
t=37~38
t=38~39
t=39~40
(a)
(b)
Degree of Coupling k (N/m)

(f)

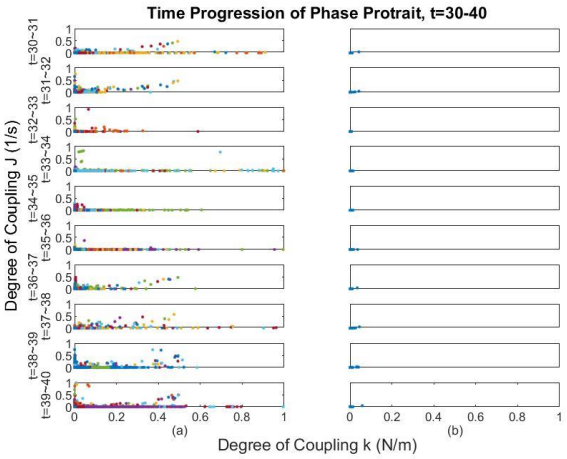
Time Progression of Phase Protrait, t=30-40
Degree of Coupling J (1/s)
t=30~31
t=31~32
t=32~33
t=33~34
t=34~35
t=35~36
t=36~37
t=37~38
t=38~39
t=39~40
(a)
(b)
Degree of Coupling k (N/m)

(n)

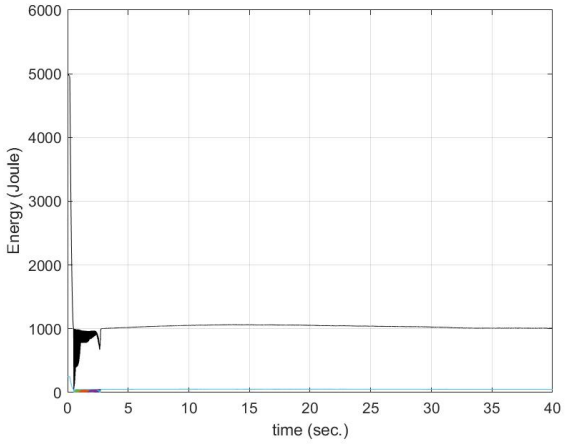
Energy (Joule)
time (sec.)

(g)

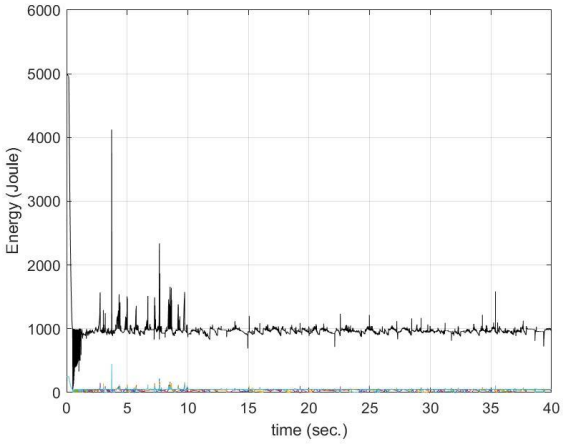
Energy (Joule)
time (sec.)

(o)

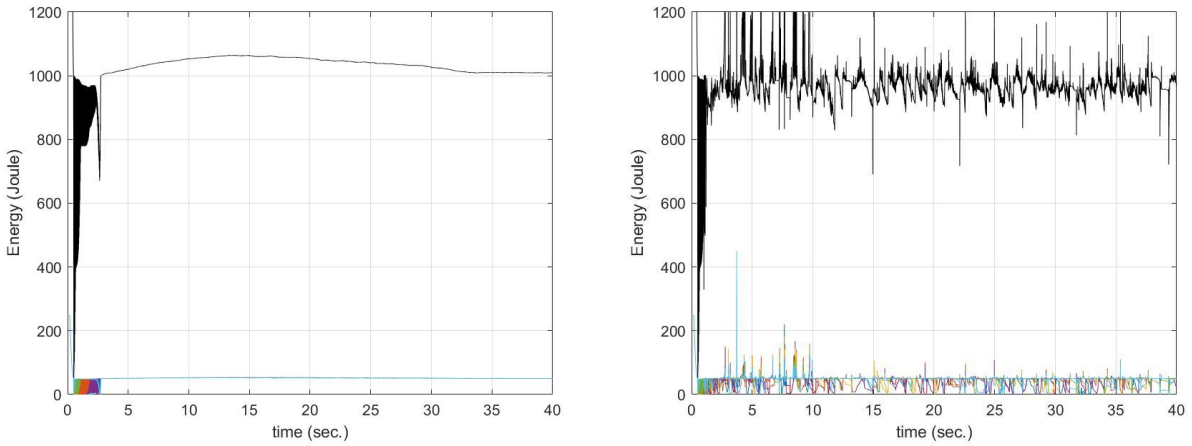

(h) (p)

Fig. 17 Case B in Scenario 1 (left column) – 20-constituent network under no disturbance with 1 constituent being controlled in (a) through (h). Case C in Scenario 1 (right column) – 20-constituent network under no disturbance with 20 constituents being controlled in (i) through (p). (a) and (i) entropy, (b) and (j) instantaneous frequency of entropy, (c) and (k) time progression of k-J phase during t=0~10s, (d) and (l) time progression of k-J phase during t=10~20s, (e) and (m) time progression of k-J phase during t=20~30s, (f) and (n) time progression of k-J phase during t=30~40s, (g) and (o) constituent energy, and (h) and (p) constituent energy (zoomed-ins on Fig. 17(g) and Fig. 17(o), respectively.)

The right column in Fig. 17 displays the results of Case C in Scenario 1 in which control is applied to all the constituents of the 20-constituent network. Entropy in Fig. 17(i) is seen to reach the target level at t=1s at a rate that is faster than Case B in Scenario 1. The broadband IF response of the entropy in Fig. 17(j) indicates that the 2 degrees-of-coupling, k and J, are swiftly adjusted. Column (a) in Figs. 17(k)- 17(n) shows that k-J phase approaches the origin with the corresponding averaged k-J phase in Column (b) seen to converge to the origin as a cluster at t=10~11s, indicating that constituent synchronization is reached essentially at the moment the controller is engaged. The network is stabilized at low degrees-of-coupling requiring minimal energy for constituents to stay connected. The total constituent energy in Fig. 17(o) stabilizes at 1,000 joules at t=10s. Fig. 17(p) shows that individual constituent energies oscillate between 0 and 50 joules which was not observed in Fig. 17(h) where Case B in Scenario 1 was considered.

With both k's and J's being low in magnitudes individual constituent energies as seen in Fig. 17(p) together manifest the lowest energy state of the collective behavior emerged at t=38s.

Case B in Scenario 2

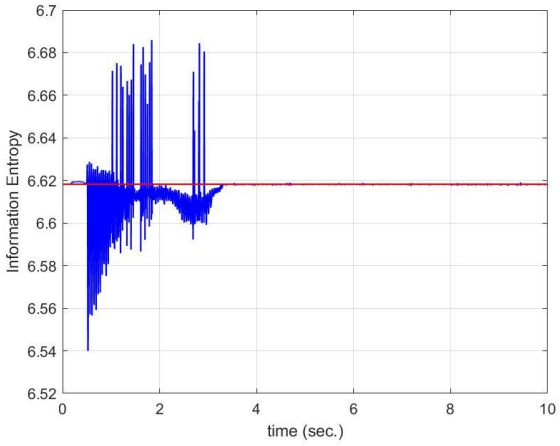

(a)

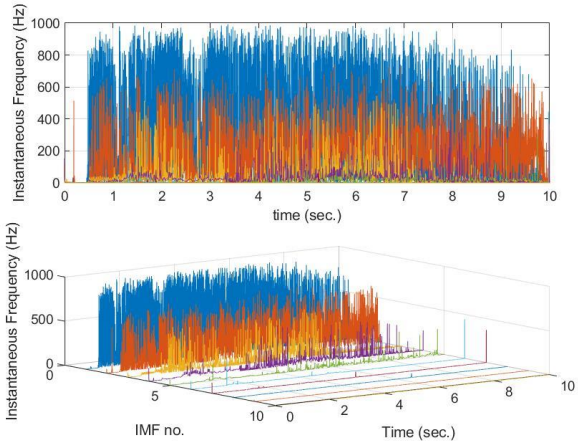

(b)

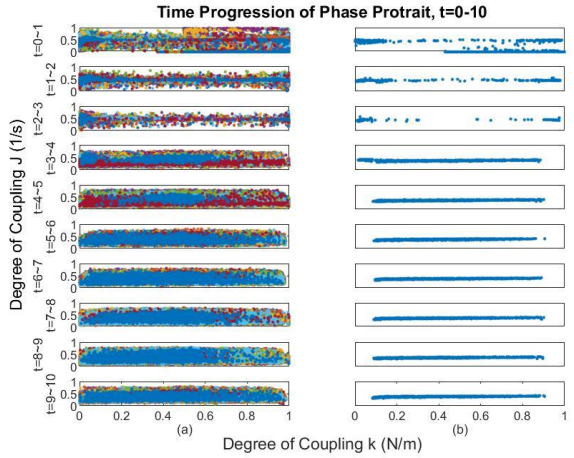

Case B in Scenario 3

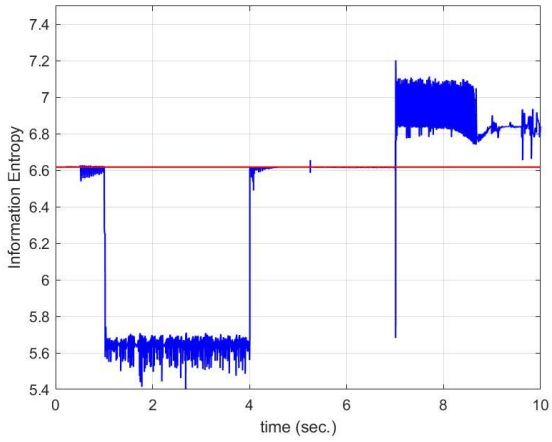

(f)

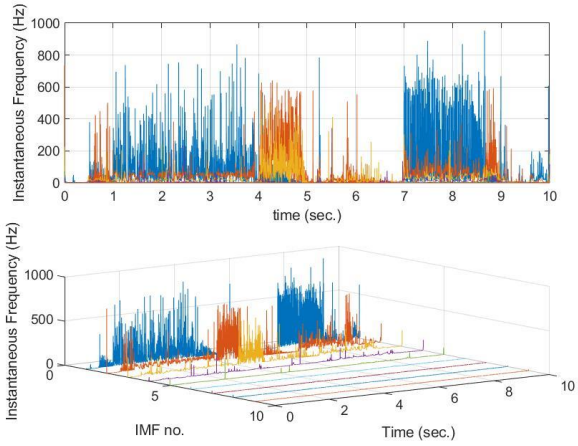

(g)

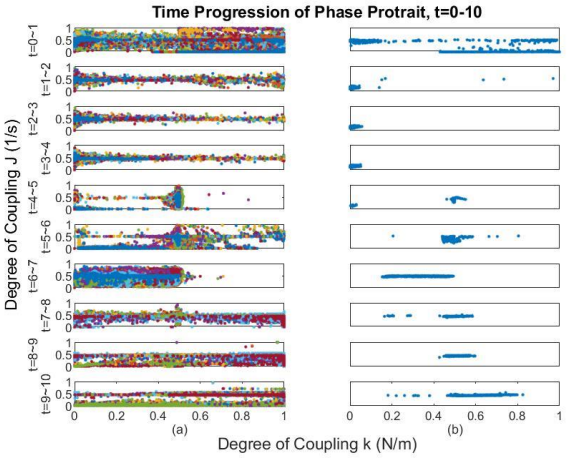

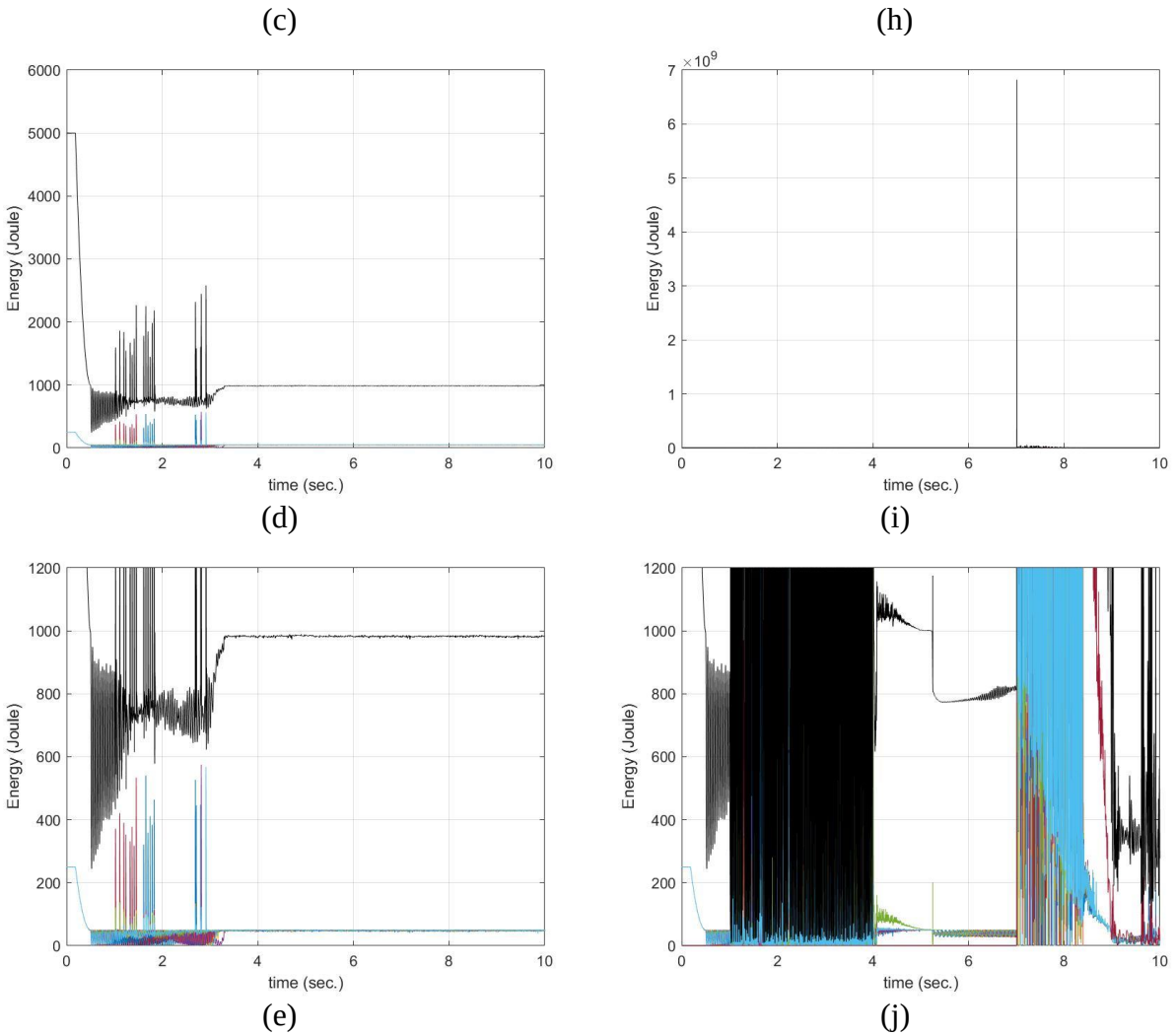

Fig. 18 Case B in Scenario 2 (left column) – 20-constituent network experiencing random temporary connection breakage with 1 constituent being controlled in (a) through (e). Case B in Scenario 3 (right column) – 20-constituent network experiencing random temporary connection breakage with 1 constituent detached from the network at t=1s and re-join the network at t=4s and a constituent join the network at t=7s with 1 constituent being controlled in (f) through (j). (a) and (f) entropy, (b) and (g) instantaneous frequency of entropy, (c) and (h) time progression of k-J phase during t=0~10s, (d) and (i) constituent energy, and (e) and (j) constituent energy (zoomed-ins on Fig. 18(d) and Fig. 18(i), respectively.)

Fig. 18 shows the results of Case B with Scenario 2 in the left column and Scenario 3 in the right column. Entropy variations of Case B in both Scenarios 2 and 3 as seen in Figs. 18(a) and 18(f) are effectively controlled. Entropy amplitudes of Case B in Scenarios 2 and 3 are less than those of Case A in Scenario 2. Instability in Scenario 3 is signified by oscillating entropy in

Fig. 18(f) when one constituent detaches from the ensemble at t=1~4s and after a constituent joins the network at t=7~8.5s. However, network synchronization is expedited despite the disruptions of constituents' joining and exiting from the ensemble. As is evident from Figs. 18(b) and 18(g), the broadband responses of the entropy observed in Case A in Scenario 2 are now being mitigated. While Figs. 16(c) and 18(c) show no significant difference in the k-J phases for Case A and Case B in Scenario 2, nevertheless, Figs. 16(h) and 18(h) suggest that Case B in Scenario 3 reaches synchronization markedly faster than Case A. The total constituent energy in Figs. 18(d) and 18(i) are seen to fast converge with their respective entropies in Figs. 18(a) and 18(f) rapidly becoming stabilized. Constituent dynamics depicted in Figs. 18(e) and 18(j) for Scenarios 2 and 3 are different from their counterparts in Figs. 16(e) and 16(j) that correspond to Scenario 1. While the perturbed states of the network illustrated in Fig. 18 are clearly controlled, however, as observed in Figs. 18(d) and 18(i), steep variations of individual constituent energies ensue from endeavoring to keep all the couplings intact – an indication that network control applied to one constituent would be insufficient in maintaining the integrity of the network structure had the disruption been more severe.

Case C in Scenario 2

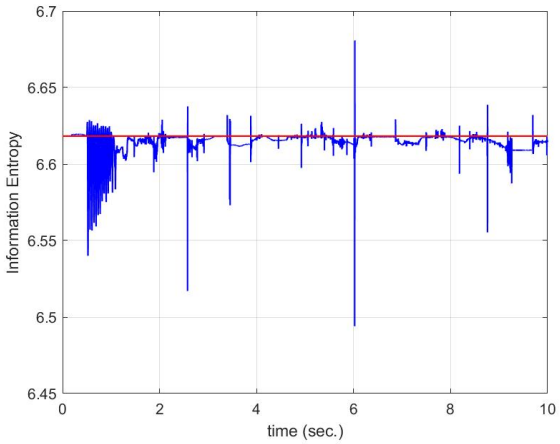

(a)

Case C in Scenario 3

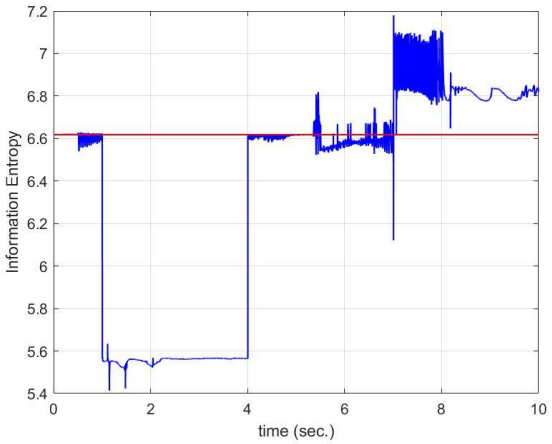

(f)

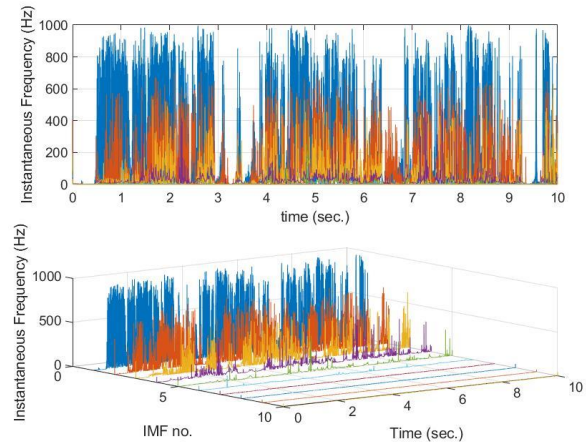
Instantaneous Frequency (Hz)
time (sec.)
IMF no.
Time (sec.)

(b)

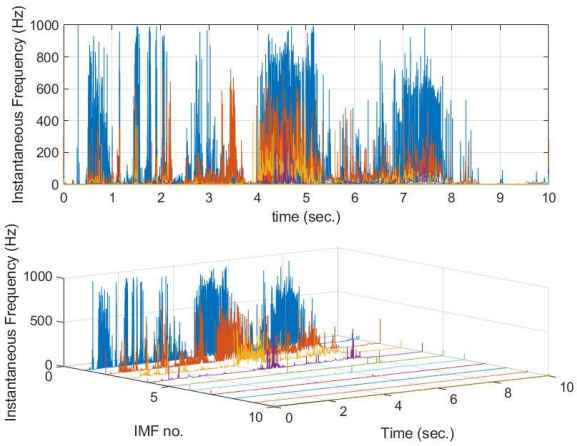
Instantaneous Frequency (Hz)
time (sec.)
IMF no.
Time (sec.)

(g)

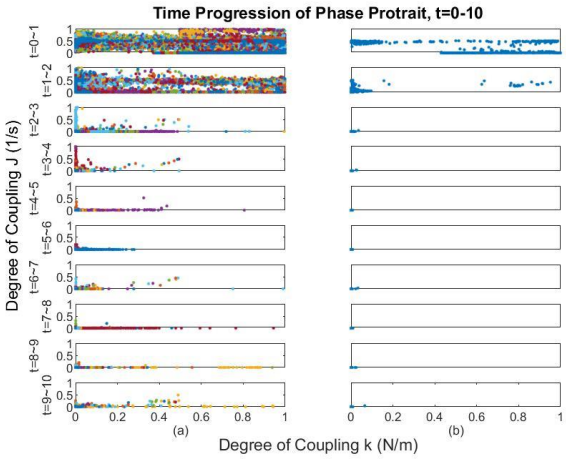
Time Progression of Phase Protrait, t=0-10
Degree of Coupling J (1/s)
Degree of Coupling k (N/m)

(c)

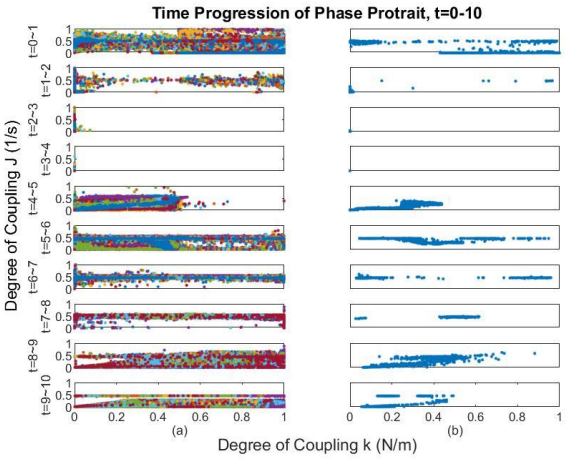
Time Progression of Phase Protrait, t=0-10
Degree of Coupling J (1/s)
Degree of Coupling k (N/m)

(h)

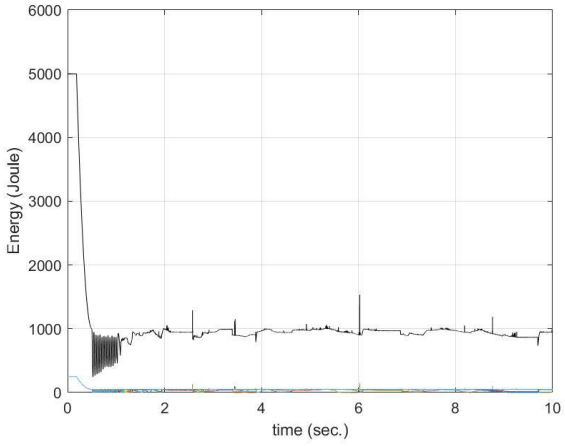
Energy (Joule)
time (sec.)

(d)

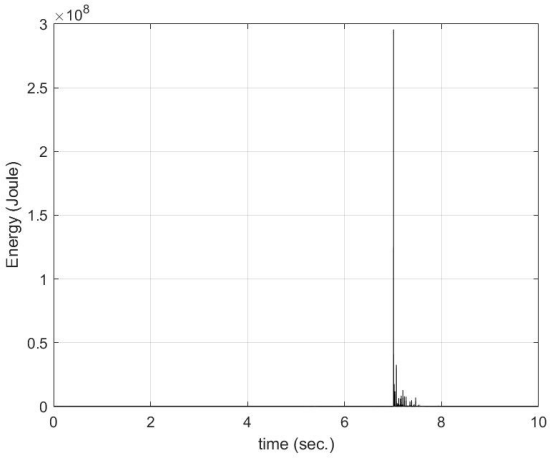
Energy (Joule)
time (sec.)

(i)

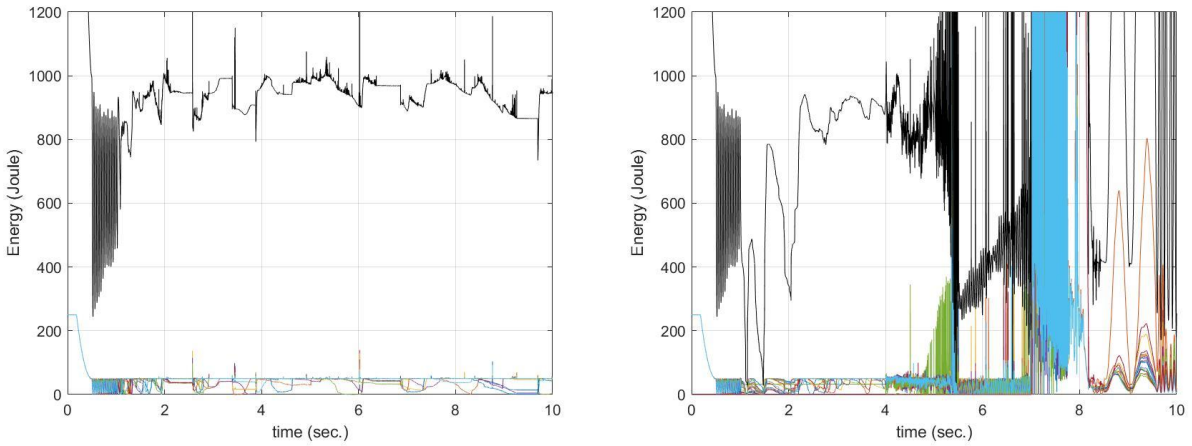

(e) (j)

Fig. 19 Case C in Scenario 2 (left column) – 20-constituent network experiencing random temporary connection breakage with all 20 constituents been controlled in (a) through (e). Case C in Scenario 3 (right column) – 20-constituent network experiencing random temporary connection breakage with 1 constituent detach from the network at t=1s and re-join the network at t=4s and a constituent join the network at t=7s with 20 constituents being controlled in (f) through (j). (a) and (f) entropy, (b) and (g) instantaneous frequency of entropy, (c) and (h) time progression of k-J phase during t=0~10s, (d) and (i) constituent energy, and (e) and (j) constituent energy (zoomed-ins on Fig. 19(d) and Fig. 19(i), respectively.)

Figs. 16, 18, and 19 indicate that network dynamics evolves at a faster rate in Case C than in Case B and Case A (See Fig. 15) under the jurisdiction of the nonlinear time-frequency control scheme. Target entropy is quickly met with more controlled constituents. It is seen that k's and J's are adjusted less frequently in Figs. 19(b) and 19(g), thus implying a greater degree of network structure stability than when control is applied to only 1 constituent. It is evident from the k-J phase plots and their averages in Figs. 19(c) and 19(h) that Case C in both Scenarios 2 and 3 reaches synchronization faster than Cases B and A while Case B in Scenario 2 shows no significant difference from Case A. Energy plots in Figs. 19(d) and 19(i) also indicate that less energy is required for constituents to stay connected when control is exerted to multitudes of constituents. The total constituent energy of Case C in Scenario 3 in Fig. 19(i) is one order of magnitude lower than that of Case B in Scenario 3 in Fig. 18(i). Constituent dynamics in Figs. 19(e) and 19(j) are

very different with less oscillation of constituent energies in both Scenarios 2 and 3. Moreover, Figs. 18(j) and 19(j) show that energy oscillations caused by loss of constituent at t=1~4s are significantly less prominent in Case C than in Case B. As seen in Fig. 19 the network with a greater number of controlled constituents demonstrates a higher degree of robustness. Unlike Scenario 1, the IF of entropy of the network in Case C in Scenario 2 and 3 indicates that, when subject to random and brief breakage of connections, (1) both target entropy and eventual synchronization are reached significantly faster and (2) network structure is of a greater degree of stability. In other words, a network with more controlled constituents is more robust to disruption with less energy required for maintaining network structure stability.

3.3 Discussion and Summary

It was shown that static small-world and scale-free network models were rigid, thus inadequate for properly characterizing network dynamics. Simulation results showed that the general complex network, Case 1, resolved disturbances significantly faster than the two static network models, Case 2 and Case 3, with properly defined and well-described connections and couplings. It was also discussed that (1) it is improper to use time snapshots to establish network dynamics, (2) the two graph theory-based network models considered in the study do not differentiate themselves in resolving network dynamics, and (3) in the context of the general framework, small-world networks are less centralized networks while scale-free networks are more centralized. Through considering constituent energy and ensemble entropy defined under the general framework, the collective behaviors of Case 1 complex network were properly characterized and comprehensively studied at the global, network level. In contrast to defining network dynamics at the constituent level, studying collective behaviors in complex networks at the ensemble level demands much less computational effort. The general framework is applicable

to explore complex networks for network vulnerability and emergent phenomena such as synchronization and asynchronization. It is also a preferred tool for generating policy of natural disaster management, strategy for pandemic prevention and control, and guidelines for securing infrastructures such as power grids and highway systems from being compromised, to name only a few.

A multivariable nonlinear time-frequency control configuration was developed in the context of the general framework for dynamic complex networks for the mitigation of network instability induced by disruptions such as severed constituent couplings and addition of new connections (links). The controller design was shown to be fast in response and robust in sustaining collective behaviors and network structure stability. It was shown in all the 3 scenarios considered in the presentation that while under the steering of the modified Kuramoto law, eventual synchronization of the 20-constituent network was expedited with robustness and stability through adjusting k and J, the degrees-of-couplings. The controller allowed constituent couplings (connections) to be updated in response to the desired entropy in the time and frequency domains simultaneously. In addition to requiring fewer adjustments to the degree-of-couplings to meet the target entropy, (1) the time required to reach synchronization was shortened, (2) the stability and integrity of network structure were improved, and (3) the network with the most number of controlled constituents demonstrated the best performance in mitigating the impact caused by temporary breakage of connection and permanent change to network structure due to constituents leaving, rejoining and external constituents joining the network. The multivariable time-frequency network control scheme was also shown to render flexible constituent couplings that are low in connection energy and fast in response to control action.

4. 6-NEURON BRAIN NETWORK MODEL

In the previous section, the dynamics of a 20-constituent complex network was comprehensively studied in the context of the general framework. The multivariable time-frequency network control scheme was shown to be fast in response and robust in sustaining collective behaviors and network stability. To show that the general framework is applicable to study the dynamics of the brain which represents an example from a different physical domain, a brain network model was developed in section 2 following the guidelines outlined in the general framework. A 6-neuron brain network model is studied in the present section to (1) show in section 4.1 that individual neuron dynamics indeed capture the various characteristic time scales seen in the membrane potential acquired through physiological experiments, and (2) describe in section 4.2 the dynamics of the 6-neuron brain network. As aforementioned, to describe network dynamics, individual constituent dynamics must be established using energy and coupling dynamics using physical laws at the microscopic (constituent) level. At the macroscopic (network) level, information entropy is to be employed to define network dynamics as a function of constituent energies. Once the dynamics of the 6-neuron system is established using energy and synaptic dynamics is defined using proper physical laws, the general framework can be applied to describe the dynamics of the 6-neuron brain network model.

4.1 Neuron Dynamics

A 6-neuron brain network is constructed in this section. At the microscopic level, individual neuron dynamics is investigated to enable a realistic brain network dynamics at the macroscopic level. Microscopic dynamics is the time evolution of the membrane potential of each neuron, thus named neuron dynamics. Per the general framework for dynamical complex networks, individual neuron dynamics at the microscopic level is defined using energy and

network dynamics at the macroscopic level is defined using information entropy. Membrane potential profiles observed in reported physiological studies is used to compare with the individual neuron dynamics obtained from the 6-neuron network model for agreements in prominent features. Proper ranges of Na^+, K^+, and Ca^{2+} concentrations are determined to show that ion pumps dynamics as defined by the network model induces realistic membrane potential dynamics.

To validate the model a set of physiological neuron properties is selected. Only the prominent time scales featured in physical membrane potential data are considered when comparing with the neuron dynamics generated by the network model. The reason is that the time evolution of membrane potential is the manifestation of postsynaptic dynamics, action potential dynamics, and ion pump dynamics. However, consider that (1) the time progression of postsynaptic potential is random due to the dependency of the signal (neurotransmitters) received from the presynaptic neuron, (2) each action potential firing is roughly repeating at the same time scale due to the correlated ion channels are triggered by the voltage of the membrane, and (3) ion pump dynamics is dependent on ion concentration that fluctuates in time, action potential time profiles would serve better as a reference of choice. The magnitude of the computed neural membrane potential is credible for the reason that the model is developed obeying physical laws.

In regard to the time scale of membrane potential, this study uses the neuron response on the faster end of the spectrum documented in [34] where the action potentials are observed to come with a time scale of 2 milliseconds in duration. This action potential profile features a depolarization of 1 millisecond in duration and a repolarization of 1 millisecond in duration including a 2 milliseconds pump refractory time. In regards to the time scale of postsynaptic potential, although the profile is dependent upon the signal transmitted by the presynaptic neuron, the postsynaptic potential of the postsynaptic neuron usually requires 10 to 20 milliseconds to rise

from the resting potential to the threshold potential if the presynaptic neuron fires action potential and releases neurotransmitters continuously [50]. Note that the referenced membrane potential profile is not universal. Different types of neurons have their unique membrane potential characteristics.

Systems with faster system response are usually of smaller mass and higher nature frequency. Therefore, choices of neuron volume are those on the smaller end of the observed data [51]. Assume that ion density is the same for all neurons, smaller the volume of a neuron, less the number of ions required to flow across the membrane to induce the same amount of changes in membrane potential. Moreover, for a neuron to have a faster response in action potential firing, the number of ligand gated ion channels has to be on the higher end of the physical data. The more ligand gated ion channels a neuron has, the higher ion flux can be allowed to flow across the membrane per unit time. As a result, postsynaptic potential would arise faster to reach the threshold potential and fire action potential. Due to the very small number of neurons in the brain network considered in simulation experiment, a proper number of dendritic spines are considered to ensure that threshold potential can be sufficiently attained within a reasonable amount of time. This is necessary so that the timescale of the ion flux across the ligand gated channels that causes postsynaptic potential is similar to observations made in electrophysiological measurements. A neuron can be connected to 10,000 presynaptic neurons to have enough amplitude rise through time in voltage to be observed. As each individual neuron receives signals from 5 presynaptic neurons, the number of inputs to each postsynaptic neuron in the simulation environment must be scaled up to allow enough ion fluxes across the membrane to induce membrane potential rise to trigger action potential firing. Otherwise, it will take significantly longer time for each neuron to reach the threshold potential. Individual neurons in the 6-neuron network with 5 coupled

presynaptic neurons are connected to a large number of presynaptic neurons as neurons usually do in reality. The scaling must align with real-life presynaptic-postsynaptic neuron connection scenarios. However, the range of possible number of input a postsynaptic neuron can have from presynaptic neurons is quite wide. A neuron can have as many as 1.5×10^4 dendritic spines [52] while in some cases a neuron can receive 1×10^5 inputs [53]. Since each dendritic spine serves as an input terminal to a postsynaptic neuron, it is reasonable to assume that some neural structures are too small to be observed. The number of dendritic spines of any neuron is not clear. As a result, this study assumes that on each of the 5 postsynaptic sites of a postsynaptic neuron that exists 3×10^4 dendritic spines, each having 3 colonies of 25 AMPARs and 6 NAMARs (both receptors are ligand gated ion channels) [54, 55]. Consequently, the number of ligand gated ion channels must be scaled up to allow sufficient ion flux to cause a proper postsynaptic potential response to trigger action potential firing.

All the 6 neurons are assumed to have the same biophysical properties. Key parameters that are significant to generate characteristic neuron dynamics are tabulated in Table 3. All the 6 neurons serve as both presynaptic and postsynaptic neurons to one another. They do not transmit signals to or receive signals from to themselves. Membrane potentials of all the 6 neurons are assumed to be at the threshold potential at t = 0s. That is, all the 6 neurons are under the same initial conditions.

Table 3. Parameters of individual neurons

Time step of simulation iteration	$1 \times 10^{-4}\ s$ = 10000Hz
Fastest responding ion channel	Δt_{AMPARi}
Δt_{AMPARi}	$1.5 \times 10^{-3}\ sec.$
Characteristic system frequency of neuron	$\frac{1}{\Delta t_{AMPARi}} = 666.667\ Hz$
Neuron cell volume	$524 \mu m^3$
Na^+ concentration	5-15 [mM] (millimole)
K^+ concentration	140-150 [mM]
Ca $^{2+}$ concentration	0.1 [mM]
Number of dendrites per neuron	6
Number of dendritic spins per neuron	$3 \times 10^4\ per\ dendrit\ \times 6\ dendrits$
Number of AMPAR per neuron	$25\ per\ cluster \times 3\ clusters$
Number of NMDAR per neuron	$6\ per\ cluster \times 3\ clusters$
AMPAR opening area	NTD area
NMDAR opening area	NTD area
NTD area [56]	3.2×10^{-16}
Synaptic cleft area [57]	1.6×10^{-15}

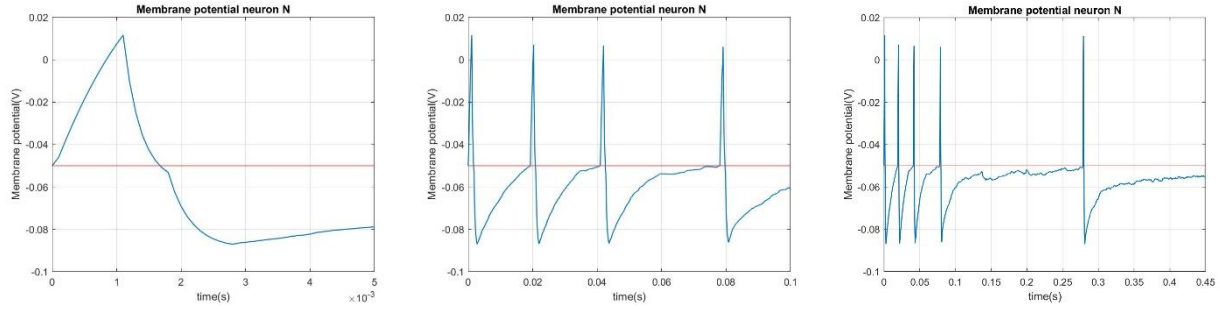

(a) (b) (c)

Fig. 20 Membrane potential of neuron N – The individual neuron N dynamics

Fig. 20 shows the dynamics of neuron N where the corresponding membrane potential is plotted. Fig. 20(c) shows the membrane potential of the neuron over a 0.45s time window. Figs. 20(a) and 20(b) are zoom-ins on Fig. 20(c) with the former showing the profile of 1 action potential firing and 4 in the latter. The dynamics of neuron N shows the features typical of a fast response action potential. At t=0, the membrane potential registers a threshold potential at -50mV with both voltage gated Na^+ and K^+ channels being triggered. Voltage gated Na^+ channels are triggered as

soon as threshold potential is reached while voltage gated K^+ channels have a 1 millisecond delay before fully opened. Fig. 20(a) shows depolarization caused by Na^+ influx through voltage gated Na^+ channels started at t=0s and terminated at approximately t=1ms due to fully opened voltage gated K^+ channels. The membrane potential then enters the repolarization phase. Note that at t > 1ms, the decreasing membrane potential shows a change of slope due to the closing of the voltage gated Na^+ channels. Similarly, voltage gated K^+ channels are closed at t=2.8ms, 1 millisecond after the membrane potential drops below the threshold value. The whole action potential firing lasts about 2.5 milliseconds. The various time scales in the profile are in agreement with physiological observations. That is, the governing law defined in Eqs. (16), (17), (18), (26), and (44) correctly describes the mechanism behind the voltage gated ion channels. Moreover, the 20 milliseconds duration seen in Fig. 20(b) for the postsynaptic potential are also in excellent agreement with published postsynaptic potential data. Therefore, the governing laws defined in Eqs. (26) and (44) also describes well the mechanism behind the ion pumps.

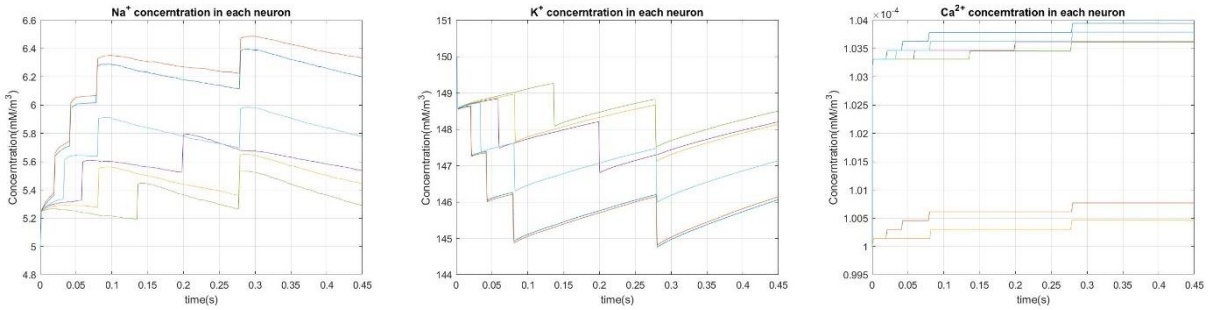

Fig. 21 Ion concentration in each neuron

Fig. 21 shows the time evolution of ion concentration of all the 6 neurons over the 0.45 seconds simulation time window. All three ion species oscillate in the range of concentration that is physically observed: 5~15 millimole for Na^+ concentration, 140~150 millimole for K^+ concentration, and 0.0001~0.0015 millimole for Ca^{2+} concentration [58]. It is seen that the ion

pumps defined in the brain network model are able to maintain ion concentrations in ranges that are commonly observed. Fig. 21 also shows that the ion pumps are able to restore the membrane potential to the resting value after firing in a time span (approximately 5 ms) that is in agreement with [59]. It is noted that each of the rise or drop in ion concentration seen in Fig. 21 is synchronized with the firing of action potential. Steps of ion concentration are caused by the sudden large Na^+ and Ca^{2+} influx and K^+ efflux across the voltage gated ion channels when each action potential fires. The slope of each ion concentration indicates the corresponding ion flux through the ligand gated ion channels. Ion concentrations are effectively maintained by the ion pumps as where zero slopes are indicated. It is seen that the time evolution of postsynaptic potential, action potential, and ion pumps are all properly described by their respective governing law of dynamics. Note that the observations made in the case of Na^+ and K^+ ion concentration are not as significant for the case of Ca^{2+} because the range of Ca^{2+} concentration fluctuation is smaller. Also, the Mg^{2+} blockage of NMDARs (the ligand gated ion channels allow Ca^{2+} flux) are only unblocked briefly after each action potential firing (See Fig. 22(n)).

In summary, the results given in Figs. 20 and 21 show that the various time scales featured in the computed action potentials agree with physical data. Computed postsynaptic potentials also fall in the time range reported in literature. Ion pumps are able to maintain the ion concentrations of the 3 ion species within a reasonable range. With the feasibility of the neuron model demonstrated, individual neuron dynamics can now be defined using energy and the general framework can be applied to describe brain network dynamics using information entropy.

4.2 Validation of Brain Network Model

In the last section, the governing laws of neuron dynamics were shown to describe the time evolution of membrane potentials in ways that agree with biophysics. Characteristic temporal signatures commonly observed in electrophysiologically acquired membrane potentials were faithfully resolved by the neuron model with excellent time resolution. Following the guidelines in the general framework for dynamical complex networks, individual neuron dynamics are defined in Eqs. (16), (17), (18), (26), and (44) using energy. Individual neuron energies must follow a normal distribution. The results presented in the last section for the 6-neuron brain network indicate the feasibility of the general framework in modelling neurons and brain dynamics. Responses of network dynamics using the general framework and biophysics (ion charges of neurons) are compared to show the benefits of modelling complex network dynamics using the general framework.

The response of the 6-neuron brain network at the individual neuron (microscopic) level is presented in Fig. 22 and the response at the network (macroscopic) level is shown in Fig. 23. The column on the lefthand side of the figure, Figs. 22(a)-(g), shows the response obtained using the general framework. The corresponding biophysical response is plotted in the column on the righthand side of Fig. 22. Individual neuron dynamics is defined in Eq. (48) using energy. Individual neuron energies in Fig. 22(a) are of the identical trend as Fig. 22(h), suggesting that individual neuron dynamics are properly defined using energy. The relationship between each pair of coupled neurons can be described by degree-of-couplings. Constituent dynamics consists of potential energy and kinetic energy. The potential energy portion of the individual neuron dynamics defines degree of coupling k (DOC k) in terms of the ion charge a neuron carries. The kinetic energy portion of the individual neuron dynamics defines the degree of coupling J (DOC

J) in terms of the number of ions per mole allowed to flow across the available ligand gated ion channels triggered by the neurotransmitter released by the presynaptic neurons. Figs. 22(b), 22(c), and 22(d) show the DOCs k of Na^+, K^+, and Ca^{2+} with the corresponding biophysical responses being shown in Figs. 22(i), 22(j), and 22(k). Responses of DOCs J of Na^+, K^+, and Ca^{2+} are shown in Figs. 22(e), 22 (f), and 22 (g) with the corresponding biophysical responses given in Figs. 22(l), 22 (m), and 22 (n). It is evident that DOCs k and J demonstrate the same characteristics as their biophysical counterparts. The relationship between each pair of presynaptic and postsynaptic neurons are properly described by the degree of couplings of the general framework. It is noted that, although the right column of Fig. 22 shows the corresponding biophysical responses to DOCs J, each response is a coupled result of the electrochemical gradient in Eq. (19), the availability of ligand gated ion channels in Eq. (22), and the ion flux in Eq. (21). Each of these biophysical properties is a function of other physical properties. It is not easy to describe the coupled relationship of the postsynaptic neuron toward the presynaptic neuron through biophysical measurements. However, the general framework defines the coupling relationship using degree of couplings. Moreover, all the data seen in Fig. 22 show a similar trend indicating synchronization. At each action potential spike, there are prominent oscillations in DOCs k and J and rapid variations of ion charges. Evidently the time response of each measurement is in agreement with the oscillations of membrane potential observed in the real-world, suggesting the feasibility of the general framework properly in describing neuron dynamics at the microscopic level.

General framework measurements

Biophysical properties

Microscopic Level

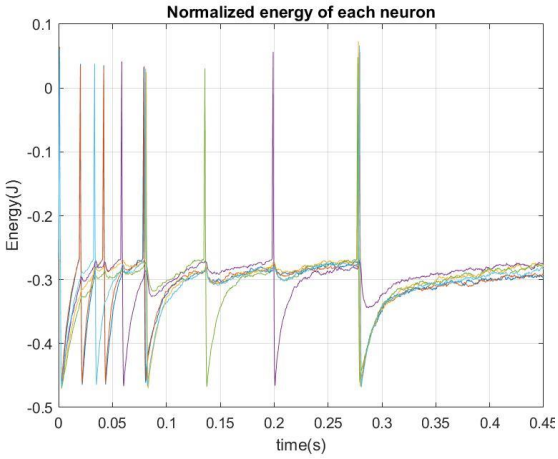

(a)

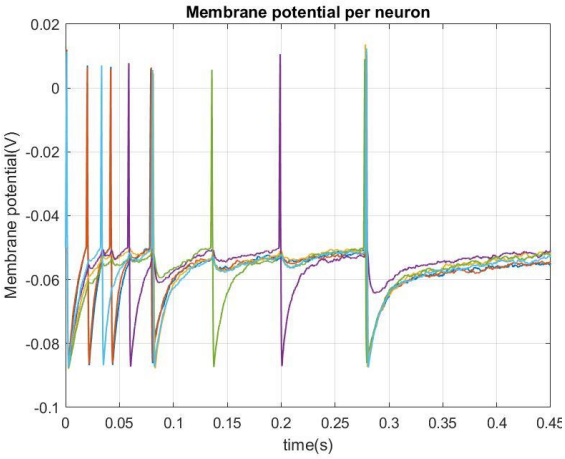

(h)

Microscopic Level

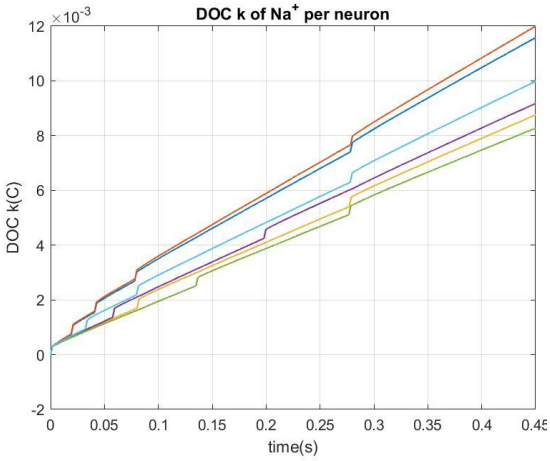

(b)

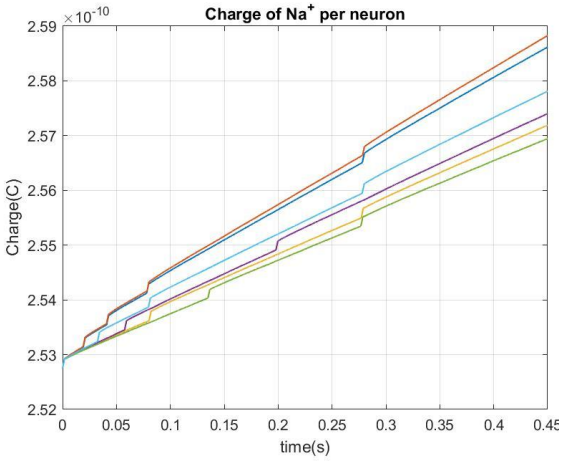

(i)

Microscopic Level

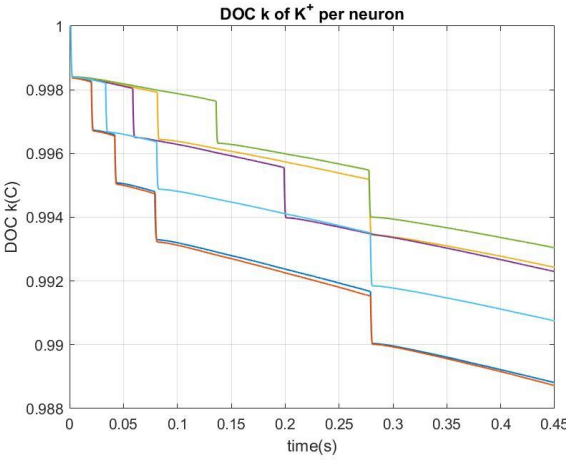

(c)

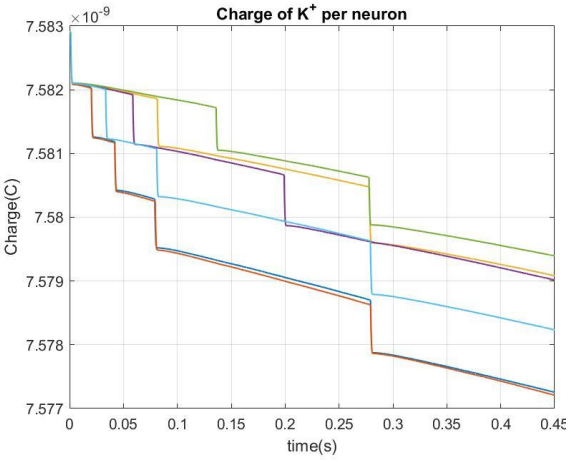

(j)

Microscopic Level

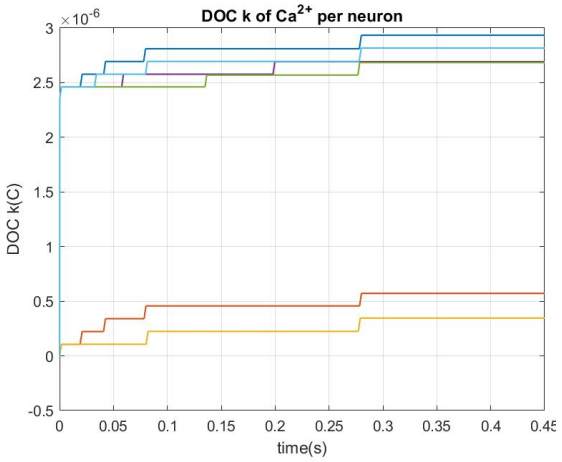

(d)

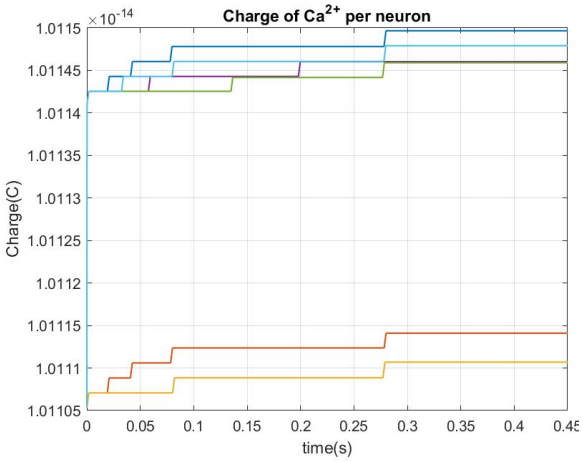

(k)

Microscopic Level

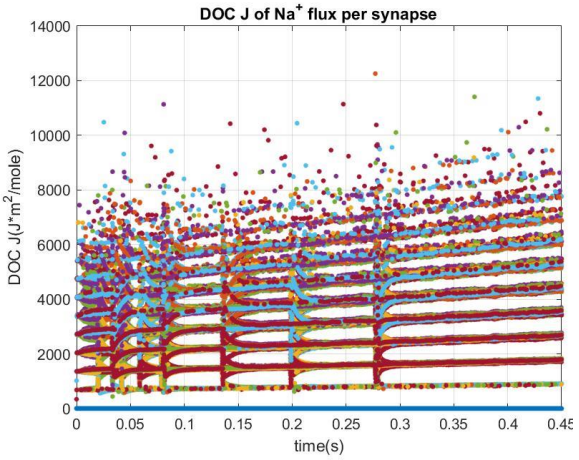

(e)

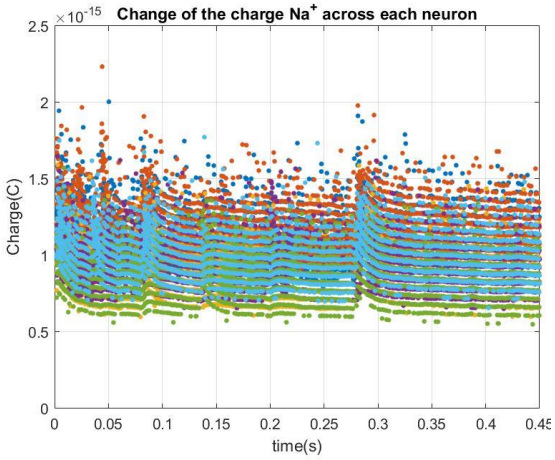

(l)

Microscopic Level

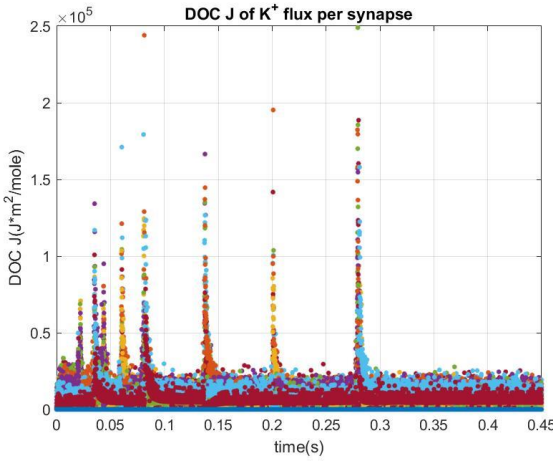

(f)

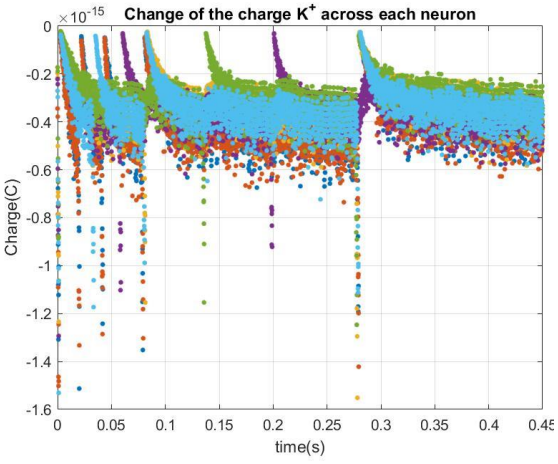

(m)

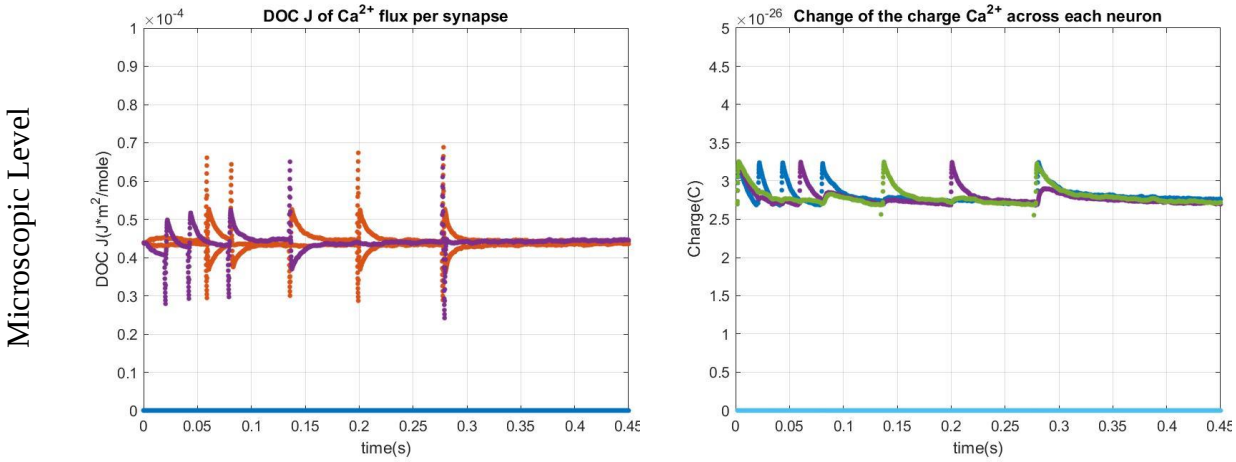

(g) (n)

Fig. 22 6-neuron brain network dynamics at the individual neuron (microscopic) level

General framework measurements Biophysical properties

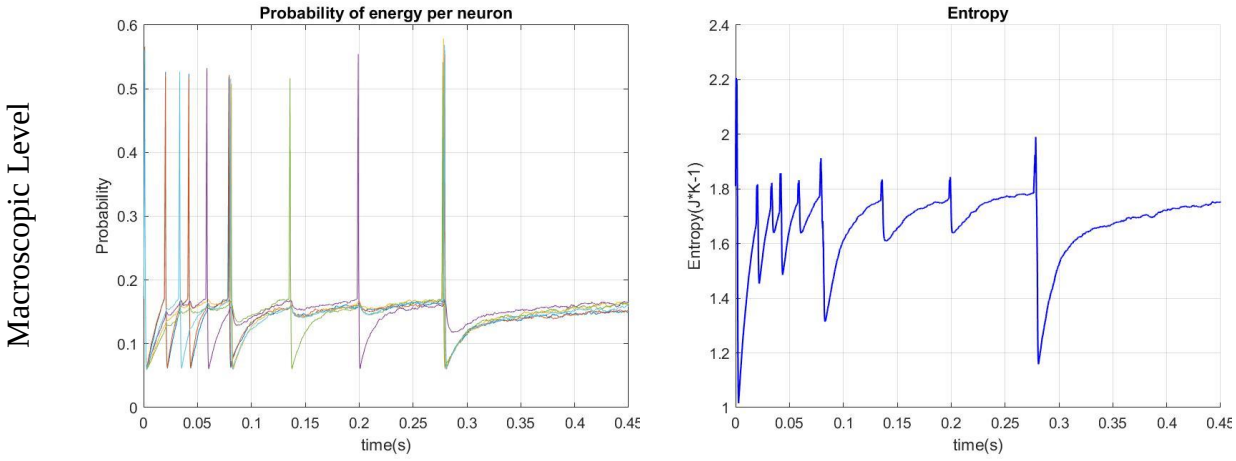

(a) Probabilities of individual neuron energies

(b) Information Entropy – The direct measurement of brain network dynamics

Fig. 23 6-neuron brain network dynamics at the global (macroscopic) level

Now that individual neuron dynamics at the microscopic level is shown to be described properly using the governing laws, the general framework is to be applied to define the brain network dynamics at the macroscopic level. As aforementioned, the distribution of individual neuron energies must follow a normal distribution defined in Eq. (12). The dynamic state of the brain network model at the network (macroscopic) can be determined using information entropy

which is a function of the individual neuron energies. Fig. 23 shows the response of the brain network. Fig. 22(a) shows the time evolution of the probability of each individual neuron energy. Fig. 22(b) shows the time evolution of entropy of the 6-neuron brain network. At the individual neuron level, the probability of individual neuron energies and the entropy are of the same trend as the membrane potentials.

As seen in Eq. (56), information entropy is the summation of the probability of neuron energy. Magnitude of entropy is therefore correlated with the membrane potentials of all the 6 neurons. Larger value of the entropy at each spike indicates more simultaneous neuron firing of action potentials at the same time. That is, higher is the entropy, more synchronized are the neurons and vice versa. As a result, the entropy data also convey synchronization of the 6-neuron brain network at the network (macroscopic) level.

4.3 Discussion

In this section, the general framework for dynamical complex networks was applied to a problem from a physical domain that is different from the statistical mechanics system investigated in the previous section. The general framework for dynamical complex networks was shown to properly describe the dynamics of the 6-neuron brain network at both the individual neuron level and the network level. The 6-neuron brain network is a complex network in the biology domain whose dynamics is dominated by magnetic flux and exhibits electrical voltage oscillations of neuron membranes. The responses of the 6-neuron brain network obtained from using the general framework featured the same temporal characteristics as biophysical responses in excellent agreement. Moreover, the dynamics of the 20-constituent network presented in section 3 was a complex network of statistical mechanical system whose network dynamics is defined using the general framework. Albeit from different physical domains, the two networks examples were

exemplary in showing the applicability and feasibility of the general framework for modelling complex network dynamics using energy and information entropy.

As opposed to the need for generating large amounts of biophysical data through laborious physical testing, the general framework is a viable alternative to describing brain network dynamics at both the microscopic and the macroscopic levels. The degree of couplings defines the relationship between coupled neurons by describing the mechanism of synaptic dynamics using laws of physics. DOC k indicates the ion charge a neuron cell possesses and the DOC J is a function of electrochemical gradient, availability of the ligand gated ion channels, and ion flux. Current physiological measurement techniques are inadequate in resolving the coupling of biophysical properties. The degree of couplings defined in the general framework provides a way to resolve the coupled dynamics that governs the relationship of individual constituents. The approach is generally applicable to complex networks regardless of the domain they are from.

The presented brain network model captured individual neuron dynamics and synaptic dynamics by their fundamental characteristics. The laws of physics that govern individual neuron dynamics make explicit the mechanism that drives the dynamics. The computed membrane potential profiles are more realistic than those of HH based models and mathematically fitted models.

5. CONCLUDING REMARKS

Real-life networks are complex networks whose responses are nonlinear and nonstationary. They are sensitive to disturbance, easily perturbed, and highly unpredictable. Real-life complex networks are known to be resilient to disturbance. However, there are times they collapse under a slight change of condition. Therefore, it is important to develop a better understanding for complex networks and their dynamics. Complex networks are statistical mechanical systems where the dynamics exist at both the microscopic and macroscopic levels. At the microscopic level, individual constituent has its own dynamics while maintaining a coupled relation with neighboring ensemble. Individual constituent dynamics and coupling dynamics are both time-dependent. At the macroscopic level, the ensemble exhibits a global behavior that is also time-dependent. Therefore, it is challenging to describe complex networks dynamics. Controlling a complex network without having a comprehensive knowledge of its underlying local and global properties is even more demanding.

Aiming to address the issue, this study developed a general framework for defining complex network dynamics using energy and information entropy. The general framework provides a guideline to describe network dynamics both from the individual constituent level (the local level) and the network level (the global level). At the local level, constituent dynamics is defined in energy terms and the coupling of constituents is defined using degree of couplings, DOC k and DOC J. Because energy is used to define individual constituent dynamics and entropy is used to describe network dynamics, the general framework is generally applicable to complex networks regardless of their inherent physical attributes.

A multivariable time-frequency control scheme for complex network is presented to ensure the integrity of network structure and a fast response time in stabilizing complex network dynamics

when undergoing disturbance is maintained. Different scenarios of disturbance to the network structure and control cases of constituents were investigated. Through the control scheme, the network dynamics is able to maintain its integrity with a lower effort in maintaining the relationships between the constituents. Therefore, under the effect of the control scheme, a complex network reaches synchronization faster and is more robust to environmental disturbance.

In proving the generality of the general framework, this study applies the general framework to describe the dynamics of a 6-neuron brain network. To ensure realistic brain network dynamics, a procedure to develop a model of real-life network dynamics is also provided. First, the network dynamics must be investigated thoroughly in locating the physical state that drives the individual constituent dynamics and the mechanisms that cause the coupling dynamics. Secondly, the individual constituent dynamics must be defined through energy while the mechanism of coupling must be described properly through physics laws. As aforementioned, energy of all systems in nature must follow a normal distribution. Therefore, the real-life network dynamics can be defined through information entropy. Following this network modeling procedure, a preliminary brain network model is developed. The dynamics of the 6-neuron brain network is defined properly through the general framework. The individual neuron dynamics generated through the preliminary brain network model captures the signature characteristic in time evolution of neuron membrane potential commonly observed in the physiology experiments. The individual neuron dynamics is described through energy. The synaptic dynamics is properly defined through the degree of couplings. Information entropy is able to describe brain network dynamics at the global level.

In summary, the general framework is a proper and a true dynamic description to complex networks. In short, the general framework serves as a building block by providing a proper

guideline in describing complex network dynamics which opens a new door in real-life network studies.

5.1 Contribution

The study addresses the needs for resolving the true nature of dynamical complex networks. To meet the objective, the study developed (1) a general framework for describing complex networks dynamics, (2) a multivariable time-frequency network control scheme for the robust control of complex networks to achieve network structure integrity and desired collective behaviors, and (3) a brain network model to show the applicability of the general framework. Complex networks dynamics can be defined and quantified under the general framework. With the multivariable time-frequency network control architecture, control can be designed to steer network dynamics toward desired states. The followings are contributions of the study:

1. *The proposed general framework defines the dynamics of complex network properly*

Complex networks are dynamic systems whose dynamics is nonlinear and nonstationary. Also, since complex networks are special case of statistical mechanical systems with the dynamics of individual constituents coupled with the neighboring ensemble, the network dynamics has to be defined both at the individual constituent level (microscopic level) and the network level (macroscopic level). At the microscopic level, the individual constituent dynamics is defined through energy. The coupling relationship is defined through the degree of couplings (DOC k and DOC J). The DOC k is defined according to the potential energy of the individual constituent dynamics and DOC J is defined according to the kinetic energy. Both the individual constituent dynamics and degree of couplings are time-dependent. At the macroscopic level, the network dynamics is defined through information entropy. Under the constraint of a natural law of all physical systems that the energy distribution of all systems has to follow a normal distribution.

The distribution of individual constituent energies has to follow a normal distribution as well. Therefore, information entropy defines the randomness of the probability of individual constituent energies. The entropy measurement of complex network is also time-dependent since it's a function of individual constituent energies. As the energy defines the individual constituent dynamics at the microscopic level and the information entropy defines the randomness of the individual energies at the macroscopic level, the dynamics of a complex network is defined properly.

2. The general framework is a true dynamic guideline in describing complex network dynamics

The general framework not only accounts the dynamics of individual constituents but also describes the time evolution of the coupling relationship accordingly through the degree of couplings. Unlike traditional static network models that define static network structures that is rigid through time, the degree of couplings of the general framework defines a flexible and time-dependent coupling relationship of constituents. Depends on the interaction between the constituents through time, the degree of coupling of each connection (link) can be measured to a very small value that registered to a very weak coupling relationship or a very high value that registered to a very strong coupling relationship of the connected constituents. Therefore, the time-dependent degree of couplings describes a dynamical network structure of complex networks. Since 1) at the microscopic level, the energy describes the individual constituents and the degree of coupling described the interaction relationship, and 2) at macroscopic level, information entropy that describes ensemble dynamics are all time-dependent, the general framework is a true dynamic guideline that is time-dependent in describing complex networks dynamics.

3. The general framework is general to all complex network

The general framework is proven to describe the dynamics of 1) a 20-constituent point mass network and 2) a 6-neuron brain network. The 20-constituent network is a translational system whose network dynamics is dominant by translational motions of the constituents in space. The 6-neuron brain network is a biological system whose dynamics is significantly dominated by magnetic flux and exhibited in the form of electrical voltage fluctuations of the neurons membranes. It is obvious that both case of networks are network systems of different physical domains. Using energy to define individual constituent dynamics, the general framework is able to describe the complex network dynamics disregarded to the physical domain where each network exists. As a result, the general framework is general to all complex networks that exist in the world of physics in describing the network dynamics.

4. A guideline in describing real-life network dynamics

While the general framework is general to all complex networks, this study also provides a guideline of the procedure to describe the dynamics of real-life network through the general framework. Each real-life network is a special case of complex networks that the network dynamics is driven by different physical properties. Therefore, to describe network dynamics, one should 1) investigate the cause of dynamics of the complex network of interest in realizing the procedure of the mechanism that drives the individual constituent dynamics and the coupling dynamics, 2) describing the mechanism that causes the coupling dynamics through physics laws and define the individual constituent dynamics through energy so the dynamics at the microscopic level is properly defined, and 3) following the general framework, the dynamics at the macroscopic level can be defined through information entropy.

5. *The multivariable time-frequency complex network control scheme ensures the integrity of network structure and a fast response of the network dynamics in reaching synchronization and resilience against disturbance*

Since the general framework defines the network dynamics through entropy measurement, complex network dynamics has to emerge to the collective behavior that registers to the measurement of entropy. However, applying the multivariable time-frequency control scheme to the constituents, the constituents are able to adjust the degree of couplings and further maintain the desirable relationship. As a result, the ensemble is able to reach synchronization in a shorter time so that the integrity of the network structure is ensured. Consequently, the complex network dynamic is more robust to disturbance.

5.2 Impact of The Study

Since the general framework describes the individual constituent dynamics through energy with a proper time-dependent description to the coupling relationship of the constituents and measures the network dynamics through entropy, many contemporary challenging task of dynamical network systems can be approached. Through the complex network example cases this study shown, dynamics models of spatial translational network systems (drone fleets, traffic networks, and automatic package delivering network, etc.) and brain network (brain network, cell networks such as brain-nerve-muscle network, prosthetic design, etc.) can be better studies. The impact of this study is stated as followings:

1. *The spatial translational network system*

As the individual constituent dynamics be defined through energy, dynamics of systems such as drones and autocars is clearly defined and easy to apply control inputs. With the multivariable time-frequency network controller operates on constituents, the relationship between

the constituents become easier to maintain. Compared to how this system be approached with a static network structural model through a linear controller traditionally, the general framework coupled with the time-dependent network control scheme capture the true nature of the complex networks since the general framework as well as the network control scheme are time-dependent. As a result, contemporary control issues of drone fleets, autocars, and automatic package delivering networks can be easy to control, fast in response, and resilience to disturbance, change of fleet formation, and numbers of constituent.

2. The preliminary brain networks

The dynamics of brain network is defined properly through the general framework. At the local level, the individual neuron dynamics is defined properly in terms of the time evolution of membrane potential. At the global level, the brain dynamics is clearly defined through information entropy. Since the mechanisms that cause the brain network dynamics is properly described through physics laws, the preliminary brain network model captures the true nature of brain networks. The brain network model provides a novel tool for neuroscientists, pharmacists, and biochemists, etc., for addressing their work of interests such as depression and Alzheimer study, treatment, and medicine formulation design.

5.3 Recommendations for Future Work

1. Novel computing algorithms are needed

The simulation results of this study were generated using nonlinear regression. Maintaining desired information entropy requires the code of the model to scan through all possible outcomes for all parameters in every time iteration. Constrained by current regression algorithms, each numerical run performed for the study demanded a tremendous amount of computing resources and was excruciatingly time consuming. This also put a cap on the number

of constituents used for the model. Novel computing algorithms that demand less computing resources and is more efficient in speed is required for accounting for more constituents.

2. *Proper physiological measurement and observation of neurons are required for improving the brain network model*

The brain network model developed for this study describes neurons and the underlying mechanisms with physical laws. The brain network dynamics described is realistic in capturing the signature characteristics observed in real-life brain networks. However, many key parameters required by the brain network model are not available. Some mechanisms that dictate individual neuron dynamics are yet to be fully understood. To achieve a better understanding of brain dynamics using the brain network model, novel physiological measuring device and methodologies are needed. The insufficiency noted of the brain network model could serve to guide neuroscience, physiology, electrophysiology research and medical instrument design to chart future paths. With improved physiological measurement and better understanding for neurons, the brain network model can be refined to realize greater capability and capacity.

REFERENCES

[1] Gibbs, J.W. (1902), Elementary Principles in Statistical Mechanics, Charles Scribner's Sons, NY.

[2] Callen, H.B. (1985), Thermodynamics and an Introduction to Thermostatistics, John Wiley and Sons, NY.

[3] Bianconi, G. (2009), Entropy of Network Ensembles, Phys. Rev. E, 79, 036114.

[4] Shannon, C.E., and Weaver, W. (1949), The Mathematical Theory of Communication, University of Illinois Press, 1949. Print, Urbana.

[5] Yang, C.-L. and Suh, C.S. (2021), A General Framework for Dynamic Complex Networks, Journal of Vibration Testing and System Dynamics, 5, 87-111.

[6] Winfree, A. T. (1967), Biological rhythms and the behavior of populations of coupled oscillators, Journal of theoretical biology, 16(1), 15-42.

[7] Kuramoto, Y. (1975), Self-Entrainment of a Population of Coupled Non-Linear Oscillators, In: Araki H. (eds) International Symposium on Mathematical Problems in Theoretical Physics. Lecture Notes in Physics, 39. Springer, Berlin, Heidelberg.

[8] Kuramoto, Y. (1984), Chemical Oscillations, Waves, and Turbulence, Springer-Verlag, NY Tokyo.

[9] Kuramoto, Y. (1984), Cooperative Dynamics of Oscillator Community: A Study Based on Lattice of Rings, Progress of Theoretical Physics Supplement, 79, 223–240.

[10] Strogatz, S. (2000), From Kuramoto to Crawford: Exploring the Onset of Synchronization in Populations of Coupled Oscillators, Physica D: Nonlinear Phenomena, 143, 1-20.

[11] Acebrón, J.A., Bonilla, L.L., Pérez-Vicente, C.J., Ritort, R. and Spigler, R. (2005), The Kuramoto Model: A Simple Paradigm for Synchronization Phenomena, Rev. Mod. Phys., 77, 137.

[12] Watts, D. and Strogatz, S. (1998), Collective dynamics of 'small-world' networks, Nature, 393, 440–442.

[13] Barabási, A.-L., and Albert, R. (1999), Emergence of Scaling in Random Networks, Science, 286(5439), 509-512.

[14] Liu, Y.-Y., Slotine, J.-J. and Barabási, A.-L. (2011), Controllability of Complex Networks, Nature, 473, 167–173.

[15] Yang, C.-L. and Suh, C.S. (2021), On Controlling Dynamic Complex Networks, Physica D: Nonlinear Phenomena. Under review.

[16] Kitzbichler MG, Smith ML, Christensen SR, and Bullmore E (2009) Broadband Criticality of Human Brain Network Synchronization. PLOS Computational Biology 5(3):e1000314. https://doi.org/10.1371/journal.pcbi.1000314.

[17] Freche, D., Pannasch, U., Rouach, N., and Holcman, D. (2011). Synapse geometry and receptor dynamics modulate synaptic strength. PloS one, 6(10), e25122.

[18] Lyon, A. (2014), Why are Normal Distributions Normal? Brit. J. Phil. Sci., 65, 621–649.

[19] Erdős, P. and Rényi, A. (1959), On Random Graphs. I, Publicationes Mathematicae, 6, 290–297.

[20] Bianconi, G. and Barabási, A.-L. (2001), Bose-Einstein Condensation in Complex Networks, Phys. Rev. Lett., 86, 5632.

[21] Bianconi, G. and Barabási, A.-L. (2001), Completition and Multiscaling in Evolving Networks, Europhys. Lett., 54 (4), 436-442.

[22] Albert, R. and Barabási, A.-L. (2002), Statistical Mechanics of Complex Networks, Reviews of Modern Physics, 74(1), 47-97.

[23] Boccaletti, S., Latora, V., Moreno, Y., Chavez, M., and Hwang, D.-U. (2006), Complex Networks: Structure and Dynamics, Physics Reports, 424(4–5), 175-308.

[24] Rossetti, G. and Cazabet, R. (2018), Community Discovery in Dynamic Networks, ACM Computing Surveys, 51(2), 1–37.

[25] Strogatz, S.H., (2001), Exploring complex networks, Nature, 410, 268–276.

[26] Lewis, M.A. and Tan, K.-H. (1997), High Precision Formation Control of Mobile Robots Using Virtual Structures, Autonomous Robots, 4, 387–403.

[27] Consolini, L., Morbidi, F., Prattichizzo, D. and Tosques, M. (2008), Leader–Follower Formation Control of Nonholonomic Mobile Robots with Input Constraints, Automatica, 44(5), 1343-1349.

[28] Strogatz, S.H., Marcus, C.M., Westervelt, R.M. and Mirollo, R.E. (1989), Collective Dynamics of Coupled Oscillators with Random Pinning, Physica D: Nonlinear Phenomena, 36(1–2), 23-50.

[29] Strogatz, S., Mirollo, R. and Matthews, P. (1992), Coupled Nonlinear Oscillators below the Synchronization Threshold: Relaxation be Generalized Laudau Damping, Phys. Rev. Lett., 68, 2730.

[30] Ren, W., Beard, R.W. and Atkins, E.M. (2005), A Survey of Consensus Problems in Multi-Agent Coordination, Proceedings of the 2005, American Control Conference, 2005., Portland, OR, USA, 3, 1859-1864.

[31] Lin, C.-T. (1974), Structural Controllability, IEEE Transactions on Automatic Control, 19, 201-208. https://doi.org/10.1109/TAC.1974.1100557.

[32] Liu, Y.-Y. and Barabási, A.-L. (2016), Control Principles of Complex Networks, Review of Modern Physics, 88(3), 035006. https://doi.org/10.1103/RevModPhys.88.035006.

[33] Yang, C.-L. and Suh, C.S. (2021), A General Framework for Dynamic Complex Networks, Journal of Vibration Testing and System Dynamics, 5(1), 87-111. http://dx.doi.org/10.5890/JVTSD.2021.03.006.

[34] Bean, B. The action potential in mammalian central neurons. Nat Rev Neurosci 8, 451–465 (2007). https://doi.org/10.1038/nrn2148

[35] Yang, C.-L., Suh, C.S. and Karkoub, M. (2018), Impact of Coupling Strength On Reaching Network Consensus, Journal of Applied Nonlinear Dynamics, 7, 243-257.

[36] Liu, M.-K. and Suh, C.S. (2012), Temporal and Spectral Responses of a Softening Duffing Oscillator Undergoing Route-to-Chaos, Communications in Nonlinear Science and Numerical Simulation, 17(12), 5217-5228. https://doi.org/10.1016/j.cnsns.2012.04.015.

[37] Liu, M.-K. and Suh, C.S. (2012), Simultaneous Time-Frequency Control of Bifurcation and Chaos, Communications in Nonlinear Science and Numerical Simulation, 17(6), 2539-2550. https://doi.org/10.1016/j.cnsns.2011.10.008.

[38] Suh, C.S. and Liu, M.-K. (2013), Control of Cutting Vibration and Machining Instability: A Time-Frequency Approach for Precision, Micro and Nano Machining, John Wiley and Sons. https://doi.org/10.1002/9781118402795.

[39] Liu, M.-K. and Suh, C.S. (2013), Synchronization of Chaos in Simultaneous Time-Frequency Domain, Applied Mathematical Modelling, 37(23), 9524-9537. https://doi.org/10.1016/j.apm.2013.05.008.

[40] Liu, M.-K., Halfmann, E.B. and Suh, C.S. (2014), Multi-Dimensional Time-Frequency Control of Micro-Milling Instability, Journal of Vibration and Control, 20(5), 643-660. https://doi.org/10.1177/1077546312463716.

[41] Wu, X-H.., Song, Z.-H, Du, Y.-F, Mao, E.-R., and Suh, C.S., (2017) “A Time-Frequency PID Controller Design for Improved Anti-Interference Performance of A Solenoid Valve Applicable to Hydraulic Cylinder Actuation,” Vibration Testing and System Dynamics, 1(4), pp. 281-294. https://doi.org/z10.5890/JVTSD.2017.12.001.

[42] Wu, X., Du, Y., Suh, C.S., Mao, E, and Song, Z., and (2017) “On The Design and Physical Validation of A Time-Frequency Controller,” Control Theory and Applications, 34(3), pp. 329-336. https://doi.org/10.7641/CTA.2017.60334.

[43] Wang, X. and Suh, C.S. (2017) “Time-Frequency Based Field Oriented Control of Permanent Magnet Synchronous Motors,” International Journal of Dynamics and Control. https://doi.org/10.1007/s40435-017-0327-5.

[44] Kuo, Chi-Wei and Suh, C.S., (2017) “A Case of Mitigating Non-Autonomous Time-Delayed System with Cubic Order Feedback,” Journal of The Franklin Institute, 354(15), pp. 6651-6671. https://doi.org/10.1016/j.jfranklin.2017.08.023.

[45] Wang, X. and Suh, C.S., (2017) “Precision Concurrent Speed and Position Tracking of Brushed DC Motors using Nonlinear Time-Frequency Control,” Journal of Vibration and Control, 23(19), pp. 3266-3291. https://doi.org/10.1177/1077546316628974.

[46] Hodgkin AL, Huxley AF (August 1952). "A quantitative description of membrane current and its application to conduction and excitation in nerve". The Journal of Physiology. 117 (4): 500–544. doi:10.1113/jphysiol.1952.sp004764. PMC 1392413. PMID 12991237.

[47] Bear MF, Connors BW, and Paradisio MA. 2007. Neuroscience: Exploring the Brain, 3rd ed. Lippincott, Williams & Wilkins

[48] Zahler, R., Zhang, Z. T., Manor, M., & Boron, W. F. (1997). Sodium kinetics of Na,K-ATPase alpha isoforms in intact transfected HeLa cells. The Journal of general physiology, 110(2), 201–213. https://doi.org/10.1085/jgp.110.2.201

[49] Blom, H., Bernhem, K., & Brismar, H. (2016). Sodium pump organization in dendritic spines. Neurophotonics, 3(4), 041803. https://doi.org/10.1117/1.NPh.3.4.041803

[50] Azouz, R., & Gray, C. M. (2000). Dynamic spike threshold reveals a mechanism for synaptic coincidence detection in cortical neurons in vivo. Proceedings of the National Academy of Sciences, 97(14), 8110-8115.

[51] Swiegers, J., Bhagwandin, A., Sherwood, C. C., Bertelsen, M. F., Maseko, B. C., Hemingway, J., Rockland, K. S., Molnár, Z., & Manger, P. R. (2019). The distribution, number, and certain neurochemical identities of infracortical white matter neurons in a lar gibbon (Hylobates lar) brain. The Journal of comparative neurology, 527(10), 1633–1653. https://doi.org/10.1002/cne.24545

[52] Koch, C.; Zador, A. (February 1993). "The Function of Dendritic Spines: Devices Subserving Biochemical Rather Than Electrical Compartmentalization". The Journal of Neuroscience. 13 (2): 413–422. doi:10.1523/JNEUROSCI.13-02-00413.1993. PMC 6576662. PMID 8426220.

[53] Alberts, Bruce (2009). Essential Cell Biology (3rd ed.). New York: Garland Science. ISBN 978-0-8153-4129-1.

[54] Park, M. (2018). AMPA receptor trafficking for postsynaptic potentiation. Frontiers in cellular neuroscience, 12, 361.

[55] Myme, C. I., Sugino, K., Turrigiano, G. G., & Nelson, S. B. (2003). The NMDA-to-AMPA ratio at synapses onto layer 2/3 pyramidal neurons is conserved across prefrontal and visual cortices. Journal of neurophysiology, 90(2), 771-779.

[56] García-Nafría, J., Herguedas, B., Watson, J. F., & Greger, I. H. (2016). The dynamic AMPA receptor extracellular region: a platform for synaptic protein interactions. The Journal of physiology, 594(19), 5449–5458. https://doi.org/10.1113/JP271844

[57] The Dana Foundation-a private philanthropic organization that supports brain research through grants, publications, and educational programs. link 4th paragraph, http://www.dana.org/media/detail.aspx?id=31294#_edn2

[58] Tagluk, M. E., & Tekin, R. (2014). The influence of ion concentrations on the dynamic behavior of the Hodgkin-Huxley model-based cortical network. Cognitive neurodynamics, 8(4), 287–298. https://doi.org/10.1007/s11571-014-9281-5

[59] Yeomans, J. S. (1979). The absolute refractory periods of self-stimulation neurons. Physiology & behavior, 22(5), 911-919.